MODELLING AND SIMULATION OF A PHYSIOLOGICAL SYSTEM PRODUCING OCULAR PULSE

by

Yansheng Yan

A thesis
presented to the University of Manitoba
in partial fulfillment of the
requirements of the degree of
Master of Science
in
Electrical Engineering

Winnipeg, Manitoba, Canada
© Yansheng Yan, August 1988

Permission has been granted to the National Library of Canada to microfilm this thesis and to lend or sell copies of the film.

The author (copyright owner) has reserved other publication rights, and neither the thesis nor extensive extracts from it may be printed or otherwise reproduced without his/her written permission.

L'autorisation a été accordée à la Bibliothèque nationale du Canada de microfilmer cette thèse et de prêter ou de vendre des exemplaires du film.

L'auteur (titulaire du droit d'auteur) se réserve les autres droits de publication; ni la thèse ni de longs extraits de celle-ci ne doivent être imprimés ou autrement reproduits sans son autorisation écrite.

ISBN 0-315-47888-8

MODELLING AND SIMULATION OF A PHYSIOLOGICAL SYSTEM PRODUCING OCULAR PULSE

BY

YANSHENG YAN

A thesis submitted to the Faculty of Graduate Studies of the University of Manitoba in partial fulfillment of the requirements of the degree of

MASTER OF SCIENCE

© 1988

Permission has been granted to the LIBRARY OF THE UNIVERSITY OF MANITOBA to lend or sell copies of this thesis, to the NATIONAL LIBRARY OF CANADA to microfilm this thesis and to lend or sell copies of the film, and UNIVERSITY MICROFILMS to publish an abstract of this thesis.

The author reserves other publication rights, and neither the thesis nor extensive extracts from it may be printed or otherwise reproduced without the author's written permission.

ABSTRACT

This thesis presents an extension of a recent model of a physiological system producing ocular pulse, including the models of the left side carotid vascular system, stenosis, and the eye. The method is intended for early screening of both stenosis and elevated intraocular pressure for preventing stroke and glaucoma. The validity of the carotid vascular system model is shown through its (i) stability, (ii) accuracy, (iii) sensitivity to degrees of the model, and (iv) linearity of the system. The stenosis model is improved with respect to the integration algorithm and the displacement along the carotid vascular system. The eye model is also modified to achieve the relationship between the ocular blood pressure and intraocular pressure with respect to different severity levels of stenosis. The ocular pulse is analyzed, both in spatial and frequency domains, with its associated signals such as the ocular blood pressure, and the intraocular pressure. Computer simulation has shown that the model compares well with the previously published results, while revealing details not available before. The sensitivity of the ocular pulse waveform to the stenosis and intraocular pressure is studied through a differential differencing analysis, and shows that it is possible to use the ocular pulse waveform to detect the severity level of stenosis from 10% to 90% with precision of the level difference of 20%, and its location in either the common carotid, or the external carotid, or the internal carotid, as well as the intraocular pressure levels from 15 to 40 mmHg.

ACKNOWLEDGEMENTS

I wish to express my sincere thanks to my advisor, Dr. Witold Kinsner, for his excellent guidance, endurable motivation and consistent support throughout the course of this research, and for his suggestion of this research topic.

Thanks also go to Mr. Larry Leblanc for his co-operation of the partial computer program.

Thanks to Dr. A.B. Thornton-Trump and Dr. G.W. Swift for their valuable comment and examination on this thesis.

I would like to express my gratitude to my wife, my parents and the family for their consistent encouragement and financial support.

Finally, the partial financial support from the Natural Sciences and Engineering Research Council (NSERC) of Canada and the Manitoba Strategic Research Program is gratefully acknowledged.

TABLE OF CONTENTS

		Page
ABSTRACT		ii
ACKNOWLEDGEMENTS		iii
TABLE OF CONTENTS		iv
LIST OF FIGURES		vii
LIST OF TABLES		xi
LIST OF ABBREVIATIONS		xii
I. INTRODUCTION		1
1.1	Motivation	1
1.2	Research Methodology	4
1.3	Thesis Objectives and Structure	5
II. Existing MODELS		7
2.1	Modelling of the Human Arterial System	8
2.2	Stenosis Modelling	10
2.3	Eye Modelling	12
2.4	Summary	14
III. THE OCULAR PULSE SYSTEM MODEL		15
3.1	The Model of the Carotid Vascular System	15
	3.1.1 CVS Topology	15
	3.1.2 Haemodynamic/Electrical System Analogy	17
	3.1.3 The Model of the CVS	21
	3.1.4 Computer Modelling of the CVS Model	29

3.1.5 Evaluation of the CVS Model Performance 31
3.1.6 Summary 46
3.2 The Model of Stenosis 47
3.2.1 Description of the Stenosis Model 47
3.2.2 Integration and Displacement of the Stenosis in the CVS 50
3.2.3 Three Term Index Numbers of the Stenosis Model 53
3.2.4 OBP Waveforms With 10 level Stenosis 54
3.2.5 Summary 58
3.3 The Model of the Eye 58
3.3.1 Vascular Blood Circulation in the Eye 61
3.3.2 Aqueous Humour Dynamics 63
3.3.3 Ocular Rigidity Function 64
3.3.4 OBP-IOP Relationship 65
3.3.5 Ocular Pulse 71
3.3.6 Summary 76
3.4 Description on the System Structure 77

IV. A SENSITIVITY STUDY AND PATTERN EXPLORATION OF OCULAR PULSE 80
4.1 Stenosis 82
4.1.1 Spatial Analysis 82
4.1.2 Spectral Analysis of OPW 99
4.2 Elevated IOP 117
4.3 Summary 124

V. CONCLUSIONS AND RECOMMENDATIONS 125

REFERENCES 131

APPENDIX A ELEMENTS OF STATE EQUATIONS OF THE CVS 135

APPENDIX B PARAMETER CHANGES IN VARIATION CASES OF CHAPTER IV 137

APPENDIX C SIMULATION PROGRAM STRUCTURE 139

APPENDIX D PROGRAM LISTING 141

LIST OF FIGURES

Figure		Page
1.1	A decision tree for the screening process of stenosis and glaucoma	3
2.1	Ocular pulse waveform (OPW) characteristics	11
3.1.1	Topology of the carotid vascular system (CVS)	16
3.1.2	Analogy between haemodynamic system and electric system	19
3.1.3	The carotid vascular system (CVS) model with 22 reactive elements	22
3.1.4	The carotid vascular system (CVS) model with the 14 reactive elements	25
3.1.5	DC equivalent of the carotid vascular system (CVS) model	28
3.1.6	Network representation of the 22nd degree CVS model with 22 reactive elements denoted by bold characters and segments denoted by circled numbers	30
3.1.7	The aorta blood pressure waveform (ABPW)	32
3.1.8	Discrete Fourier transform of the ABPW in Fig. 3.1.7	33
3.1.9	Step response of the 22nd degree CVS model	36
3.1.10	Step response of the 14th degree CVS model	37
3.1.11	The ocular blood pressure waveform (OBPW) for the 22nd degree CVS model with input shown in Fig. 3.1.7	39
3.1.12	The ocular blood pressure waveform (OBPW) for the 14th degree CVS model with input shown in Fig. 3.1.7	40
3.1.13	Discrete Fourier transform of OBP in Fig. 3.1.11 (the 22nd degree model)	42
3.1.14	Discrete Fourier transform of OBP in Fig. 3.1.12 (the 14th degree model)	43

3.1.15 Absolute difference between spectrum magnitude values in Fig. 3.1.13 and Fig. 3.1.14 45
3.1.16 The spectral transfer function of the 22nd degree CVS model (Ratio of magnitude values in Fig. 3.1.13 to those in Fig. 3.1.8 45
3.2.1 Geometric configuration of stenosis 48
3.2.2 OBPWs as a function of stenosis severity in segment 8 of the CVS 55
3.2.3 Percent OBP mean values as a function of stenosis in segment 8 of the CVS 56
3.2.4 Percent mean value reduction of stenosis blood flow in segment 8 of the CVS 56
3.2.5 Relationship between mean value reductions of OBP and stenosis blood flow in segment 8 of the CVS 56
3.3.1 Causal diagram for the eye 59
3.3.2 OBP-IOP relationship as a function of stenosis severity located in segment 8 of the CVS 70
3.3.3 Cornea model 72
3.3.4 OPW without stenosis 74
3.3.5 OPWs as a function of stenosis severity located in segment 8 of the CVS 75
3.4.1 System structure chart 79
4.1.1 OBPWs as a function of stenosis severity in segment 2 of the CVS 85
4.1.2 OBPWs as a function of stenosis severity in segment 5 of the CVS 86
4.1.3 Mean values of IOP as a function of stenosis severity 88
4.1.4 OPWs as a function of stenosis severity in segment 2 of the CVS 89

4.1.5 OPWs as a function of stenosis severity in segment 5 of the CVS 90
4.1.6 Mean values of OBP as a function of stenosis severity in segment 8 of the CVS for CASE1 and CASE8–CASE21 91
4.1.7 Mean values of IOP corresponding to mean values of OBP in Fig. 4.1.6 91
4.1.8 Spectrum of human heart beat cycle with systolic (S) and diastolic (D) portions 92
4.1.9 ABPWs with (a) cycle 0.4 sec, (b) cycle 1.5 sec 93
4.1.10 OBPWs as a function of stenosis severity in segment 8 of the CVS with the input ABP shown in Fig. 4.1.9a 95
4.1.11 OBPWs as a function of stenosis severity in segment 8 of the CVS with the input ABP shown in Fig. 4.1.9b 96
4.1.12 OPWs as a function of stenosis severity in segment 8 of the CVS with the input ABP shown in Fig. 4.1.9a 97
4.1.13 OPWs as a function of stenosis severity in segment 8 of the CVS with the input ABP shown in Fig. 4.1.9b 98
4.1.14 MAGDIF spectrum of the OPW for CASE1 102
4.1.15 PHADIF spectrum of the OPW for CASE1 103
4.1.16 Trend patterns from MAGDIF spectra for different slots 105
4.1.17 MAGDIF pattern of the OPW as a function of stenosis severity for CASE1 and CASE8–CASE21 106
4.1.18 PHADIF pattern of the OPW as a function of stenosis severity for CASE1 and CASE8–CASE18 107
4.1.19 PHADIF pattern of the OPW as a function of stenosis severity for CASE7 and CASE19–CASE21 108
4.1.20 MAGDIF patterns of the OPW as a function of

stenosis severity in different locations 111
4.1.21 PHADIF patterns of the OPW as a function of stenosis severity in different locations 112
4.1.22 DIF patterns of the OPW as a function of stenosis severity for CASE22 114
4.1.23 DIF patterns of the OPW as a function of stenosis severity for CASE23 115
4.2.1 Relationship between transmural pressure and ocular vascular volume 118
4.2.2 OBP-IOP relationship as a function of the elevated IOP 120
4.2.3 OPWs as a function of IOP levels 121
4.2.4 MAGDIF spectrum of the OPW as a function of IOP levels 122
4.2.5 PHADIF spectrum of the OPW as a function of IOP levels 123

LIST OF TABLES

Table		Page
3.1.1	The analogy of haemodynamic/electrical quantities	20
3.1.2	Component values of the 22nd degree CVS model	23
3.1.3	Component values of the 14th degree CVS model	26
3.1.4	Eigenvalues of matrix A for the 22nd degree CVS model	35
3.1.5	Eigenvalues of matrix A for the 14th degree CVS model	35
3.2.1	Coefficients of stenosis in segment 8 of the CVS	52
3.2.2	Three index numbers of the stenosis in segment 8 of the CVS	52
3.3.1	Mean values of IOP and ocular vascular volume as a function of stenosis severity located in segment 8 of the CVS	69
4.1.1	Three index numbers for stenosis in segment 2, 5 and 8 of the CVS	83
4.2.1	IOP level and ocular vascular volume	118

LIST OF ABBREVIATIONS

CVS	The carotid vascular system
ABP	Aorta blood pressure
ABPW	Aorta blood pressure waveform
OBP	Ocular blood pressure
OBPW	Ocular blood pressure waveform
IOP	Intraocular pressure (the pressure within the eye)
OPW	Ocular pulse waveform

CHAPTER I

INTRODUCTION

1.1 Motivation

Stroke and glaucoma are of major concern to preventive medicine due to their toll on human life and health care system. In 1980, over 1 million Americans died of diseases of the heart and blood vessels. The majority of these patients died of acute problems such as heart attack (566,900 persons) and stroke [Bron86]. Stroke accounts for 11% deaths [Wolf77] (approximately 500,000 persons per year in the U.S. alone). 40% to 70% of the people who had the cardiovascular diseases are rendered disabled and require billions of dollars per year in continuing care. For example, in 1983, over $56 billion was spent or lost due to cardiovascular diseases, with over $32 billion spent on hospital or nursing home care. Glaucoma accounts for 15% of blindness in the U.S. [ScAl69]. Therefore, early detection of the diseases could be very important to preventive medicine.

Stroke may be caused by an effective blood vessel narrowing (an arterial stenosis, possibly combined with arterial spasm) which obstructs the blood flow to the brain, leading to a possible damage of the brain or even death. Glaucoma may be caused by an elevated intraocular pressure (IOP) which may reduce blood supply to the nerve fiber in the retina, thus leading to possible blindness. Therefore, early screening for the stenosis and elevated IOP in an outpatient environment should be very important and an effective way to prevent the two diseases.

Although the plausible causes of stroke (an arterial stenosis without or with the spasm) and glaucoma (an elevated IOP) are not related, they can be detected by a common method based on an analysis of an ocular pulse waveform (OPW), which is defined as the pulsatile radial displacement of the cornea due to choroidal pulsations under a given IOP. The method is highly sensitive to the level and location of carotid occlusions causing stroke because the choroidal arteries are connected to the ophthalmic artery which, in turn, is the first major division of the internal carotid . In his study on rabbits, Best [Best70 to Best74] has shown that carotid occlusions can alter the ocular pulse. The method is also sensitive to the level of the IOP because the spectral contents of the OPW change as the function of the IOP due to their direct correlation [Mow68].

Work on finding a single screening method for both diseases started in 1977 [Kins79, CKKJ81] and summarized in [Kins87]. The method is to analyze the OPW measured by an accurate and repeatable technique to achieve its relationships with either the carotid stenosis or the elevated IOP. These relationships can be used to screen for the existence of the carotid stenosis and the elevated IOP in an outpatient environment. An example of a decision tree can be compiled in Fig. 1.1 to explain the screening process.

Separate screening methods presently used for the two diseases have been studied [Kins79, JuKi84a, Jull84a]. They include (i) the non-invasive methods (Doppler sonography, phonoangiography, thermography) and the invasive methods (angiography) for blood vessel narrowing encountered in stroke, (ii) the contact methods for IOP measurement (tonometry and its derivatives), (iii) the non-contact method (Doppler shift with ultrasound) for the ocular pulse measurement. However, all of these methods have serious

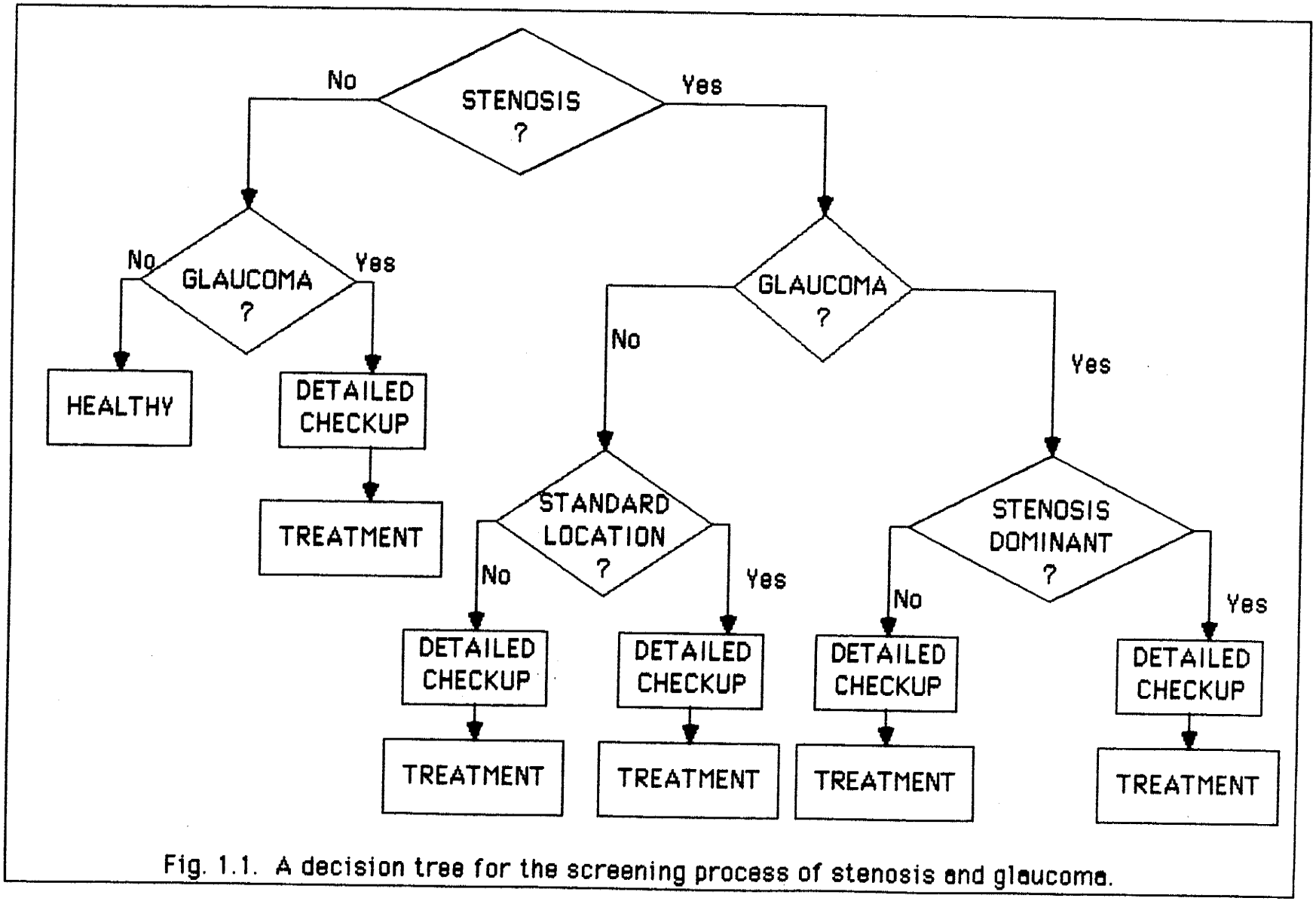

Fig. 1.1. A decision tree for the screening process of stenosis and glaucoma.

and essential drawbacks that eliminate their use for the ocular pulse screening method. These drawbacks have proved to be (i) the non-invasive methods are not reliable and simple enough for the outpatient screening, (ii) the invasive methods, due to its danger to human beings, is usually used after stroke has occurred, (iii) the contact methods do not produce accurate results, and (iv) the ultrasound measurement of OPW is too sensitive to environmental conditions and noise. A laser interferometry method has been selected [JuKi84b] as the most promising, which is non-invasive, non-contact, and accurate enough to be applied in the outpatient environment.

1.2 Research Methodology

The ultimate goal of this research topic is to establish a non-invasive, non-contact, reproducible, economical, and outpatient method for early screening of the stenosis and the elevated IOP. In order to achieve this goal, a sequence of research phases were proposed [CKKJ81, Kins87], including (i) the preliminary study by modelling and simulation of the ocular pulse system (the physiological system producing ocular pulse), (ii) the development of a new laser interferometer for measuring the ocular pulse, (iii) the clinical study of the screening method, and (iv) the development of a practical apparatus.

Since the presently used methods cannot obtain the accurate ocular pulse, the ocular pulse and its interrelationship with the stenosis and elevated IOP for an accurate non-contact screening method need to be first investigated. In phase (i), a model of the ocular pulse system has been developed [Jull84a, JuKi84a], including the models of the carotid vascular

system (CVS), stenosis, and the eye. Through this system model, the sensitivity of OPW to the carotid stenosis and the elevated IOP within the eye can be extensively studied. The results are intended to assist in further clinical studies. This thesis has been done to improve the present model, including the re-evaluation and validity study of the system. Furthermore, this thesis is also focused on the sensitivity of OPW to the stenosis and the elevated IOP.

1.3 Thesis Objectives and Structure

The objectives of this thesis work follow the selected research methodology and include:

1. Further development and detailed improvement of the present system model, including the models of CVS, stenosis, and the eye;
2. Evaluation and validity study of the system, and establishment of more detailed formulation of the ocular pulse analysis structure in both spatial and frequency domains; and
3. The sensitivity study of the OPW to the stenosis and the IOP levels, and the study of methods for finding the corresponding OPW frequency spectrum patterns.

In Chapter II, the existing models of systemic artery, stenosis, and ocular pulse are reviewed, from which our present model is proved to be valid and improved in terms of its specificity for the OPW study. Chapter III is the description and detailed formulation of the present model including the models of CVS, stenosis, and the eye. Evaluation of results and the system analysis are also presented in that chapter. It is then followed by Chapter IV

on the sensitivity study of the OPW with respect to the stenosis and levels of IOP. In that chapter, the developed methods for finding the corresponding OPW spectrum patterns are also described. Finally, conclusions and recommendations for further research work on the accurate, non-contact OPW screening method for stenosis and elevated IOP are presented.

CHAPTER II

EXISTING MODELS

A variety of previous studies have contributed to modelling of the human arterial system, stenosis, and the eye to obtain a better understanding of the physical phenomena (i) of the human systemic arterial tree, such as pressure and flow wave propagation, properties and architectures of the arterial tree, (ii) of stenosis effect on the blood flow, and (iii) of dynamic mechanism within the eye. Two kinds of methods have been used for developing these models, physical modelling and mathematical modelling. Typical modelling involves a physical model, such as an electrical circuit, and its evaluation by measuring its voltages and currents. Such physical models have been used in the early research on the vascular systemic haemodynamics because of the advanced level of analog computing and the inability of solving large systems of equations that are required to describe the cardiovascular system. With the advent of computers and new algorithms for solving large systems, mathematical modelling has become dominant. Mathematical modelling involves a mathematical description of a physical model and its evaluation by solving pertinent equations either analytically or numerically. The results are obtained in the digital domain. All the analytical studies of large systems can be proceeded sufficiently and more effectively in the mathematical model than in the physical model although the mathematical model may be verified in some aspects by the physical model. Therefore, the mathematical modelling is chosen for our study on the development of the ocular pulse system model.

2.1 Modelling of the Human Arterial System

The first and simplest form of the mathematical models is known as the Windkessel model, in which it is assumed that all pressure fluctuations in the artery occur synchronously. Several variations of the model have been developed. This model is useful in a sense that it can approximate the input impedance of the entire arterial systemic tree. However, since it does not consider the wave propagation of the pressure (pulse), the Windkessel model cannot be used to investigate the detailed properties within the arterial system. Therefore, it has been agreed that the arterial system is not as the Windkessel model.

The limitations of the Windkessel model led to the design of other models in which it was assumed that the arteries respond to a central pulse wave as a resonant system and, therefore, the transmission line theory can be applied. Prototypes of these models was developed by Noordergraaf [Noor60, Noor63]. In this model, a passive electrical analogy was obtained by comparing the transmission line propagation equations and simplified equations of blood motion and continuity for fluid flow in a short segment of artery. There were 113 segments with 5 cm of segment length that were interconnected to construct the architecture of the human systemic arterial tree. The behavior of this model was tested to be consistent with the reality in that it exhibited the features of pulse wave travelling down the arteries. However, it was later evidenced that the pressure pulse, while travelling towards the periphery, increased more than in reality. Pater [PaVa64] in his study has developed an electrical analog model for the circulation of human heart and the major branches of entire human arterial vessels. He used

similar methods to Noordergraaf except he employed a correction factor in the calculation of the components representing blood viscosity and inertia based on the low frequency approximation. For higher frequency than 3 Hz, this method produces a marked difference. Jager [Jage65] also described the systemic arterial tree mathematically, including the wall dynamics, and attempted both analytical and numerical solutions. The detailed component parameters were obtained in his study. Snyder [SnRi68] gave his result on the model of central part of the human systemic arterial tree under the "equal-volume" principle. Operational amplifiers instead of passive electrical networks were implemented, which has the advantage of greater flexibility. The results for this model were comparable with the data recorded from the human. The model provided a means for determination of cardiac output under assumed condition such as variations of heart rate. Based on Noordergraaf's prototype and following the pulsatile flow theory by Jager, Westerhof [West69] constructed an electrical model and compared it with its real counterpart in various aspects such as the magnitude and phase of input impedance, wave propagation, and shapes of pressure and flow at different locations. In the model, some previous contradictions were avoided by including the wall dynamics and removing the assumption of thin wall. Another modification to the prototype is the use of a symmetrical network. Increase of the Young's modulus of elasticity towards the periphery was also incorporated. He showed that the model behaved very much like the real system.

All of these models have contributed to the development of a mathematical model of human systemic arterial tree. However, none of them has provided results with respect to the regulation of the ocular blood pressure (OBP) from the system. This fact, therefore, motivated us to develop

a new model of the carotid vascular system (CVS) [Jul184a] for analysis of the ocular pulse waveform (OPW) related to the stenosis in the CVS and the intraocular pressure (IOP) in the eye.

2.2 Stenosis Modelling

Several previous reports have focused on the stenosis and eye models. Best [Best71a] in his *in vivo* study on rabbits confirmed that the carotid artery occlusion causes amplitude reduction and various alterations of ocular pulse along with increase of the stenosis severity, including decreases in slopes of the anacrotic and catacrotic limbs, more notching and rounding of the crest. In his graphic (non-computer) study [Best71c], the ocular pulse was characterized by several features as shown in Fig. 2.1. The study concentrated on how those features are changed with the severity progression of the induced occlusion in the common carotid. Marked amplitude changes were found for the stenosis above 50% in the graphic study and 20% in the harmonic analysis [Best74]. However, the contact measurement by the suction cup technique on anesthetized rabbits was used throughout the study, and the suction level was used to control the regular ocular pulse output and IOP level. In this way, the results lost information leading to low sensitivity, and could not be accurate as compared with the real ocular pulse from the living subject. As shown in Fig. 2.1, the ocular pulse appears to be smoothed by a low-pass filter. The harmonic phase of the ocular pulse was not published. This phase may be an important factor indicating the ocular pulse alteration by stenosis because phase shift by the stenosis can be observed in his ocular pulse results. Nevertheless, the findings from Best's results remain valuable in that it does expose some of the fundamental

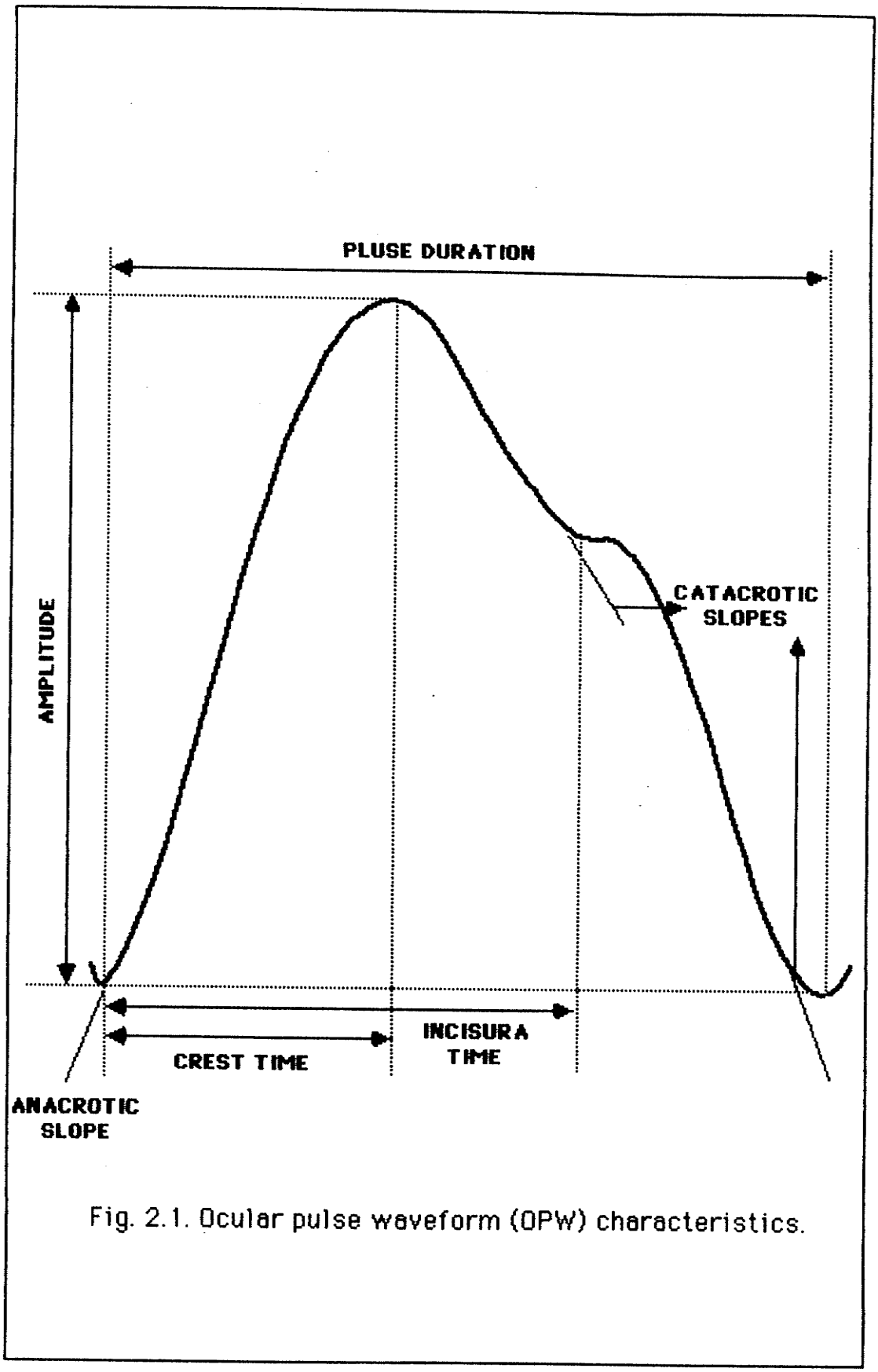

Fig. 2.1. Ocular pulse waveform (OPW) characteristics.

features of ocular pulse and its relation with the stenosis progression. All of the ocular pulse contour change in his graphic analysis reflects spectral content change as a function of stenosis

Young [YoTs73] played a major role in establishing a stenosis model, with which the results from *in vitro* studies on the stenosis performance have been achieved. The model expresses the pressure drop over the constriction of an arterial segment. The pressure drop has been studied with various conditions. A general formula expressing the pressure drop over a stenosis is

$$\frac{\Delta P}{\rho U^2} = f\left(\frac{L_S}{r}, \frac{A_0}{A_1}, \frac{Z_0}{r}, R_e\right) \qquad (2.1)$$

where ΔP is the pressure drop over the length L_S, ρ is fluid density, U is mean velocity on the unobstructed tube, r is the radius of the unobstructed vessel, A_0 and A_1 are the cross areas of the unobstructed and obstructed tubes respectively, Z_0 is half of the stenosis length, and R_e is the Reynolds number, $2\rho rU/\mu$ (an abstract number characterizing the fluid flow past the obstruction). With more detailed interpretation of this general formula, it is possible for us to study the stenosis with different formulations in terms of severity, location, etc. after it is integrated into our CVS model. A detailed description of the stenosis model will be given in next chapter.

2.3 Eye Modelling

Previous studies on modelling of the eye have contributed to revealing the ocular dynamics related to the vascular bed, the IOP, and the aqueous

volume. After an extensive review of the previous studies on the eye, Collins [CoWe80] compiled a causal diagram for understanding of the ocular dynamic relationship. Every relation in the diagram has been expressed in a mathematical formula based on the experimental result valid in certain range. Care must be taken to prevent any incorrect judgement by these relationships realizing the intraocular dynamic state changes uncertainly and nonlinearly when conditions change. Based on these results, an OBP-IOP relationship can be resolved. This allows us to embed the eye model with the CVS model to achieve the ocular pulse, which bears the effect of the carotid stenosis.

Based on the control theory, Chokhani and Kulikowski [ChKu73] studied the regulation of the IOP in order to establish a control basis for a clinical consultation program in glaucoma. Although glaucoma is characterized by an elevated IOP, other elements affecting the regulation of the human eye must be taken into account because of medical uncertainty or inability and variations of human being. The model is to interpret the human process in the eye related to the regulation of the IOP and glaucoma, which serves as a control basis in finding the relationships among various clinical states during organizing a causal network. This model has assisted us in achieving a good result for the study of glaucoma, which could, in turn, set up other factors in the causal network or the control models.

2.4 Summary

Previous studies on the modelling of human arterial system, stenosis, and the eye have been reviewed in this section. All of these models have had an essential influence on our study of a method for screening the stenosis and IOP through the OPW. Without first exposing the OBP and ocular pulse

regulation affected by the carotid stenosis, it is difficult to achieve complete results of the ocular pulse analysis. Based on the previous studies by others, models presented in this thesis are specially developed for study of OBP and OPW rather than a systemic arterial tree, which is oriented towards studying the effect of carotid stenosis and elevated IOP on the OPW.

It should be noted that our study of the elevated IOP is always associated with the causal system within the eye, and not the IOP only. The expression of elevated IOP is used only for brevity. It is also important to mention that stenosis study should include the severity levels, locations, kinds of deposits, and relationship between the shape of stenosis and blood flow past the stenosis. In this thesis, the severity levels and locations of stenosis are studied only.

CHAPTER III

THE OCULAR PULSE SYSTEM MODEL

An ocular pulse system model has been developed, which includes the models of the carotid vascular system (CVS), stenosis, and the eye. This system is capable of producing the ocular pulse for a study on a method of screening the carotid stenosis and the elevated intraocular pressure (IOP).

3.1 The Model of the Carotid Vascular System (CVS)

The CVS model is designed for studying the regulation of the ocular blood pressure (OBP), which can be affected by the carotid stenosis, and also responsible for providing the blood supply to the ocular circulation. This model gives the flexibility for any modification of the system parameters, and even more, it is specially easy to incorporate the models for the stenosis and eye.

3.1.1 CVS Topology

The topology of the CVS is illustrated in Fig. 3.1.1, in which (a) shows each side of the CVS with both the internal and external carotid arteries and their branches, and (b) illustrates the retinal and uveal circulation within the eye. We consider here the left side of the CVS. The right side requires an additional segment for the innominate artery.

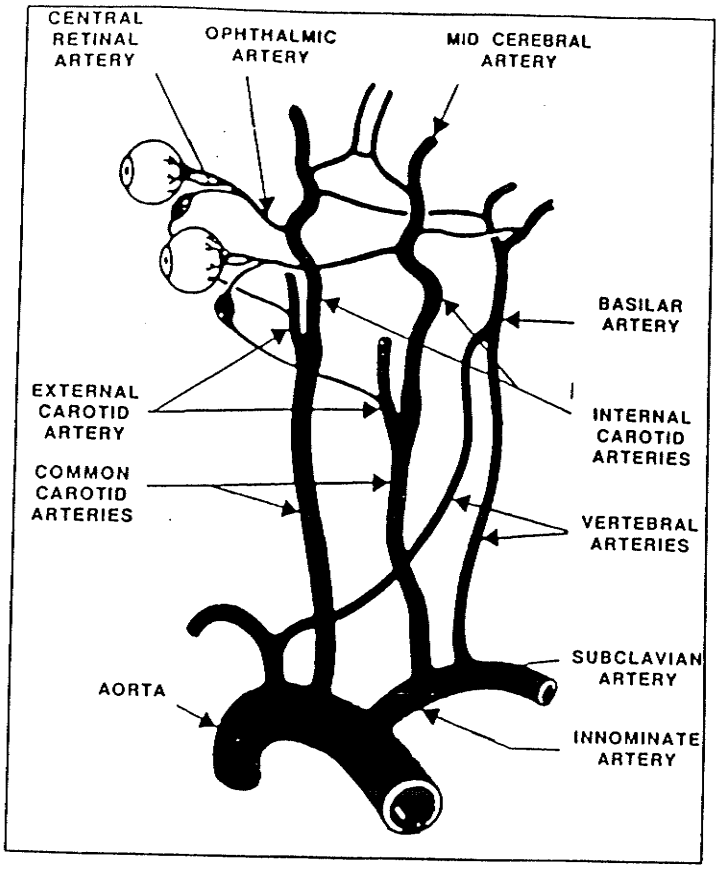

(a) Upper systemic arteries.

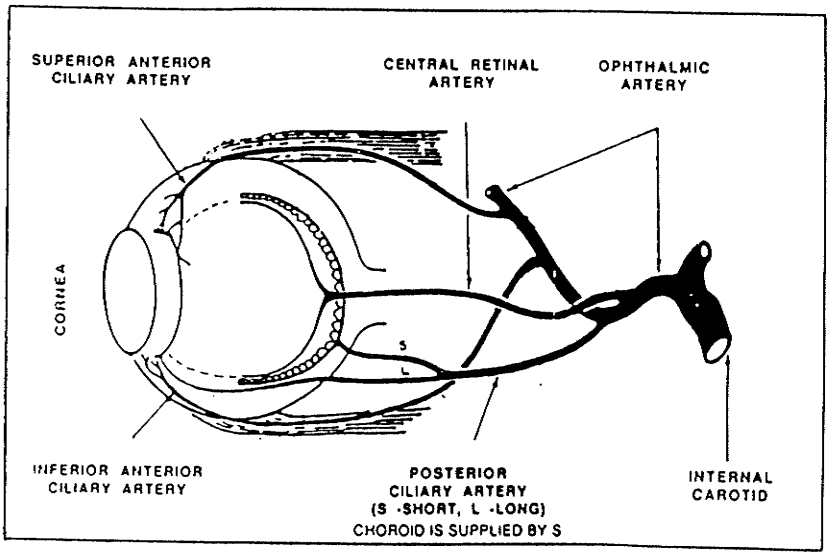

(b) Retinal and uveal circulations.

Fig. 3.1.1. Topology of the carotid vascular system (CVS) [From [Kins87]].

3.1.2 Haemodynamic/Electrical System Analogy

The artery can be considered as a cylindrical elastic tube which responds to the central pulse wave as a resonant system [Warn57]. In this study the central pulse wave is the aorta blood pressure (ABP). Motion of the fluid can be described in an original form

$$\frac{\partial P}{\partial z} = f(Q) \tag{3.1.1a}$$

$$\frac{\partial Q}{\partial z} = g(P) \tag{3.1.1b}$$

where P is the pressure, Q is the flow, ∂z is the incremental length of a segment, f(Q), g(P) are the impedance functions. This Relationship between pressure and flow within the artery can be further expressed [FoMc78], [Jage65] as

$$\frac{\partial P}{\partial z} = \frac{\rho \partial Q}{S\, \partial t} + \frac{8\pi\mu}{S^2} Q \tag{3.1.2a}$$

$$\frac{\partial Q}{\partial z} = \frac{S\, \partial P}{K\, \partial t} \tag{3.1.2b}$$

where K is the relative volume elasticity modulus, S is the cross-sectional area of the tube, μ is the viscosity of the fluid and ρ is the density of the fluid. $K = 2Eh/(3r)$ for $r \ll h$ where r is the radius of the artery, h is the arterial wall thickness, E is the Young's modulus of elasticity of the arterial wall.

An electrical analog can be found by comparing Eqs. 3.1.1 and 3.1.2 with equations describing the relationship between voltage and current in transmission line, which is

$$\frac{\partial v(z,t)}{\partial z} = R\, i(z,t) + L \frac{\partial i(z,t)}{\partial t} \qquad (3.1.3a)$$

$$\frac{\partial i(z,t)}{\partial z} = G\, v(z,t) + C \frac{\partial v(z,t)}{\partial t} \qquad (3.1.3b)$$

where v(z,t) and i(z,t) are the voltage and current as a function of the position on the line and time, R is the resistance/length, L is the inductance/length, G is the conductance/length and C is the capacitance/length.

Assuming that the arterial wall is purely elastic and there are no arterial wall losses, and considering the artery is cylindrical, the equivalent can be drawn as

$$v = P \qquad (3.1.4a)$$

$$i = Q \qquad (3.1.4b)$$

$$R = \frac{8\mu}{\pi r^4} \qquad (3.1.4c)$$

$$L = \frac{\rho}{\pi r^2} \qquad (3.1.4d)$$

$$G = 0 \qquad (3.1.4e)$$

$$C = \frac{3\pi r^3}{2Eh} \qquad (3.1.4f)$$

where R represents the viscosity effect of blood, L is the inert mass of blood, C is the distensibility of vessel or arterial compliance, G is the blood leakage

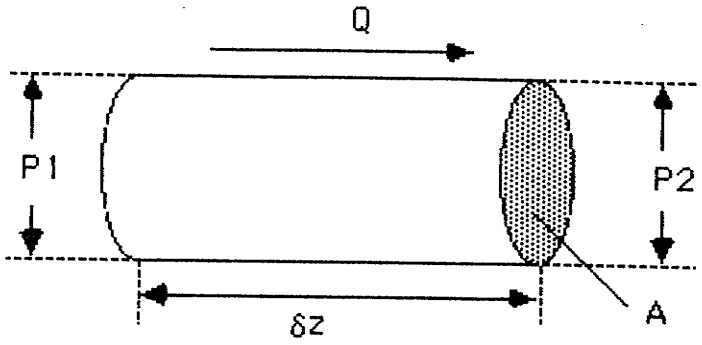

(a) A segment of artery.

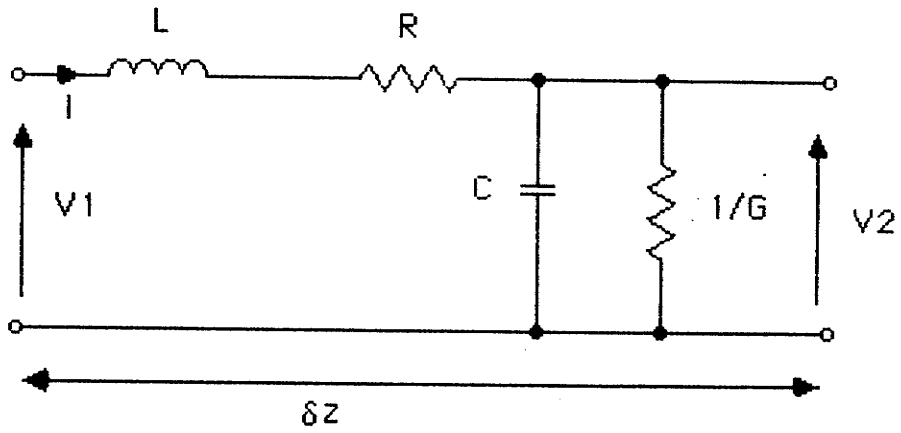

(b) A segment of transmission line.

Fig. 3.1.2. Analogy between haemodynamic system and electrical system [After [Kins87, Jul184a]].

Table 3.1.1 The analogy of haemodynamic/electrical quantities [After [Jul184a]].

Hemodynamic		Electric	
Pressure , P	mmHg	Voltage, V	V
Flow, Q	1.333E+3 cm^3/sec	Current, I	amps
Volume	1.333E+6 cm^3	Charge	coulombs
Time	1 sec	Time	1 sec
Frequency	1 Hz	Frequency	1 Hz
Viscosity	1 g cm^{-4} /sec	Resistance, R	1 ohm
Inertia	1 g cm^{-4}	Inductance, L	1 henry
Distensiblity	1 $g^{-1}cm^4$ sec^2	Capacitance, C	1 farad

which is considered to be zero for a healthy artery.

A better approximation of R and L obtained in [SnRi68] is used in this work, which is expressed as

$$R = \frac{8l\mu}{8\pi r^4} \qquad (3.1.4g)$$

$$L = \frac{9\rho}{4\pi r2} \qquad (3.1.4h)$$

Fig. 3.1.2 and Table 3.1.1 are the illustration of this analogy and the translation from electrical to haemodynamic quantities, respectively.

3.1.3 The Model of the CVS

According to the transmission line theory and the haemodynamic/electrical analogy, the artery can be segmented with certain length in lumped sections. The length affects the accuracy of the model. The higher the frequency response required, the shorter the length should be. Pater [PaVa64] found that for an artery segment with a length of about 6 cm, the errors on the longitudinal impedance were less than 2% on the modulus and 3^0 in the phase angle. Pater in his modelling of artery reported a good result for up to at least 15 Hz. Westerhof [West69] in his test obtained the same accuracy for up to 50 Hz with segments ranging from 2 to 7.5 cm. Snyder [SnRi68] also suggested the equal-volume modelling of arterial tree, which means the length of one lumped section should be approximately inversely proportional to its cross-sectional area for certain accuracy of the

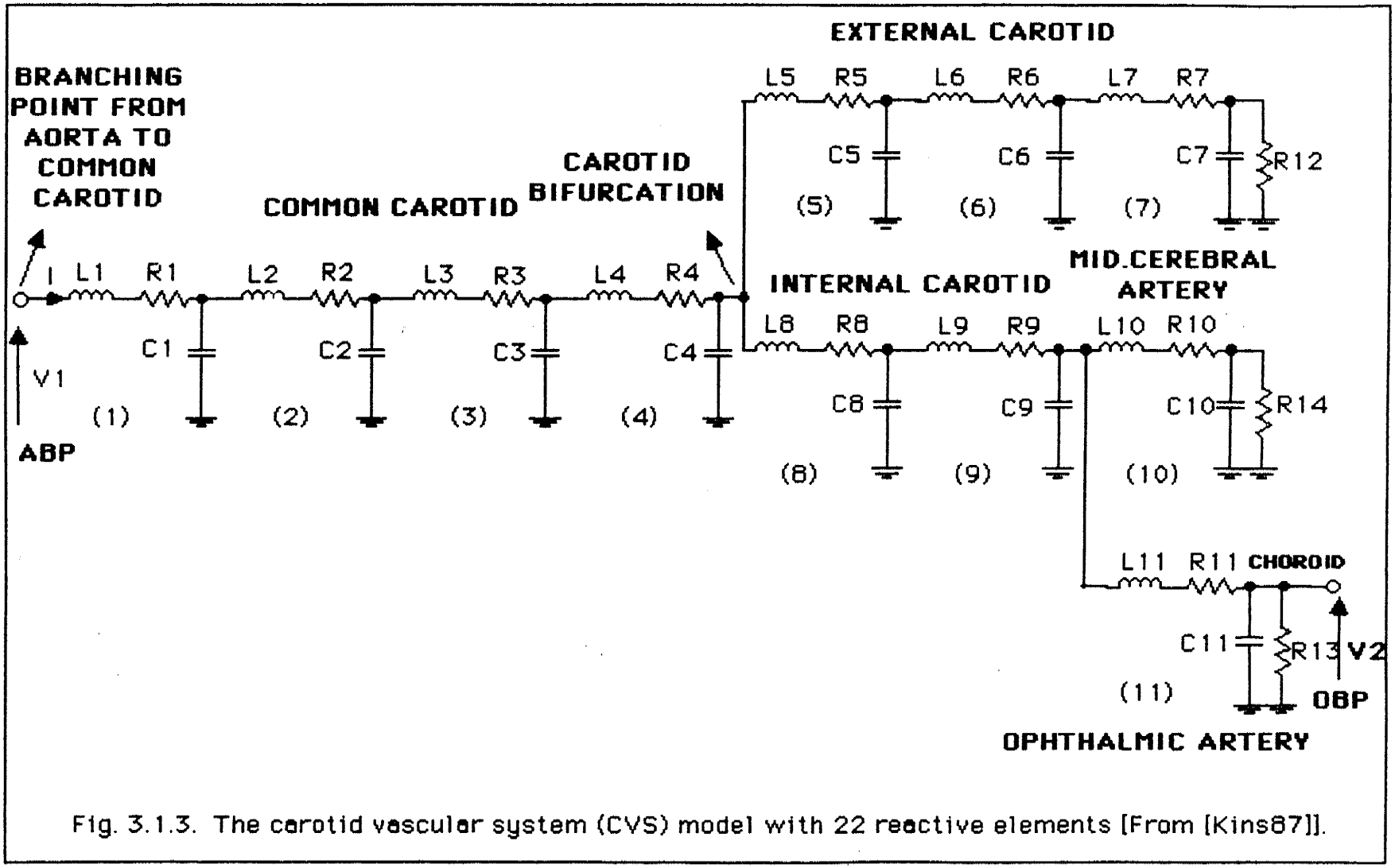

Fig. 3.1.3. The carotid vascular system (CVS) model with 22 reactive elements [From [Kins87]].

Table 3.1.2 Component values of the 22nd degree CVS model.

[After [Kins87, Jul184a]]

Segment No.	Length of segment Δz (cm)	Artery Radius r (cm)	Artery wall thickness h (cm)	Young Modulus E (10^6 gcm^{-1}s^{-2})	R (gcm^{-4}s^{-1}) $R=\frac{8l\mu}{8\pi r^4}\Delta z$	L (gcm^{-4}) $L=\frac{9\rho}{4\pi r^2}\Delta z$	C 10^{-6}g^{-1}cm^{4}s^2 $C=\frac{3\pi r^3}{2Eh}\Delta z$
1	6.0	0.4	0.06	4.0	23	28	7.5
2	6.0	0.4	0.06	4.0	23	28	7.5
3	6.0	0.4	0.06	4.0	23	28	7.5
4	3.0	0.4	0.06	4.0	11	14	3.8
5	6.0	0.18	0.045	8.0	550	139	0.46
6	6.0	0.13	0.04	8.0	2030	267	0.19
7	6.0	0.1	0.025	16.0	5800	451	0.07
8	6.0	0.18	0.045	8.0	550	139	0.46
9	6.0	0.13	0.04	8.0	2030	267	0.19
10	6.0	0.1	0.025	16.0	5800	451	0.07
11	2.0	0.08	0.02	16.0	4720	705	0.015

$\mu = 3.1 \times 10^{-2}$ [poise], $\rho = 1.05$ [g cm^{-3}]

model. For higher frequency, the results from the model will be affected by cut-off frequencies of the lumped arterial segments and, therefore, become irrelevant to the real human arterial circulation. Based on all of this principle, a model describing the left side of the CVS was established [Jul184a] as shown in Fig. 3.1.3. Table 3.2 lists the physiological data and component values. Later, we will discuss the fact that the frequency band remains below 20-50 Hz in this study.

The 22nd degree model shown in the Fig. 3.1.3 represents the left side of the CVS with its input at the branching point of the common carotid artery and the aorta. Segments 1, 2, 3, and 4 represent the common carotid artery before the branching point of the external carotid (segments 5, 6, and 7) and the internal carotid arteries (segments 8 and 9). The internal carotid artery separates into the middle cerebral artery (segment 10) and the ophthalmic artery (segment 11) which, as a first approximation, terminates into the choroid R13 (vascular lining at the posterior eyeball). The approximation of this choroidal termination is supported by the fact that the uveal vessels (ciliary and choroidal vessels) leading to the choroid carry 40 to 70 times the amount of blood presented in the retinal system [Weit73]. Both the external carotid artery and middle cerebral artery terminate into minor branches that are approximated in the model by the vascular bed resistances, R12 and R14.

Notice that the repeated solutions from the CVS model are required for the analysis of the overall ocular pulse system. Since the computation with the 22nd degree model is time-consuming, the 22nd degree model had to be reduced to a lower degree. The 14th degree model was selected [Jul184a] to preserve the same structure and frequency response bandwidth of the CVS.

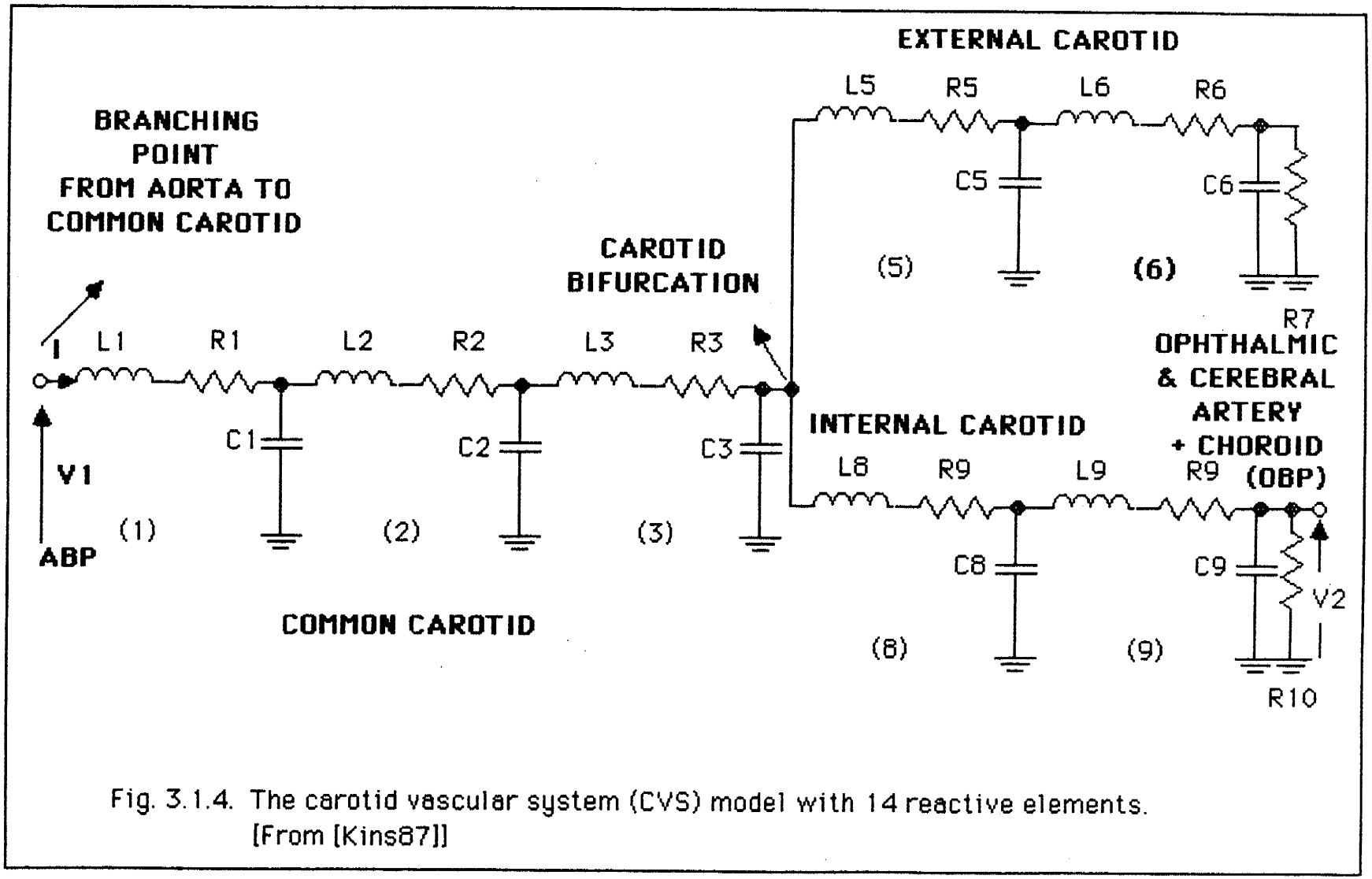

Fig. 3.1.4. The carotid vascular system (CVS) model with 14 reactive elements. [From [Kins87]]

Table 3.1.3 Component values of the 14th degree CVS model.
[After [Kins87, Jul184e]]

Segment No.	Length of segment Δz (cm)	Artery Radius r (cm)	Artery wall thickness h (cm)	Young Modulus E (10^6 gcm^{-1}s^{-2})	R (gcm^{-4}s^{-1}) $R=\frac{8l\mu}{8\pi r^4}\Delta z$	L (gcm^{-4}) $L=\frac{9\rho}{4\pi r^2}\Delta z$	C 10^{-6}g^{-1}cm^{4}s^2 $C=\frac{3\pi r^3}{2Eh}\Delta z$
1	7.0	0.4	0.06	4.0	27.3	33	8.8
2	7.0	0.4	0.06	4.0	27.3	33	8.8
3	7.0	0.4	0.06	4.0	27.3	33	8.8
5	9.0	0.15	0.045	8.0	1776.2	300	0.4
6	9.0	0.1	0.025	16.0	8991.8	677	0.1
8	6.0	0.18	0.045	8.0	571.0	139	0.46
9	6.0	0.13	0.04	8.0	2098.9	267	0.19

$\mu = 3.1 \times 10^{-2}$ [poise], $\rho = 1.05$ [g cm^{-3}]

This electrical analog model is illustrated in Fig. 3.1.4. The common carotid artery is reduced to segments 1, 2, 3. As the diameter of the vessels and the ratio of arterial radius to arterial wall decrease, the apparent viscosity of blood increases so as to make the series of artery segment almost exclusively resistive; i.e., the equivalent inductance and compliance become negligible. Based on this approximation, both the external and internal carotid arteries have been segmented into two equal segments, 5 &. 6, and 8 &. 9, respectively. Resistances R7 and R10 represent the vessel leakage. The effect of the cerebral artery is almost purely resistive and has been included in the vascular bed resistance R10 since the ophthalmic artery is a main branch of the internal carotid artery. Physiological data of the component values was also modified and is listed in Table 3.1.3.

The vascular bed terminations are expressed as the peripheral vascular bed resistances in which the pressure across R10 (for the 14th degree model) or R13 (for the 22nd degree model) accounts for the OBP as an output of the model. The resistance bed remains constant over the normal range of OBP [Best71d] so that they can be calculated by using the DC equivalent of the CVS, as shown in Fig. 3.1.5. Since R_{bed} is inversely proportional to the cross-sectional area of the blood vessel, we can write

$$R10 = K_1\, R7, \text{ for the 14th degree model, and} \qquad (3.1.5)$$

$$R12 = R14 = K_2\, R13, \text{ for the 22nd degree model} \qquad (3.1.6)$$

Notice that K_1 and K_2 have been calculated to be 0.6, 0.64, respectively. Choosing the typical systolic amplitudes of the ABP of 140 mmHg and the OBP of 75 mmHg (comparable to the result reported in [CoWe80]) we can resolve

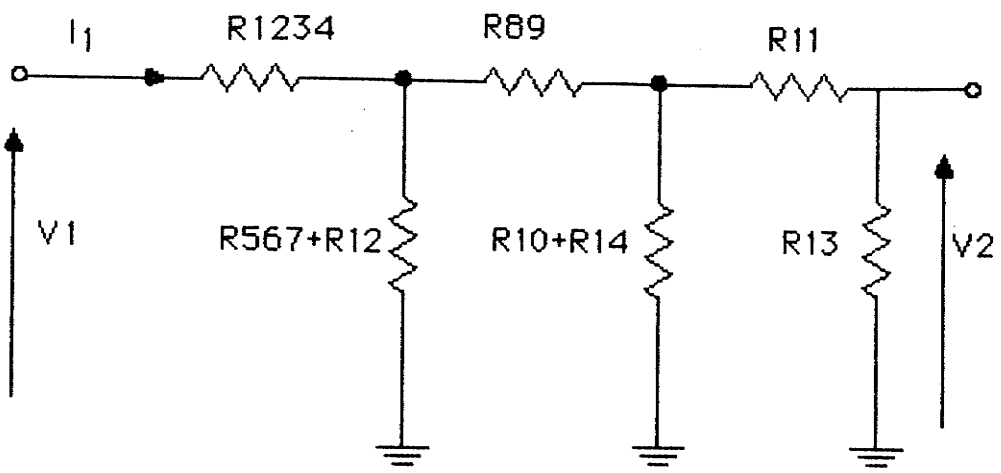

(a) DC equivalent of the 22nd degree CVS model.

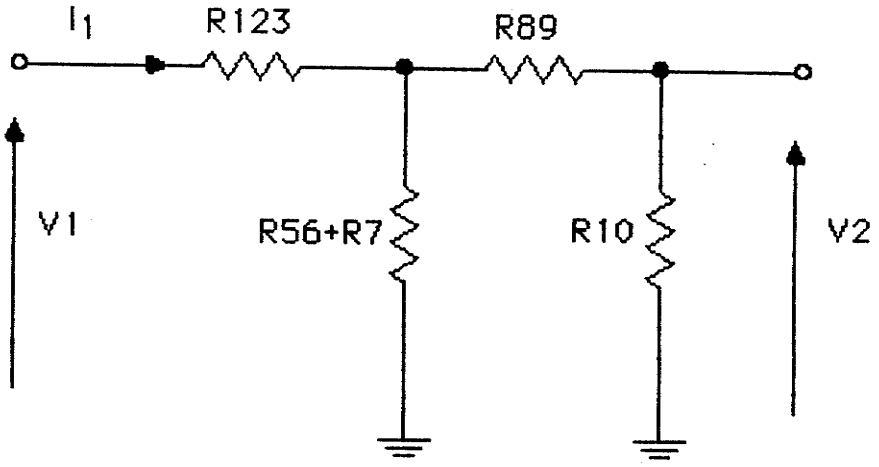

(b) DC equivalent of the 14th degree CVS model.

Fig. 3.1.5. DC equivalent of the carotid vascular system (CVS) model.

R7 = 5355.6 $gcm^{-4}s^{-1}$, R10 = 3213.4 $gcm^{-4}s^{-1}$, for the 14th degree model, and R12 = R14 = 8254.9 $gcm^{-4}s^{-1}$,

R13 = 12898.2 $gcm^{-4}s^{-1}$, for the 22nd degree model.

3.1.4 Computer Modelling of the CVS Model

For the CVS model shown in Fig. 3.1.3 or 3.1.4, a set of state equations can be systematically formulated to describe the behavior of the model. These state equations can be expressed as

$$\frac{dx(t)}{dt} = A\,x(t) + B\,u(t) \qquad (3.1.7a)$$

$$y(t) = C\,x(t) + D\,u(t) \qquad (3.1.7b)$$

where x(t) is the state vector, u(t) is the input vector, which is ABP, y(t) is the output vector, which is OBP, and A, B, C, D are constant matrices which are composed of the component values of the model. These equations can be systematically set up [Chen83] by means of a directed graph representation of this network with normal tree and cotree, given in Fig. 3.1.6 for the 22nd degree model. Since the structure of the 14th degree model is very similar with that of the 22nd degree model, similar graph representation of the network can be directly extracted from Fig. 3.1.6. From this graph, a normal tree that contains all capacitive edges can be selected, the corresponding cotree containing all inductive edges. Using Kirchhoff's current and voltage laws, each tree-branch current can be expressed as a sum of cotree-link currents, each cotree-link voltage can be expressed as a sum of tree-branch voltages. Currents on the inductive edges and voltages in the capacitive egdes

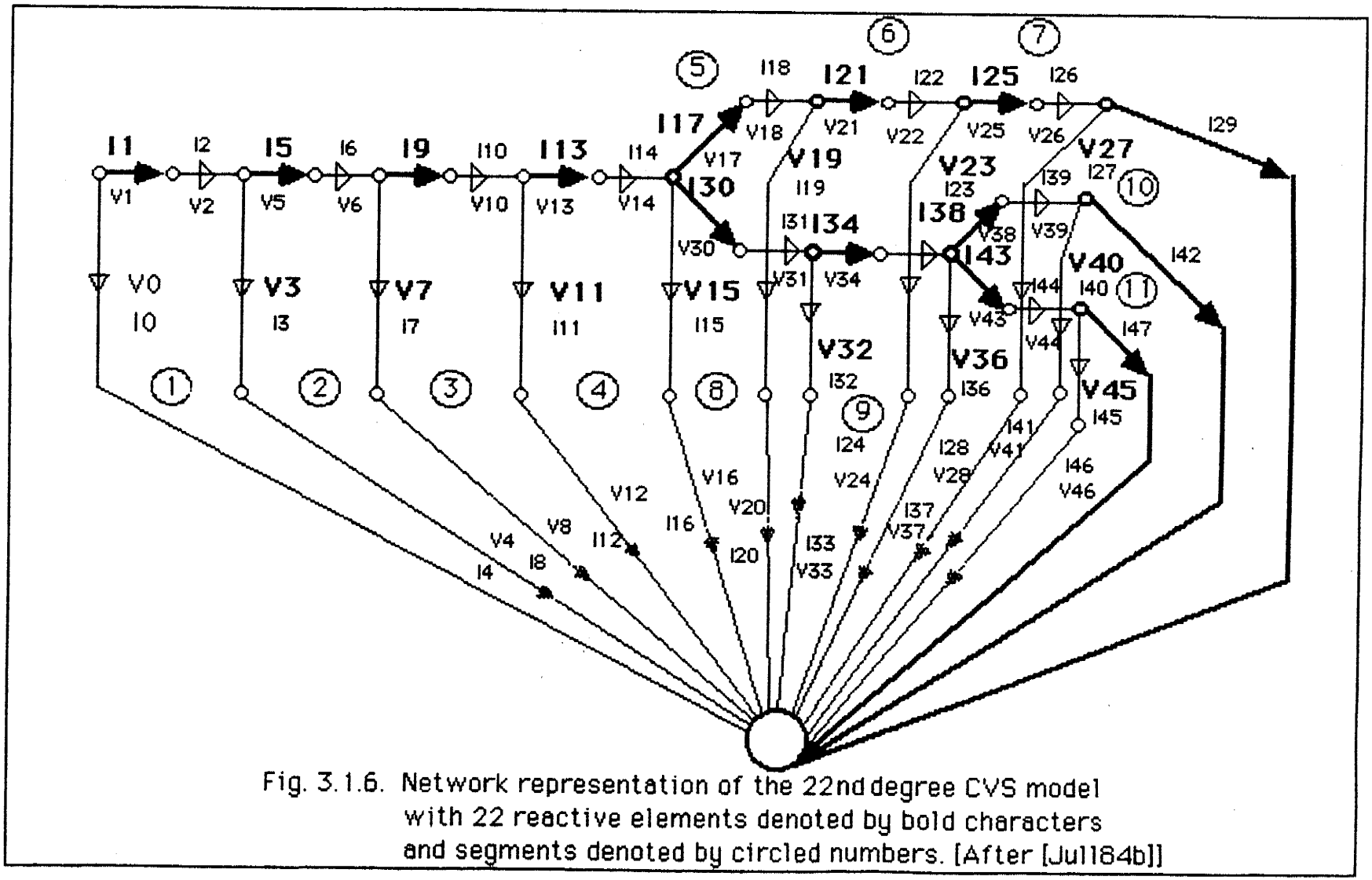

Fig. 3.1.6. Network representation of the 22nd degree CVS model with 22 reactive elements denoted by bold characters and segments denoted by circled numbers. [After [Jul184b]]

are the state variables. By combining all equations and eliminating non-state variables, a set of state equations in a normal form (Eq. 3.1.7) were obtained [Jul184b]. Elements of these state equations are presented in Appendix A.

These state equations of the model can be solved numerically using Euler's forward integration equation which can be expressed as

$$x_{i+1}(t) = x_i(t) + \frac{dx_i(t)}{dt}\Delta t \qquad (3.1.8)$$

The error introduced by this method is of the order $(\Delta t)^2$ and can be kept small by using a small Δt value.

Thus, the CVS can be fully expressed by a set of state equations. A system equation solver has been programmed [Jul184b] and improved so that this model can generate the OBP waveform (OBPW) which controls the eye blood circulation and ocular pulse, and shows the effect from stenosis. With the expression of these state equations, this system becomes flexible and may be modified for any system parameters for analytical purposes. It can also be seen that inclusion of models for stenosis and eye with this system will be convenient because every reactive element in the system is explicitly expressed in the state equations and OBP is directly related to ocular dynamics. Thus, the ocular pulse as a function of the stenosis in the CVS and elevated IOP in the eye can be obtained. These points will be more clear after two models for stenosis and eye are presented later

3.1.5 Evaluation of the CVS Model Performance

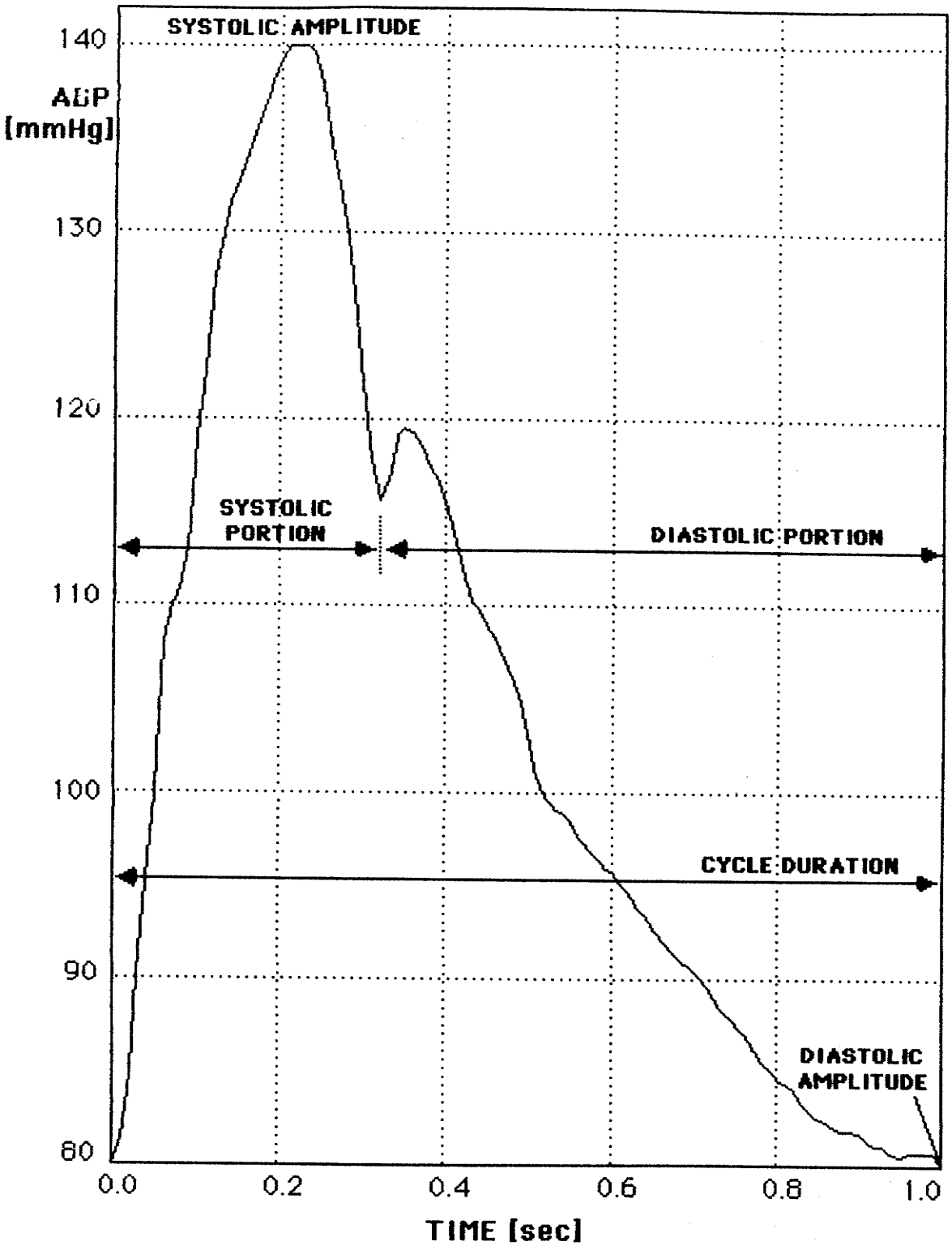

Fig. 3.1.7. The aorta blood pressure (ABP) waveform.
[After [Jul184a]]

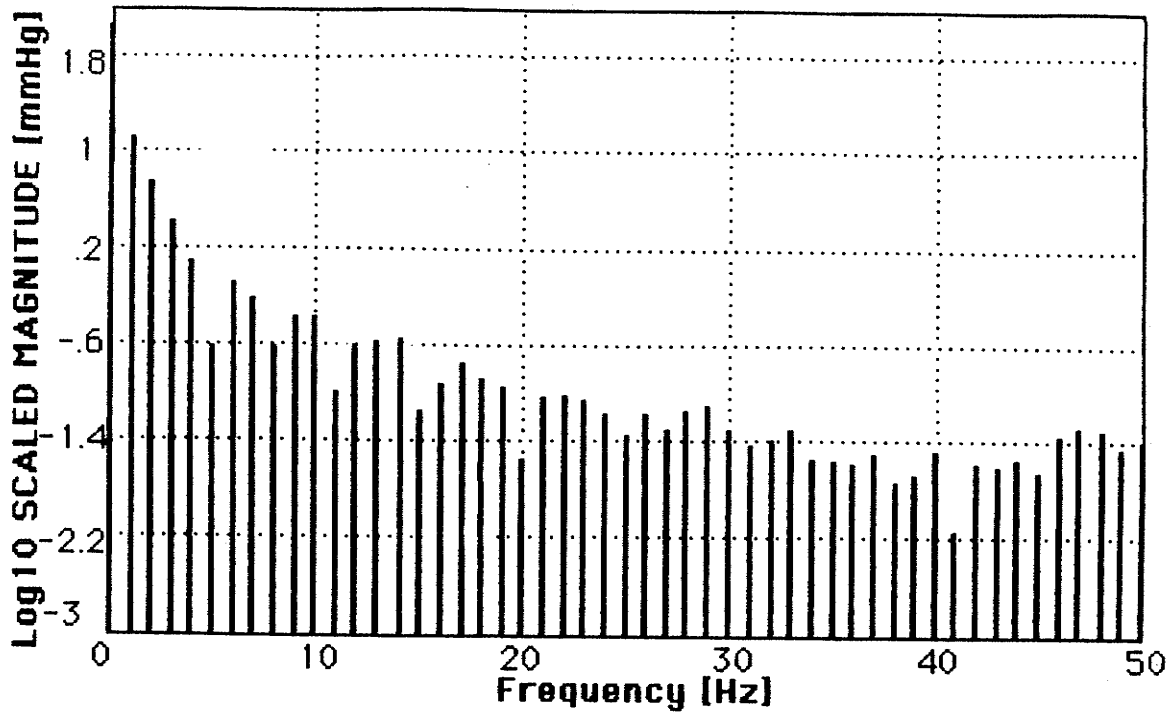

(a)

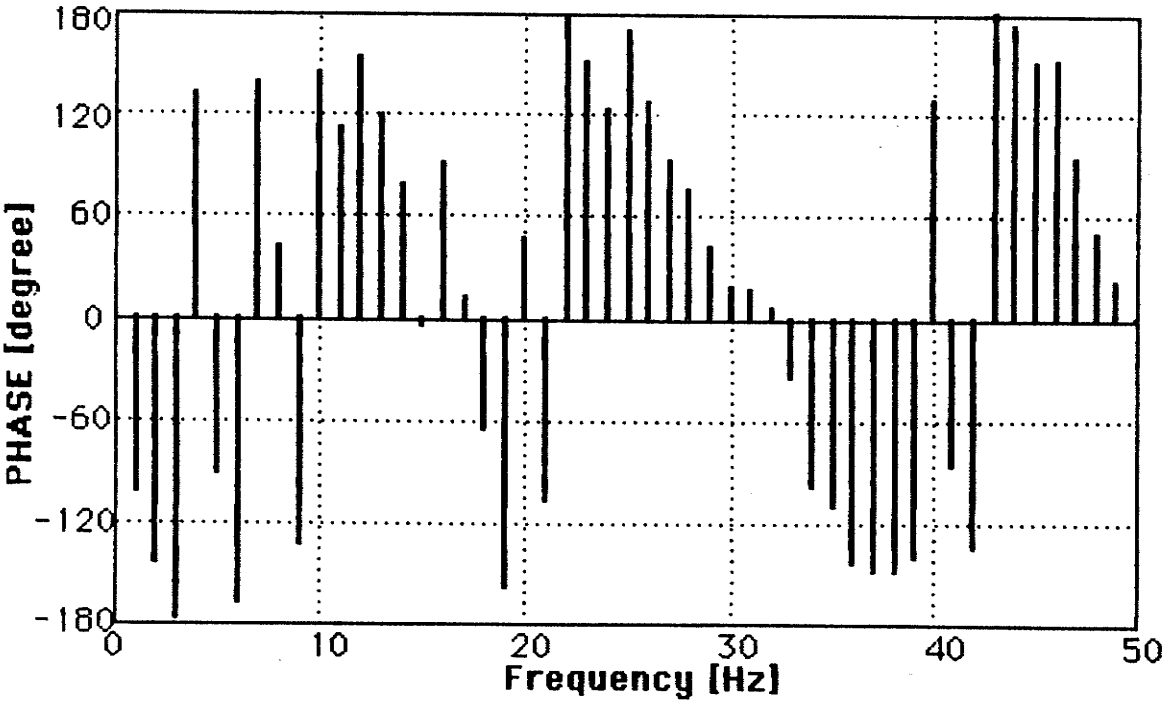

(b)

Fig. 3.1.8 Discrete Fourier transform of the ABPW in Fig. 3.1.7.

The input driving function of the CVS is the ABP waveform (ABPW). Based on the recording within 5 cm of the top of the aortic arch in a human subject [ReWo56], the ABPW has been derived [Jul184a] using polynomial regression featuring typical systole/diastole ratio 140/80 mmHg, systolic portion 0.33 sec, and duration of one cycle 1 sec. This waveform is shown in Fig. 3.1.7. In order to ease and standardize further study, both discrete Fourier magnitude and phase spectra are presented in Fig. 3.1.8. From the magnitude spectrum, it can be seen that (i) the ABPW contains high low frequency components and much lower frequency components after 20 Hz, (ii) the DC component gives the mean value of the ABP about 63 mmHg, and (iii) the oscillation of the magnitude reflects the sharp change in the ABPW, such as the transient between systolic and diastolic portions. The phase of the ABP components oscillates very much in the phase spectrum, which indicates high sensitivity of phase spectrum to its waveform.

Although the CVS model itself is a linear model, questions about its linearity and stability still hold as we use a numerical method for solving the system equations. Any numerical iterative method may produce accumulative error that could introduce nonlinearity and instability. Accuracy of the numerical method is also to be evaluated.

Eigenvalues of matrix A in Eq. 3.1.7 determines characteristics of the system. They were evaluated using a published computer software package for the 22nd degree model and listed in the Table 3.1.4. Furthermore, the step response of a system characterizes the system performance so that the accuracy and stability of a system can be analysed using step response and confirmed by the system eigenvalues. Step input of ABP from 0 to 140 mmHg

Table 3.1.4 Eigenvalues of matrix A for the 22nd degree CVS model.

i	λ_i
1	- 5085.59 + j 0.00
2	- 1695.18 + j 0.00
3	- 1695.17 + j 0.00
4	- 52.00 + j 0.00
5	- 15.21 + j 0.00
6	- 19.34 + j 0.00
7,8	- 16.85 ± j 237.41
9,10	- 5.03 ± j 203.09
11,12	-2.27 ± j 182.71
13,14	- 6.90 ± j 136.84
15,16	- 3.38 ± j 122.82
17,18	- 3.09 ± j 115.89
*19,20	- 0.91 ± j 77.70
*21,22	- 1.96 ± j 28.50

The asterisks denote the fundamental eigenvalues.

Table 3.1.5 Eigenvalues of matrix A for the 14th degree CVS model.

i	λ_i
1	- 1590.93 + j 0.00
2	- 1753.00 + j 0.00
3	- 11.80 + j 0.00
4	- 16.20 + j 0.00
5,6	- 4.58 ± j 156.56
7,8	- 4.58 ± j 111.79
9,10	- 1.03 ± j 105.13
*11,12	- 0.76 ± j 73.33
*13,14	- 1.94 ± j 28.91

The asterisks denote the fundamental eigenvalues.

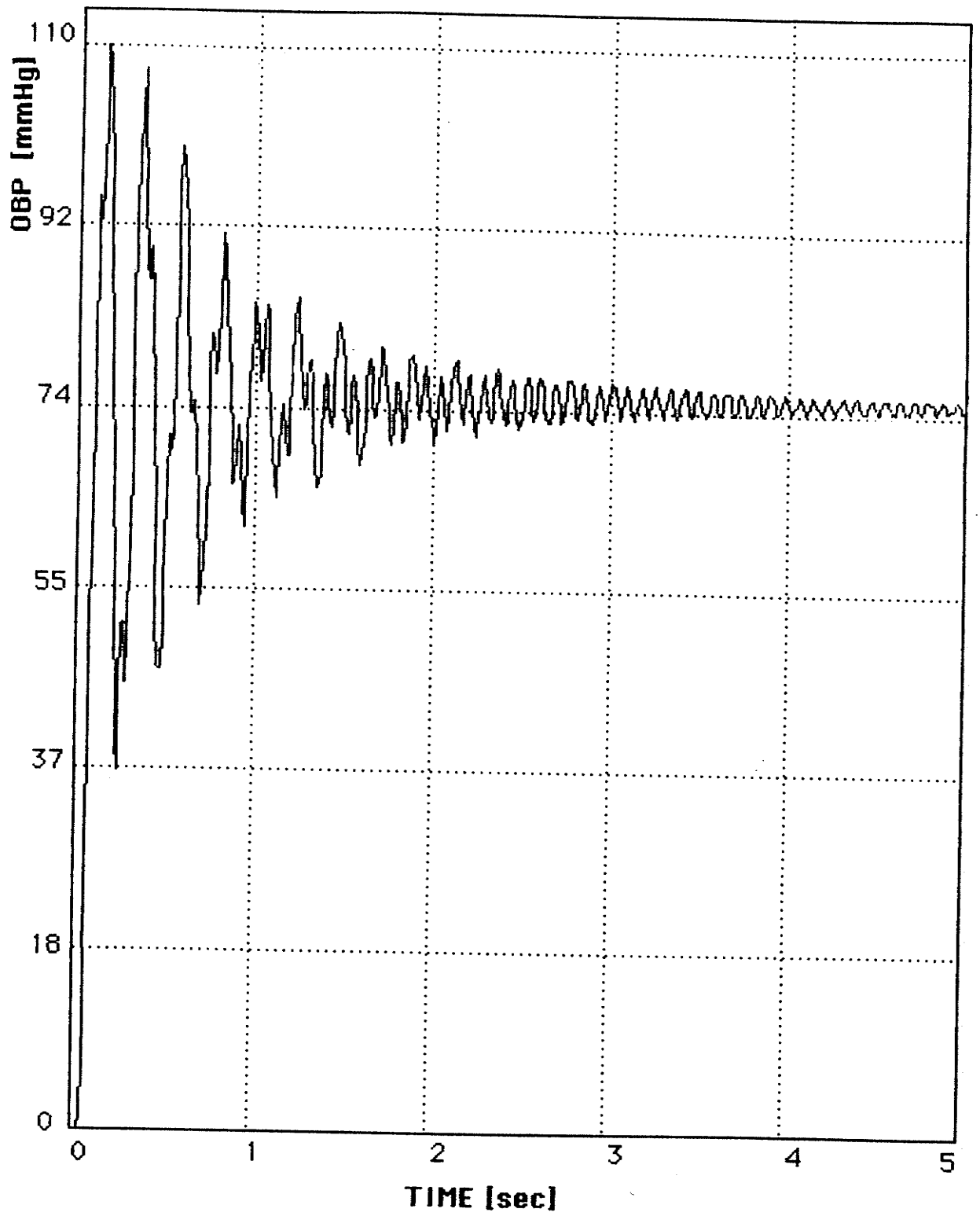

Fig. 3.1.9. Step response of the 22nd degree CVS model.

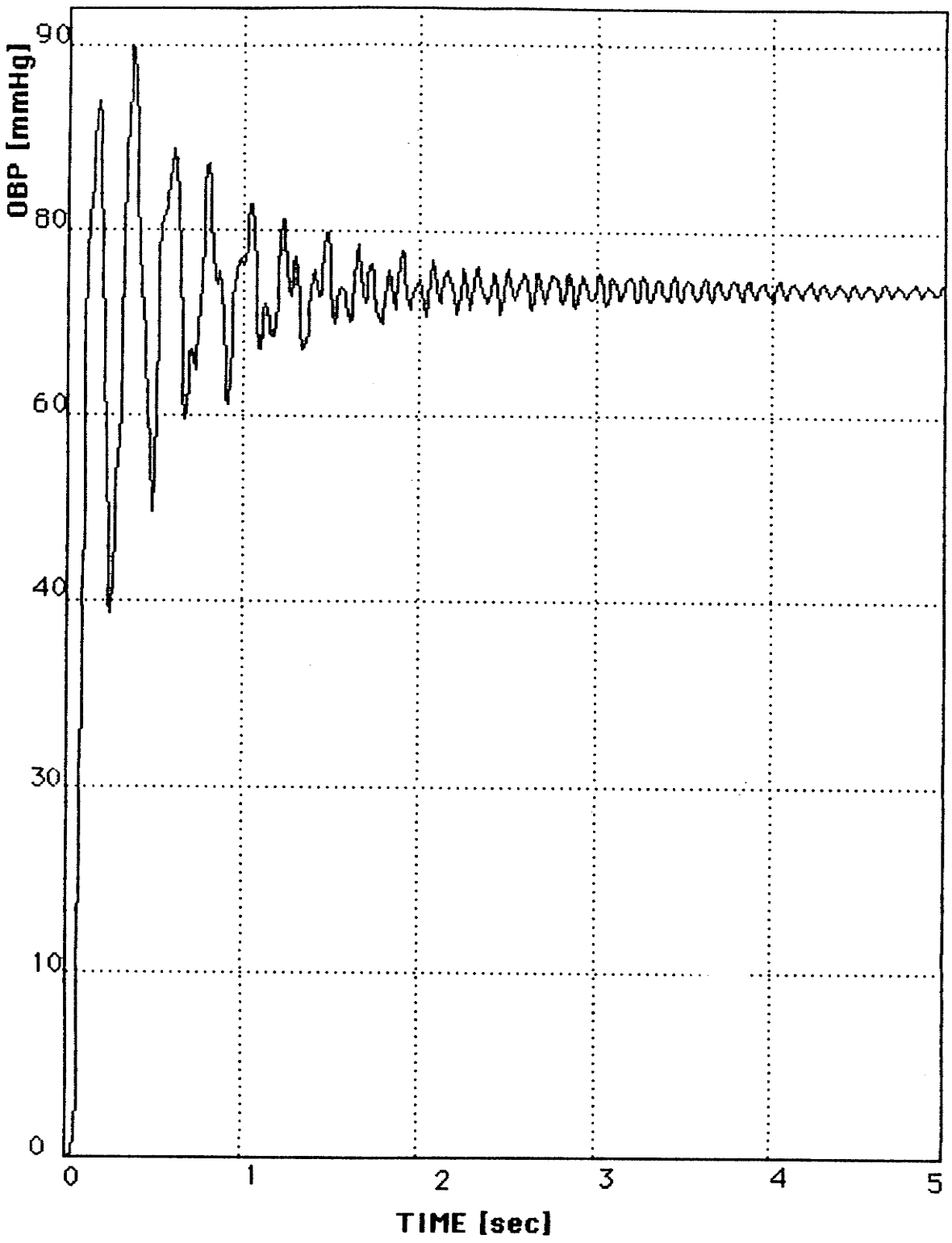

Fig. 3.1.10. Step response of the 14th degree CVS model.

was used to calculate the step response waveform of OBP, which is plotted in Fig. 3.1.9. From this waveform, we can see that after 5 seconds it converges to a steady state of 75 mmHg level with difference of less than 1 mmHg. This level of OBP is consistent as predicted in calculating the resistance bed. It is therefore concluded that the system is stable to sufficient accuracy with the implemented numerical solution. Frequency spectral change of step response can be confirmed by analyzing the system eigenvalues. The negative real parts of the eigenvalues explain the step response being a predominantly damped sinusoid. The fundamental frequency of this sinusoid can be traced to the eigenvalues with lowest imaginary values (equal to $2\pi f$) and least real part values (dominant factor). These eigenvalues are $\lambda 19$ to $\lambda 22$ in the Table 3.1.4 which indicate the step response will first show the sinusoid with the fundamental frequency of about 5 Hz, and then move to the frequency of about 10 Hz because the network experiences the least energy loss at about the 10 Hz frequency point. These features are fully shown in Fig. 3.1.9.

In order to ease the further study of the CVS, the 22nd degree model was simplified to the 14th degree model. With this simplification we expect that Fundamental spectral content of this network is still held. Sensitivity of the network to degrees of the model can be examined by difference of the step responses, eigenvalues, and OBPWs. The step response for the simplified model, (in Fig. 3.1.10) shows also a damped sinusoid with a similar set of features as in Fig. 3.1.9 for the 22nd degree model except that it is damped faster and has weaker fluctuation around the level 75 mmHg. These similarities and differences can also be seen from the eigenvalues in Table 3.1.4 and Table 3.1.5. The fundamental eigenvalues in two tables are

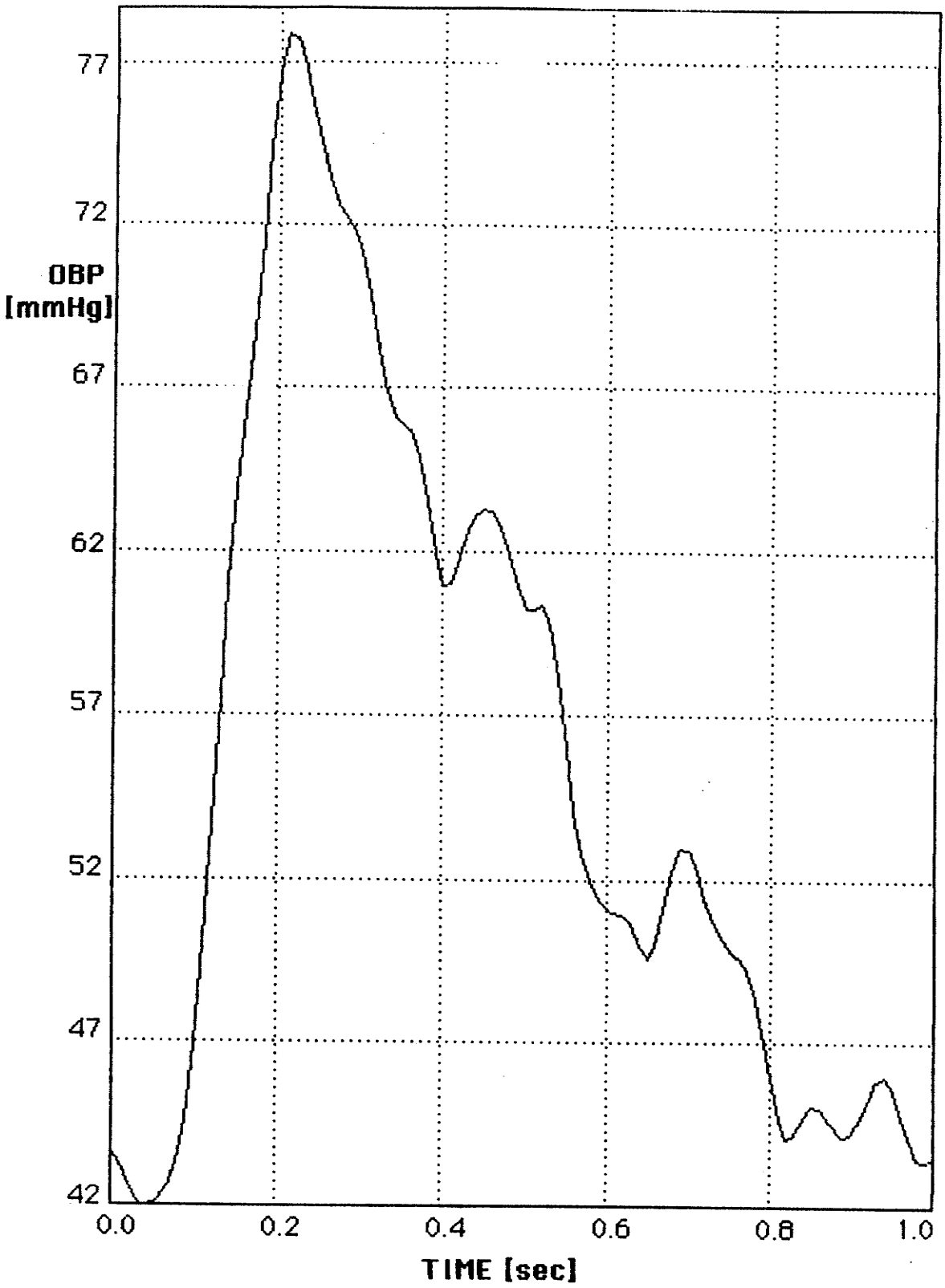

Fig. 3.1.11. The ocular blood pressure (OBPW) for the 22 nd degree CVS model with input shown in Fig. 3.1.7.

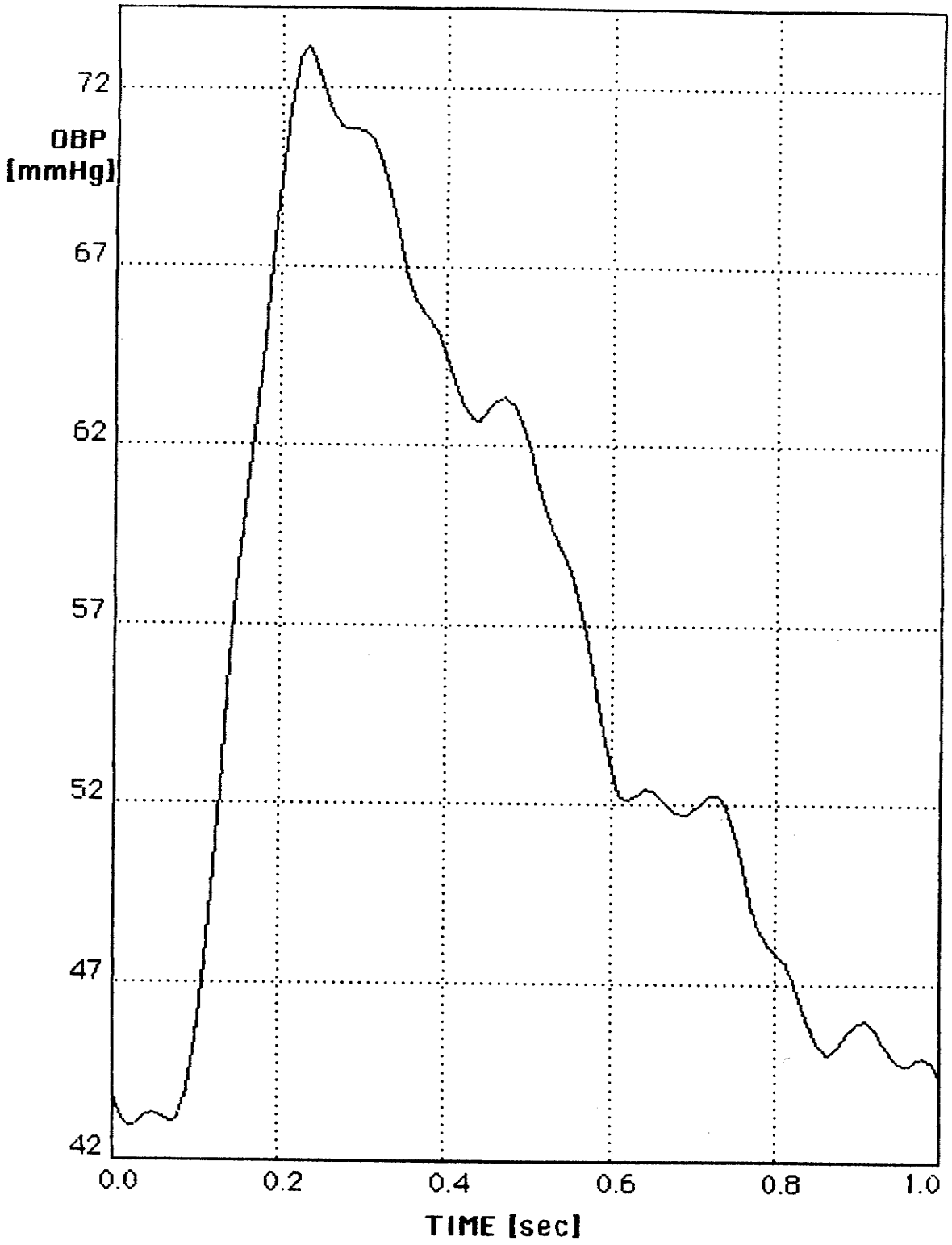

Fig. 3.1.12. The ocular blood pressure (OBPW) for the 14th degree CVS model with input shown in Fig. 3.1.7.

similar and Table 3.1.4 exhibits more eigenvalues standing for higher spectral content.

With the ABP in Fig. 3.1.7 applied to the CVS models, the associated outputs, the OBPWs at choroid, were achieved by solving the state equations for the 22nd degree and the 14th degree models and are shown in Fig. 3.1.11 and Fig. 3.1.12 respectively. The OBP amplitude is consistent with the result reported in [Adle65]. Appearance of these two waveforms is very much similar except more notchings occurred along the slope in Fig. 3.1.11, indicating higher frequency content. Their spectra are also presented in Fig. 3.1.13 and 3.1.14. These waveforms contribute to seeking the relationship between ABP and OBP, exhibit how the ABP is changed in the propagation through the CVS to the OBP at the choroidal periphery. The OBPW (can be assumed now as a approximation of ocular pulse) showed a much more complicated pattern than Fig. 2.1 in which Best classified the waveform with parameters such as pulse delay, crest time, anacrotic and catacrotic slopes. The reason for this is not only the rabbits that were used in his test instead of man, but the measuring method itself that has been discussed in Chapter II. Much more notching appeared along the catacrotic slope in Fig 3.1.11 and 3.1.12. The few features of ocular pulse will no longer be sufficient to describe this waveform. Therefore the graphic analysis method may not apply to the real human subject test. The spectral analysis is expected to be an effective method. Nevertheless, the general trend of the OBPW seems similar with Fig. 2.1 so that the amplitude and variation reduction rates of OBP with stenosis may be compared with his results.

The magnitude spectra in Fig. 3.1.13a and 3.1.14a are similar. The high

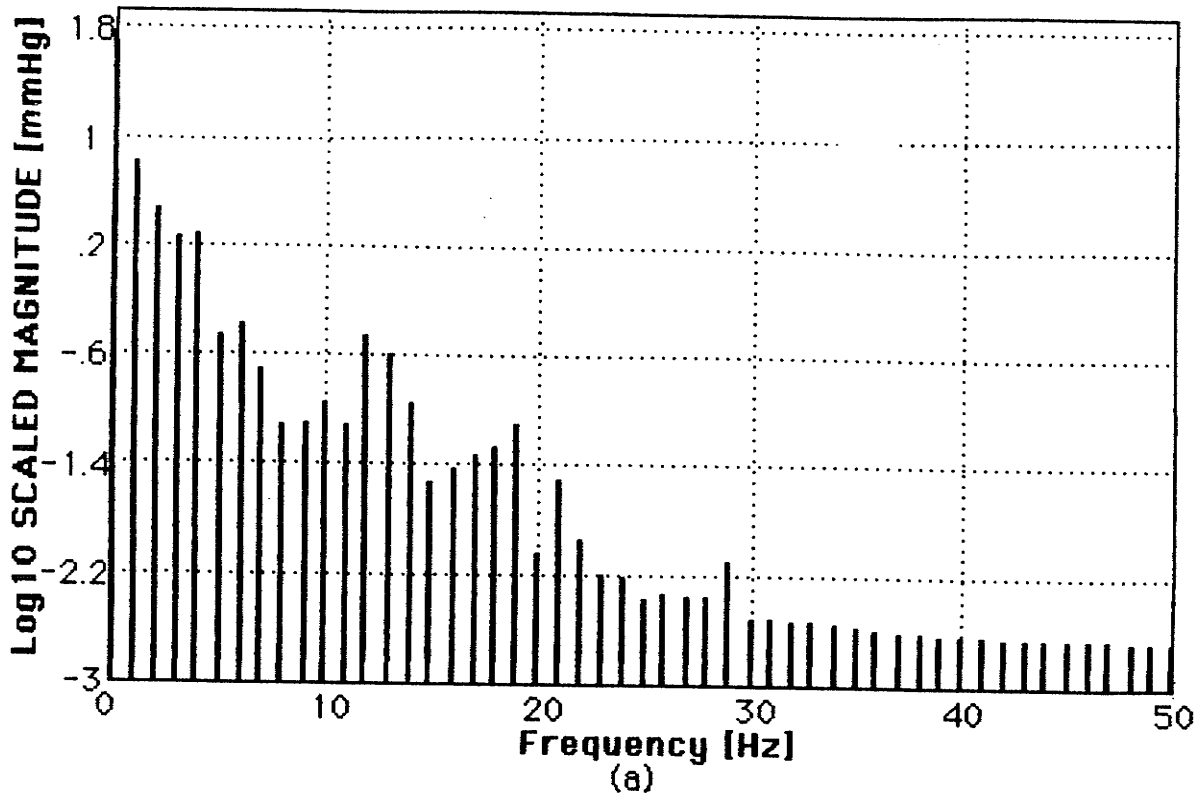

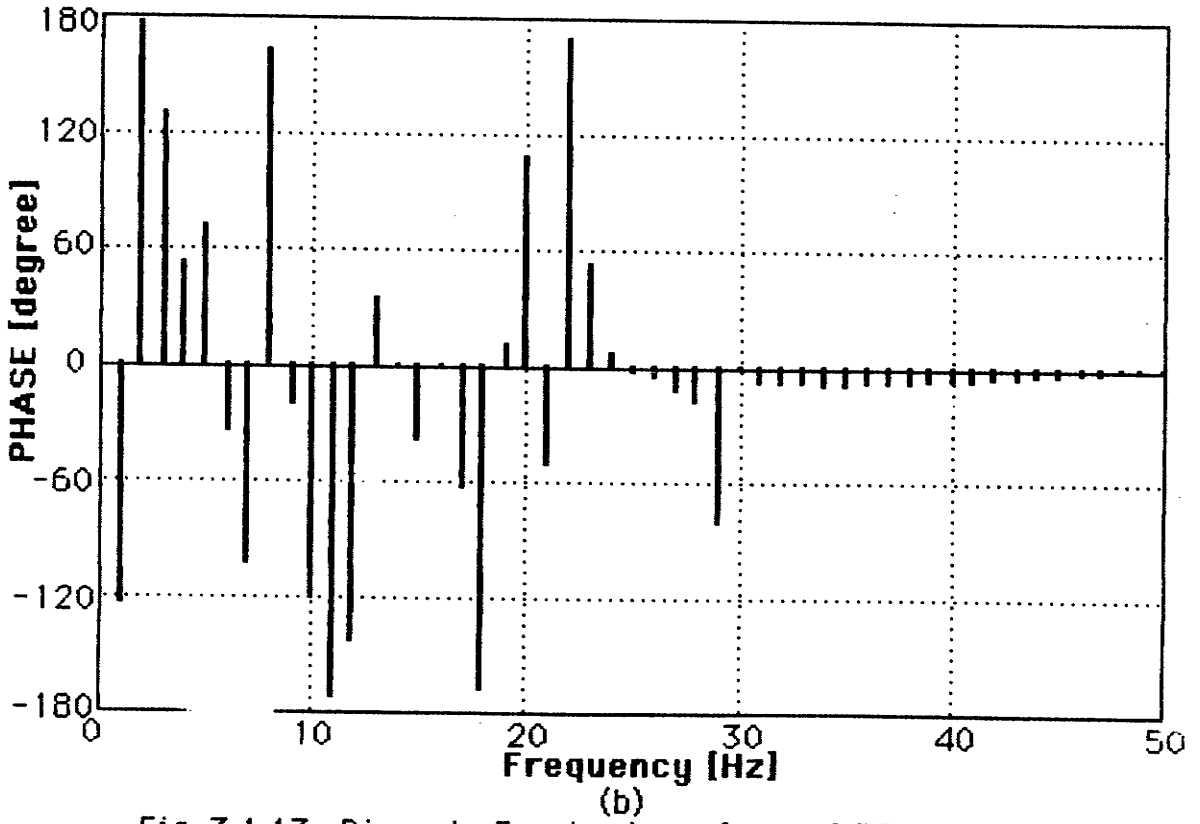

Fig. 3.1.13. Discrete Fourier transform of OBP in Fig. 3.1.11. (the 22nd degree model)

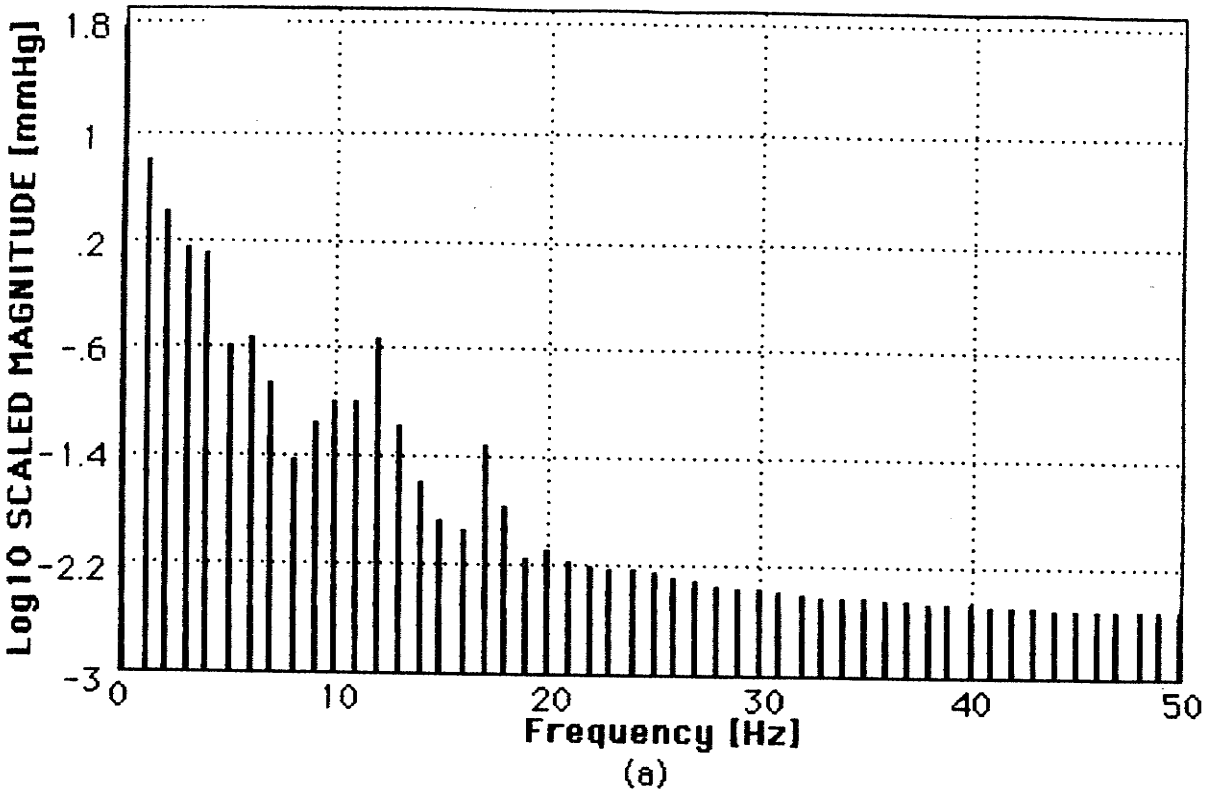

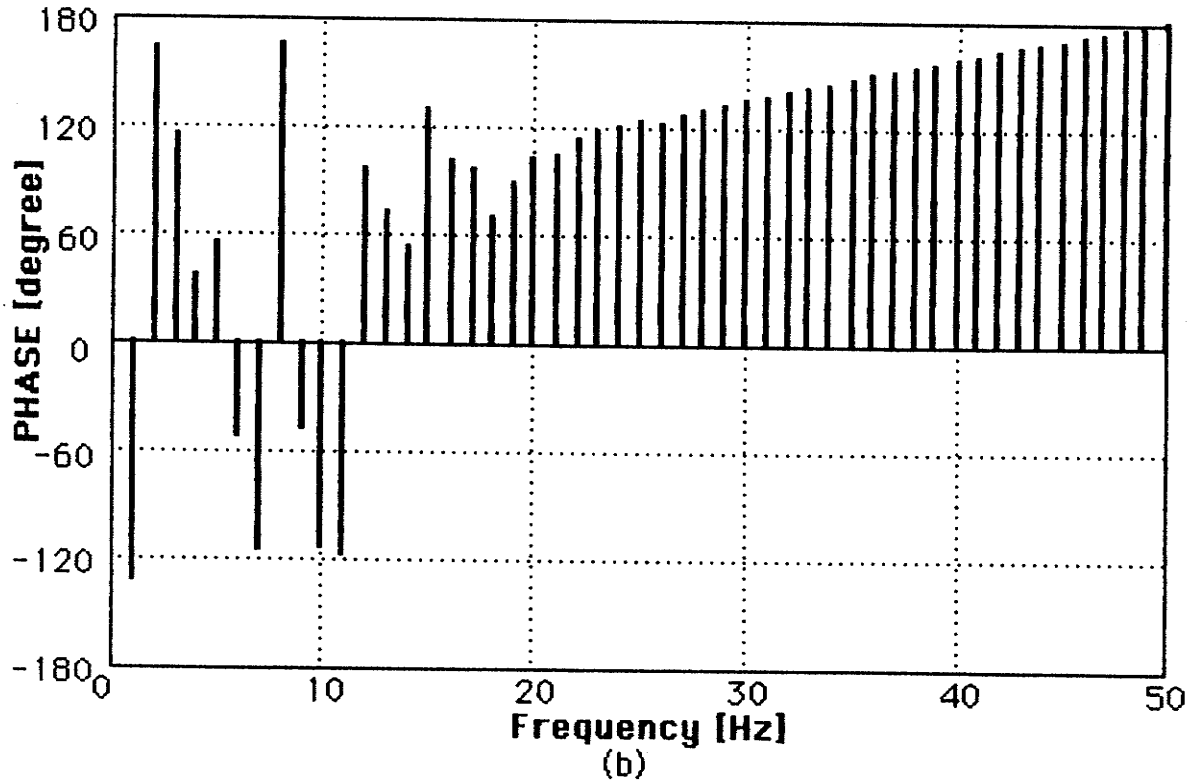

Fig. 3.1.14. Discrete Fourier transform of OBP in Fig. 3.1.12. (the 14th degree model)

frequency components (after 20 Hz) are reduced as the RLC network of the CVS model can be considered as a low-pass filter. The frequency components around 5 and 10 Hz (4, 10, 12 Hz for the 22nd degree model, 4, 11, 12 Hz for the 14th degree model) is enhanced, comparing with their adjacent components. This is because the system fundamental frequency are 5 and 10 Hz as discussed earlier.

In order to compare the difference between the two OBPWs, spectral difference of the two waveforms is displayed in Fig. 3.1.15. All of spectral magnitude differences are less than 1 and gradually fall to the negative 3rd order. This difference is small compared with their spectrum magnitude in Fig. 3.1.13a and 3.1.14a. It can also be spotted that the smaller spectral difference in the spectral band around 10 Hz and higher difference in the spectral range between 10 Hz and 20 Hz as we expected that the 22nd degree model contains higher spectral content. Phase spectra in Fig. 3.1.13b and 3.1.14b are very different due to its high sensitivity to waveforms. Since we have already known from the eigenvalue analysis that spectral magnitude attenuation after 10 Hz is much higher as seen in Fig. 3.1.13a and 3.1.14a, it can be concluded that the simplified CVS model contains most of fundamental spectral content, and can be implemented for the further study of the CVS.

It has been addressed that numerical error can introduce nonlinearities to the system. In order to prove the linearity of the CVS models, Fig 3.1.16 shows spectral magnitude transfer function from the ABP (Fig. 3.1.8) to OBP (Fig. 3.1.13). This spectral transfer function exhibits the network worked as low pass filter with relative smaller attenuation (concerning the original two magnitudes) at the frequency of about 5 HZ and 10 Hz. This is consistent

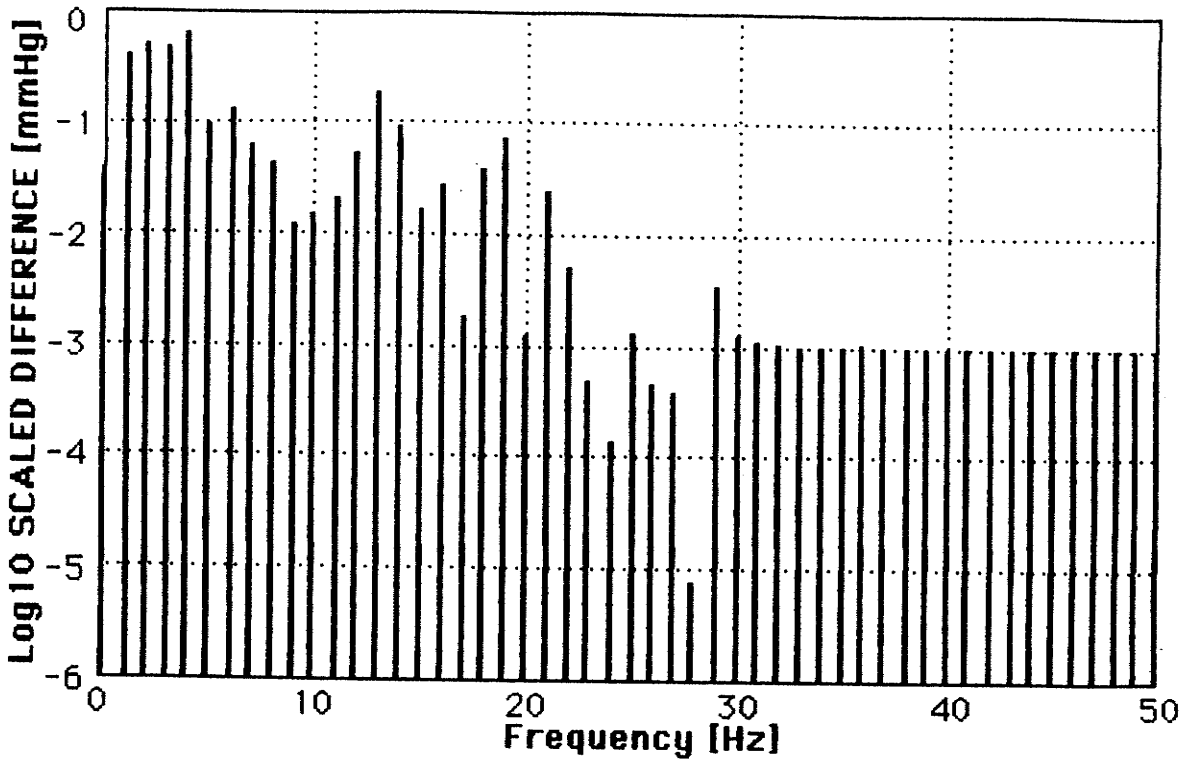

Fig. 3.1.15. Absolute difference between spectrum magnitude values in Fig. 3.1.13a and Fig. 3.1.14a.

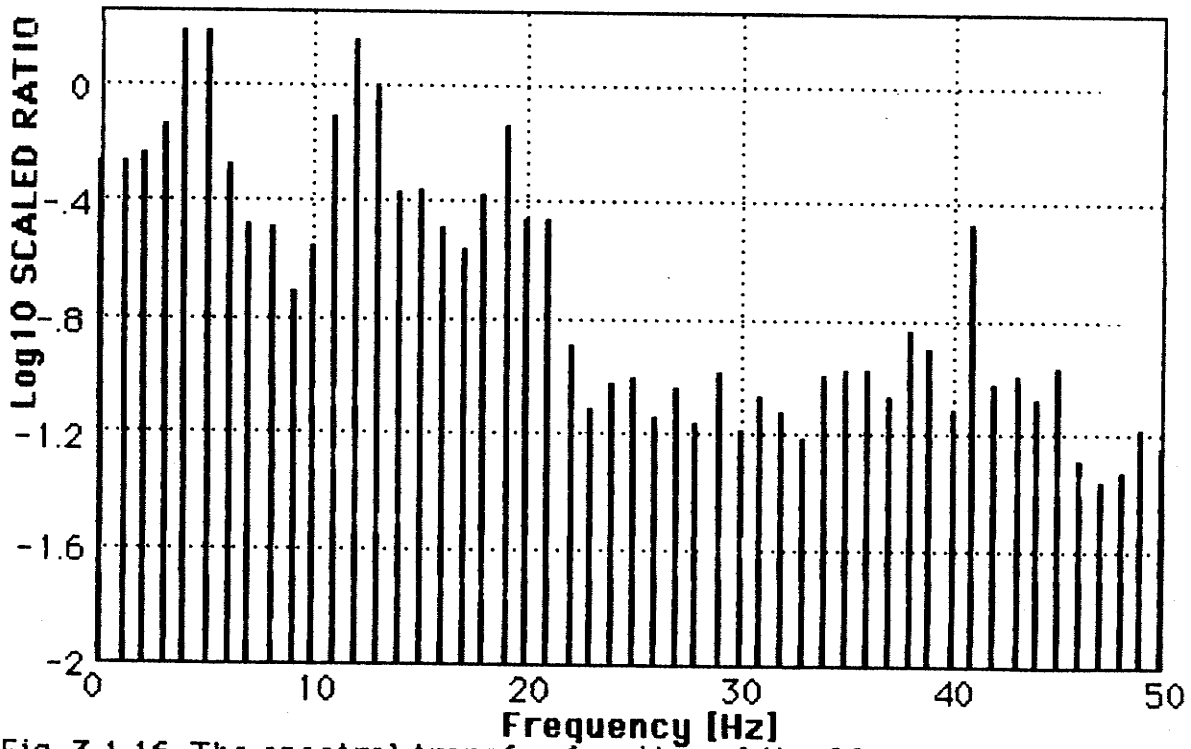

Fig. 3.1.16. The spectral transfer function of the 22nd degree CVS model. (Ratio of magnitude values in Fig. 3.1.13a to those in Fig. 3.1.8a)

with the result of the eigenvalue analysis. Linear transfer impedance from ABP to OBP has also been calculated for each frequency component. Absolute difference between the transfer impedance and its numerically obtained counterpart (Fig. 3.1.16) is 0.078 for each frequency component below 20 Hz (20 Harmonics). This small difference indicates that no new spectral content was introduced in the network, linearity is preserved under the present numerical method. The impedance magnitude calculated fell below the negative 2th order smaller than the normal value after 20 Hz and, for all the spectra shown above, magnitudes for higher frequency band after 20 Hz are all decreased to below the negative 2th order. Therefore frequency component after 20 harmonics is not considered significant and not valid for use. Our later frequency domain analysis will remain below 20 harmonics.

3.1.6 Summary

A model of the human CVS was developed. This model shows special features of specificity for OBP study and flexibility for system modification and inclusion with the two disease conditioned models. It has been evaluated that the method for developing this CVS model results in a linear, stable CVS network, accurately performing the function of CVS in the human subject. The simplified version of the CVS model was also derived and chosen as the model to be implemented for further study of the CVS. ABPW and OBPW resulted from the computer simulation method have shown a new and more complicated pattern of their relationship than the previously published result. These waveforms and their spectra give a standard for further study. By adding the eye model to the CVS model, it will give the better exhibition of the ocular pulse waveform (OPW) and effects of the elevated IOP. With the

stenosis model integrated into certain segment of the CVS, we will be able to study the sensitivity of the ocular pulse to the different presence of stenosis in the CVS. The characteristic spectral feature of the OPW can be used to screen the stenosis and the elevated IOP.

3.2 The Model of Stenosis

Stenosis was modelled based on the experimental data in the vitro study [YoTs73]. Stenosis is essentially referred to a local narrowing (a constriction or occlusion) in the blood vessel. The arterial stenosis is caused by the accumulation of fats or calcified deposits on the interior surface of the arteries. These deposits or plaques can break away from the arterial wall and flow through the blood stream, which may cause sudden acute effects [LaSe86]. The stenosis can be possibly combined with the arterial spasm, which may elevate the stenosis level uncertainly, leading to stroke. The model features the characteristic dynamics that stenosis performs in causing the pressure drop over the constriction. The pressure drop is determined by the haemodynamic and geometric condition with the stenosis. This model can be modified and integrated into the CVS model to study the stenosis effect.

3.2.1 Description of the Stenosis Model

Stenosis existing in the artery can be considered as a nonlinear resistance which causes pressure drop due to blood viscosity for low Reynolds number, turbulent losses for high Reynolds number, and inertial losses to account for the pulsatile nature of the blood flow. Quantitative description of this pressure drop also involves the geometric parameters of the vessel constriction. However, a small number of the geometric

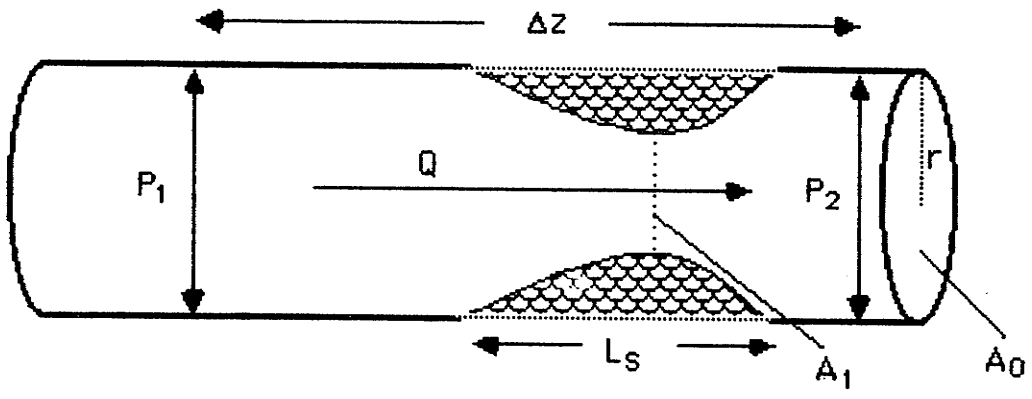

Fig. 3.2.1. Geometric configuration for stenosis.
[After [Kins87]]

parameters can be sufficient to feature the stenosis performance [YoCR75]. In this study, the symmetrical stenosis configuration was considered, which is shown in Fig. 3.2.1. The figure shows the constriction in the blood vessel and definition of geometric parameters.

The pressure drop over the stenosis can be composed as

$$\Delta P_S = \Delta P_v + \Delta P_t + \Delta P_i \tag{3.2.1a}$$

$$\Delta P_v = \frac{K_v \rho U^2}{Re} \tag{3.2.1b}$$

$$\Delta P_t = \frac{1}{2} K_t \rho U^2 \left(\frac{A_0}{A_1} - 1\right)^2 \tag{3.2.1c}$$

$$\Delta P_i = K_i \rho L_S \frac{dU}{dt} \tag{3.2.1d}$$

where R_e is the Reynolds number, ρ is the fluid density, L_S is length of the stenosis, A_0/A_1 is the ratio of the area of the unobstructed tube to the area of constriction. K_v, K_t, K_i are coefficients determined by the constriction geometry, U is the blood velocity. Three terms in Eq. 3.2.1 account for the viscous, the turbulent and the inertial losses respectively. The ratio A_0/A_1 are used to describe the severity of the stenosis. 10 levels of stenosis severity are classified from 0% to 90% of the area reduction due to the constriction.

Considering $U=Q/A_0$ and $R_e=2\rho Ur/\mu$ where Q is blood flow, μ is the blood

viscosity, and r is the radius of the unobstructed vessel. ΔP_s can be expressed in another form

$$\Delta P_s = \frac{K_v \mu}{2\pi r^3} Q + \frac{1}{2} K_t \frac{\rho}{\pi^2 r^4} \left(\frac{A_0}{A_1} - 1\right)^2 Q^2 + K_i \rho \frac{L_s}{\pi r^2} \frac{dQ}{dt} \qquad (3.2.2)$$

From Eq. 3.2.2, we can see that stenosis can be treated as a flow controlled nonlinear resistance which is expressed as

$$Rs = \frac{\Delta Ps}{Q} \qquad (3.2.3)$$

3.2.2 Integration and Displacement of the Stenosis in the CVS

Several studies [ZaGB83, BhMG82] have concluded that transitions in the artery wall configuration such as bends and bifurcation, which are associated with local modifications in rate and pattern of blood flow, are predisposed to the development of arteriosclerosis plaques. The carotid bifurcation and its associated carotid sinus is particularly subject to deposits. It has also been found that the stenosis occurred in the carotid sinus in 75 percent of the examined pathological cases. It is therefore reasonable to take the first choice to integrate the stenosis at such a location. This location corresponds to segment 8 in the CVS model. More emphasis will put on study of stenosis in this location.

Since flow Q is a state variable included in the state equations of the CVS model, this resistance can be integrated in series with the resistance R_i in the ith segment of the CVS model. Then, R_i should be modified as

$$R_i^* = R_i - R_{S0\%} \qquad (3.2.4)$$

where $R_{S0\%}$ is 0% stenosis resistance. Then, the new modified total resistance of the segment, where the stenosis is located, will be

$$R_{new} = R_i^* + R_S \qquad (3.2.5)$$

By replacing the resistance R_i with the R_{new}, we can simulate the performance of stenosis in the CVS with 10 levels of severity in different segment locations. The effect of stenosis will be reflected in the peripheral observation. In this case, we examine the ocular blood pressure (OBP). With addition of the eye model, which will be discussed in the next section, the stenosis with severity levels and locations can be screened from the ocular pulse.

In the stenosis model, coefficients K_v and K_t are determined by the geometry of stenosis. However, as stated in [YoCR75], these coefficients are primarily dependent on the limited number of basic geometrical characteristics, such as stenosis length and percent stenosis. Therefore, it may be possible to estimate K_v and K_t from a relatively small number of geometrical parameters which could be obtained in clinical situations. In this study, we chose the symmetrical pattern of stenosis. K_v is strongly dependent on the percent stenosis and length radius ratio L_S/r. K_t is much less dependent on the geometry of stenosis and falls into the range of 1.0-2.31. The value of K_i does not vary with stenosis, and is chosen to be 1.2 which has the best fit with empirical data.

K_v can be modified by the rule that 0% stenosis formula reverts to be a linear resistance as expressed in the CVS model. So, the relationship between K_v (i.e., coefficient of the linear term) and geometry parameter can

Table 3.2.1 Coefficients of stenosis in segment 8 of the CVS.

% Stenosis	K_v	K_t	K_j
0	113	0.0	0.0
10	120	1.07	1.2
20	126	1.21	1.2
30	142	1.35	1.2
40	157	1.49	1.2
50	177	1.63	1.2
60	228	1.76	1.2
70	346	1.9	1.2
80	566	2.04	1.2
90	1456	2.18	1.2

Table 3.2.2 Three index numbers of the stenosis in segment 8 of the CVS.

% Stenosis	I_v	I_t	I_j
0	0.31E-1	0.00E00	0.00E00
10	0.34E-1	0.66E-2	0.14E-1
20	0.36E-1	0.38E-1	0.15E-1
30	0.42E-1	0.12E00	0.15E-1
40	0.49E-1	0.33E00	0.17E-1
50	0.62E-1	0.82E00	0.19E-1
60	0.96E-1	0.20E01	0.25E-1
70	0.19E00	0.52E01	0.35E-1
80	0.49E00	0.16E02	0.58E-1
90	0.27E01	0.88E02	0.14E00

be deduced as

$$R_{so\%} = \frac{K_{v0}\,\mu}{2\pi r^3} \tag{3.2.6a}$$

$$R = \frac{8l\mu\, L_s}{8\pi r^4} \tag{3.2.6b}$$

$$R_{so\%} = R \tag{3.2.6c}$$

So,

$$K_{v0} = \frac{8lL_s}{4r} \tag{3.2.6d}$$

where K_{v0} is the K_v coefficient for 0% stenosis, and is used to modify the value of K_v for a given level of stenosis in the CVS model. Based on the result reported in [YoCR75], the modified K_v, K_t, K_i values for stenosis located in segment 8 of the CVS are listed in Table 3.2.1 with L_s = 1 cm and r = 0.18 cm.

3.2.3 Three Term Index Numbers of the Stenosis Model

In order to evaluate effects of stenosis from its three different terms of the model, we can rewrite Eq. 3.2.1 as

$$\frac{\Delta P_s}{\rho U_p^2} = \frac{K_v}{R_{ep}} U_m + \frac{1}{2} K_t \left(\frac{A_0}{A_1} - 1\right)^2 U_m^2 + \frac{K_i L_s A_p}{U_p^2} \frac{d}{dt}\left(\frac{U}{A_p}\right) \tag{3.2.7}$$

where U_p is the peak velocity, U_m=U/U_p, A_p is the peak value of flow acceleration dU/dt. The U_m and U/A_p can only vary within the range of less than 1. R_{ep} is the peak Reynolds number. Thus, the relative importance of the three terms can be analyzed through the three coefficients referred as three

index numbers, which are

$$I_v = \frac{K_v}{R_{ep}} \tag{3.2.8a}$$

$$I_t = \frac{1}{2} K_t \left(\frac{A_0}{A_1} - 1\right)^2 \tag{3.2.8b}$$

$$I_i = \frac{K_i L_s A_p}{U_p^2} \tag{3.2.8c}$$

Three index numbers reflect effects from viscosity for small Reynolds number, turbulence for large Reynolds number, and inertia for highly accelerated flow. With the stenosis induced in segment 8 of the CVS, three index numbers are calculated by Eq. 3.2.8. Table 3.2.2 lists the result of these index numbers changed with the stenosis varying from 10% to 90%. The viscous and nonlinear turbulence terms increase with the increasing severity of stenosis, whereas the latter increases much faster, and becomes dominant for over 20% stenosis. The viscous effect of the stenosis is specially important at lower levels of stenosis. The inertial effect is found to be relatively small and constant. The result in Table 3.2.2 accords with that in [YoTs73b]. These three terms of stenosis, especially the non-linear term, will certainly introduce new frequency components into the system, which established a basic clue for screening the stenosis from the ocular pulse.

3.2.4 OBP Waveforms (OBPWs) With 10 Level Stenosis

As described above, the stenosis with 10 level severity can be integrated in the CVS so that the OBP can be observed from the output of the CVS as a function of the stenosis changes. Here, the stenosis in segment 8 of the 14th

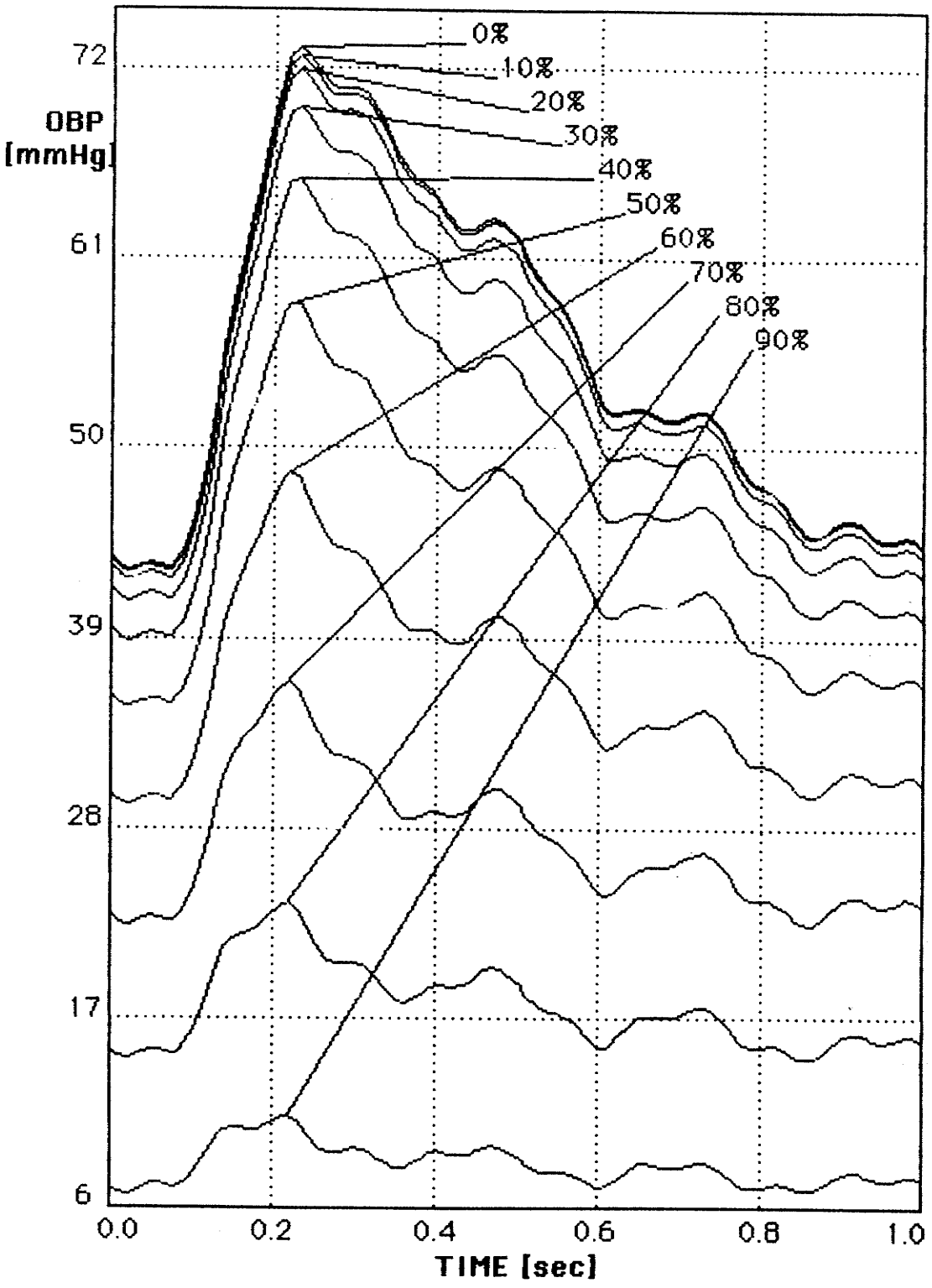

Fig. 3.2.2. OBPWs as a function of stenosis severity in segment 8 of the CVS.

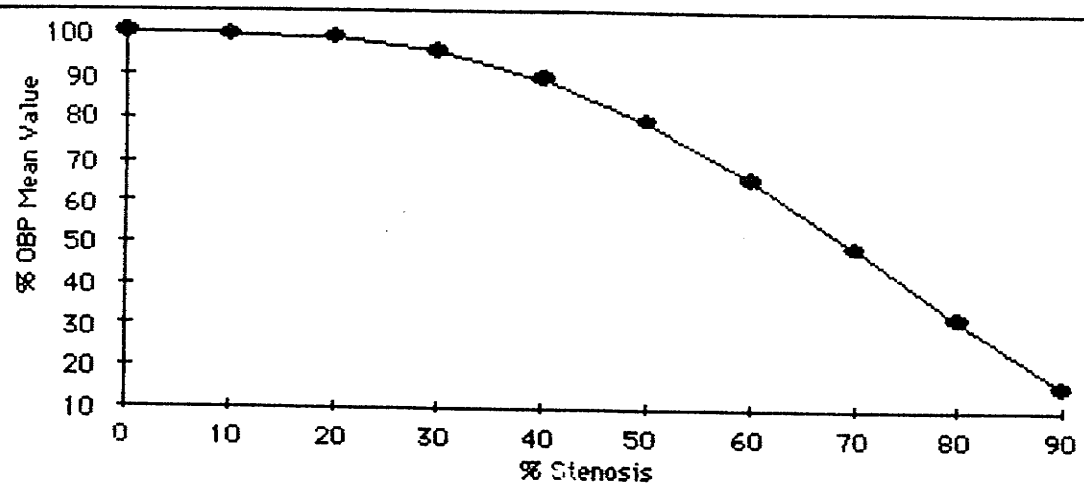

Fig. 3.2.3 Percent OBP mean values as a function of stenosis in segment 8 of the CVS.

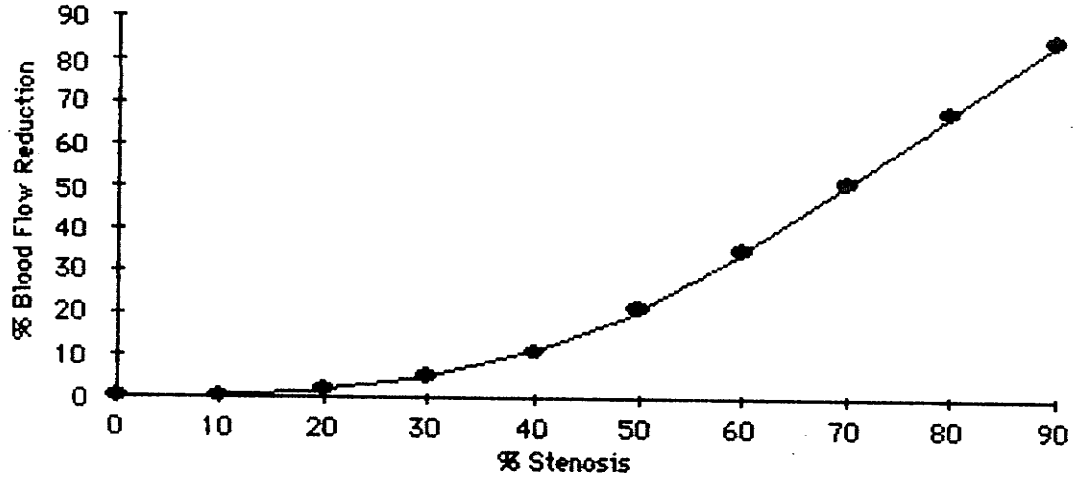

Fig. 3.2.4. Percent mean value reduction of stenosis blood flow in segment 8 of the CVS.

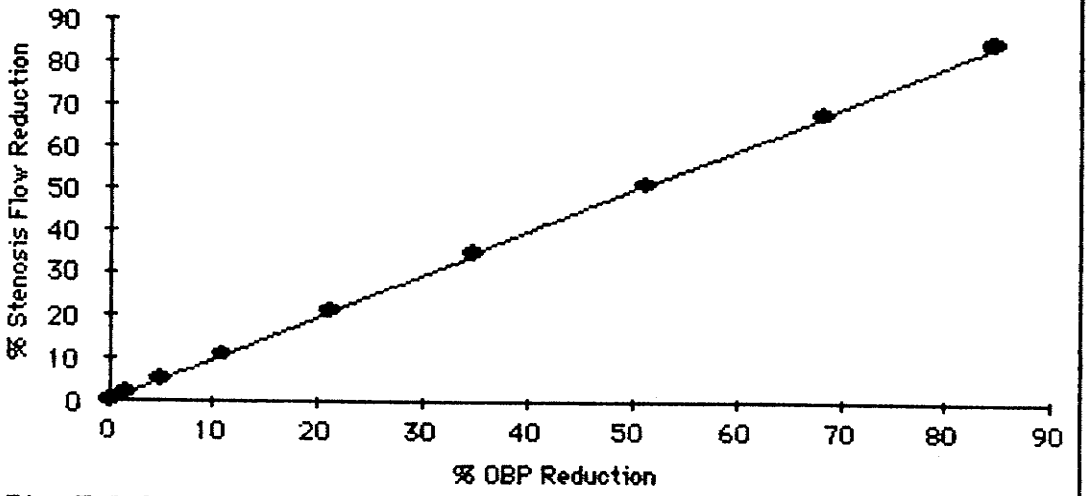

Fig. 3.2.5. Relationship between mean value reductions of OBP and stenosis blood flow in segment 8 of the CVS.

degree CVS model with 10 level severity progression is first considered. The input function (ABP) of the CVS remains to be the one in Fig. 3.1.7. The result in Fig. 3.2.2 clearly shows the OBPWs as a function of the stenosis severity. The amplitude and variation part of the OBP is attenuated as the stenosis severity increases. Still, as discussed last chapter, the OBPWs display a much more complicated pattern than the ones examined in Best's results [Best71c]. It is notable that with the more complicated pattern, these OBPWs show the shape and phase change with the stenosis severity progression. The phase shift can be observed even with 10% stenosis while the ocular pulse waveform (OPW) in Best's result can only show the pronounced change for over 50% stenosis due to the contact measuring technique. Simple graphic analysis will not be strong enough to be applied to the complicated OBPW and OPW. However, the observation of the spectral content change in the OBPW with the increased stenosis severity will trigger the study on the OBP and OPW in frequency spectral domain with higher sensitivity.

In order to give a clear pattern on how the OBP amplitude is decreased with the stenosis severity progression, the mean values of the OBP in Fig. 3.2.2 is plotted in Fig. 3.2.3 as a function of the stenosis severity levels. The mean value for each OBPW is expressed as a percentage against the OBP mean value for 0% stenosis. The mean values of the OBP drop much faster with acute stenosis than with low stenosis. Similar effects also take place in stenosis blood flow as shown in Fig. 3.2.4, where reduction rate is calculated against the values for 0% stenosis. The relationship between stenosis blood flow and OBP mean values is plotted in Fig. 3.2.5, where each point corresponds to certain level of stenosis. It can be seen that stenosis blood flow reduction is transferred to the OBP reduction. The corresponding data

points in Fig. 3.2.3 and Fig. 3.2.4 are very close to the results reported in [Best71a, Best74].

3.2.5 Summary

Based on the previous model describing the pressure drop over the stenosis in the artery [YoTs73], a model for the study on stenosis located in the CVS was developed [Jull84a]. Modification of coefficients in the model for its integration algorithm and displacement along the CVS is studied in this section. Three index numbers describing the stenosis effect from three different terms are presented. The OBPWs as a function of 10 levels of stenosis severity are achieved after the stenosis model is integrated into the CVS. These waveforms show a new pattern of the OBP altered by the induced stenosis. The simulated results presented in this section are comparable with the previous published results.

3.3 The Model of the Eye

The human eye is a complex, autoregulatory, physiological system controlled by mechanical , biochemical and neurological factors so that the stability and normal function of the eye and regulation of intraocular pressure (IOP) can be maintained. Here, only the mechanical dynamics within the eye is considered, in which pressure-volume relationship plays the most important role. Vascular blood pressure together with IOP controls the blood volume in the eye, which is directly related to the intraocular blood flow, and also a major part of intraocular volume. Intraocular pressure and volume determine the mechanical property of the eye. All of these relationships can be compiled in a causal diagram [CoWe80] shown in Fig. 3.3.1. In this figure,

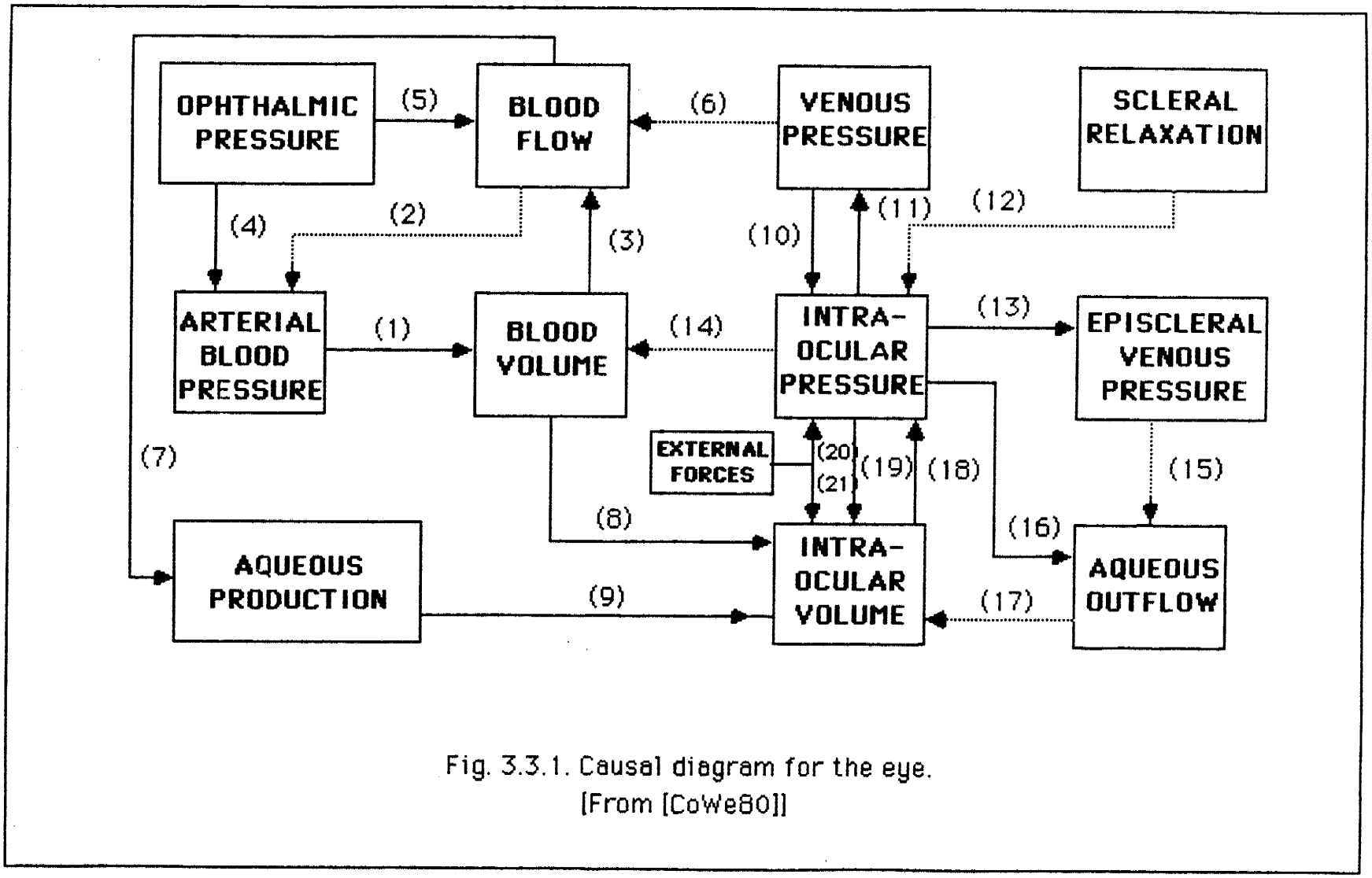

Fig. 3.3.1. Causal diagram for the eye.
[From [CoWe80]]

the arrows denote the direction of the causal relationship from cause to effect with solid lines denoting positive influence and dashed lines denoting negative influence.

In Fig. 3.3.1, the basic relationship (i.e., pressure–volume) in the eye's mechanism is well expressed, in which the homeostatic and autoregulatory nature of the eye can be seen by tracing the effects through the diagram. The blood volume is determined by the transmural pressure, i.e., difference between intraocular arterial pressure (1) and IOP (14). It is also a part of the total intraocular volume (8). The intraocular arterial (retinal or choroidal) pressure is obtained from the source, the ophthalmic artery pressure (4). Negative influence (2) by the blood flow indicates that it is the measurement of the intraocular arterial pressure drop. Blood flow is driven by the perfusion pressure, i.e. difference between ophthalmic pressure (5) and venous pressure (6). The resistance to the blood flow through the eye is primarily a function of the local radii of the blood vessels which is equivalently represented by the total blood volume in the eye. A higher blood volume means a lower resistance which in turn increases the blood flow (3) for a given perfusion pressure. Lower blood flow decreases the rate of aqueous production (7). Due to the poor distensibility of the veins, the venous pressure and intraocular pressure affects each other positively (10), (11). Part of the intraocular volume is determined by difference between production and outflow of the aqueous humour (9), (17). The difference between the intraocular and episcleral venous pressures drives the aqueous outflow (16), (15) as in (5), (6). The episcleral pressure is directly and positively influenced by the intraocular pressure (13). Intraocular pressure falls along with the scleral relaxation (12). Intraocular pressure and volume

affect each other positively (18), (19). A positive external force is also included in this diagram as it is used in some measurements like tonometry. But it will not be used if a non-contact method is implemented. This force is placed, could be in other places, to affect both intraocular pressure and volume (20), (21) as used in the experiment.

Quantitative formulation of these relations in Fig. 3.3.1 can be expressed in mathematical formulas which are derived based on the previous experimental data. The constant values are determined under certain conditions and would be subject to further refinement with new experimental findings.

3.3.1 Vascular Blood Circulation in the Eye

From Fig. 3.1.1, it can be seen that the internal carotid artery reaches the eye by the ophthalmic artery, (in cats and rabbits, the blood supply is from both the internal and the external carotid arteries [Adle65]). Man's eye comprises two separate circulatory system, retinal and uveal, both originated from the ophthalmic artery. The retinal system, formed from the central retinal artery, supplies the inner layers of the retina and is almost perfectly autoregulatory [Bill75]. The uveal (or choroidal) system, formed from the anterior and posterior ciliary arteries, supplies the outlayers of retina and the outer coats of the eye. It has also been found [Weit73] that the intraocular blood flow to the choroid is 40-70 times that to the retina. Therefore, the intraocular mechanical property is essentially due to ophthalmic arterial pressure derived from the internal carotid, and the intraocular arterial blood pressure ,Pa, or OBP as described in last chapter, can be assumed to be the ophthalmic arterial pressure. In this way, two

models, CVS and eye, are very well incorporated and stenosis in the CVS can be possibly screened from ocular pulse. This will be discussed further next.

The ocular blood flow is determined by two primary factors: the perfusion pressure and ocular vascular resistance. The perfusion pressure can be approximated with the transmural pressure due to the equality of the IOP to venous pressure [CoWe80]. The relation between flow and transmural pressure has been found [Best73] in cats as

$$Q = 0.0011\ (P_a - P_i) \tag{3.3.1}$$

where Q is uveal blood flow, P_a-P_i is transmural pressure, P_a is arterial pressure, P_i is IOP. According to this equation, blood flow is reduced with increased IOP, which indicates one of the feedback mechanism in the eye. This is left for further refinement of the model. Transmural pressure (P_a-P_i) should be positive in order to keep certain required mount of blood flow. This constitutes one of the principles governing the blood pressure in the eye, i.e., the arterial pressure always exceeds the IOP. The arterial pressure for stopping the blood flow is referred as the closing pressure.

It can also be seen that vascular resistance does not vary much and falls into the same order of values as the resistance bed in the CVS model. Concerning the resistance from P_i, values of the resistance bed in the CVS model should be higher. Previous results on blood pressure and volume relation have been studied in [CoWe80]. After comparing five different formulas with experimental data, a best fit is obtained as

$$\frac{1}{1-\alpha}\left[(P_{a2}-P_{i2})^{1-\alpha}-(P_{a1}-P_{i1})^{1-\alpha}\right]=K\alpha\ln\frac{V_{a2}}{V_{a1}} \qquad (3.3.2)$$

where V_a is the blood volume, subscripts "1" and "2" denote the initial and final states, $K\alpha$ is a constant related to the vascular vessel properties, and equal to 0.805 with $\alpha = 1.6$.

Vascular rigidity coefficient VR is defined [Best71a] as:

$$VR=\frac{\Delta\,(P_i-P_a)}{\Delta V_a}=\frac{\log\left[(P_{a2}-P_{i2})/(P_{a1}-P_{i1})\right]}{V_{a2}-V_{a1}} \qquad (3.3.3)$$

VR is a important measurement for the intraocular vascular circulation, and also implies that the vascular blood volume is decreased with the transmural pressure decreased.

3.3.2 Aqueous Humour Dynamics

The aqueous humour is a clear liquid (98.1% water) filling the anterior and posterior chambers of the eye. In addition to serving other functions for the cornea and lens, it plays a key role in maintaining the IOP. The relation between production of aqueous humour (S_p) and IOP can be expressed [CoWe80] as

$$S_p=C_p\,(P_c-P_i) \qquad (3.3.4)$$

where P_c is the cutoff pressure required to drive aqueous production, C_p is a constant.

Similarly with the blood flow, the aqueous outflow is proportional to the pressure drop between the anterior chamber and episcleral venous plexus, and expressed as

$$S_0 = C_f (P_i - P_v) \tag{3.3.5}$$

where P_v is episcleral venous pressure, which is also a function of IOP expressed as

$$P_v = c P_i + d \tag{3.3.6}$$

where c, d are constants, empirically determined to be c = 0.48, d = 4.26.

C_f is pressure dependent and can be expressed as

$$C_f = \frac{1}{aP_i + b} \tag{3.3.7}$$

where a, b are empirically determined to be a = 0.05, b=1.125.

Substituting Eq. 3.3.5 with Eq. 3.3.6 and 3.3.7, the aqueous outflow can be expressed as

$$S_0 = \frac{(1 - c) P_i - d}{aP_i + b} \tag{3.3.8}$$

3.3.3 Ocular Rigidity Function

Ocular rigidity is mainly associated with mechanical characteristics of

the corneo-scleral envelope. It can be formed as [McHe65]

$$\frac{dP_i}{dV_i} = E\,P_i + f \tag{3.3.9}$$

where dV_i is intraocular volume change, E, f are empirical constants obtained by fitting the experimental data with the so-called "unifying ocular rigidity formula", and found to be $E = 0.022\ \mu l^{-1}$, and $f = 0.208$ mmHg/μl.

3.3.4 OBP-IOP Relationship

Since the intraocular volume, V_i is comprised of a vascular blood volume, V_a, and an aqueous volume, V_{aq}, the intraocular volume change rate can be expressed as

$$\frac{dV_i}{dt} = \frac{dV_a}{dt} + \frac{dV_{aq}}{dt} \tag{3.3.10}$$

The time change rate of the aqueous volume V_{aq} is equal to a difference between aqueous production and outflow

$$\frac{dV_{aq}}{dt} = S_p - S_o \tag{3.3.11}$$

Substitute Eq. 3.1.11 with Eqs. 3.3.4 and 3.3.8 to get

$$\frac{dV_{aq}}{dt} = C_p(P_c - P_i) - \frac{(1 - c)\,P_i - d}{aP_i + b} \tag{3.3.12}$$

Through an equivalent differentiated form of Eq. 3.3.2, the time change rate of the vascular blood volume V_a can be obtained

$$\frac{dV_a}{dt} = \frac{V_a}{K_\alpha (P_a - P_i)^\alpha} \left(\frac{dP_a}{dt} - \frac{dP_i}{dt}\right) \qquad (3.3.13)$$

The IOP, P_i, change rate can be determined as follows

$$\frac{dP_i}{dt} = \frac{dP_i}{dV_i}\frac{dV_i}{dt} \qquad (3.3.14)$$

Substituting Eq. 3.3.14 with the ocular rigidity function (Eq. 3.3.9), the IOP change rate becomes

$$\frac{dP_i}{dt} = (E\,P_i + f)\frac{dV_i}{dt} \qquad (3.3.15)$$

Substituting Eq. 3.3.15 with Eqs. 3.3.12 and 3.3.13, the IOP change rate can be derived as

$$\frac{dP_i}{dt} = \frac{(E\,P_i + f)\left[\frac{V_a}{K_\alpha (P_a - P_i)^\alpha}\frac{dP_a}{dt} + C_p\,(P_c - P_i) - \frac{(1-c)\,P_i - d}{aP_i + b}\right]}{1 + \frac{V_a}{K_\alpha (P_a - P_i)^\alpha}(E\,P_i + f)} \qquad (3.3.16)$$

This equation expresses relationship between the arterial pressure (OBP) and pulsations of IOP.

The P_i and V_a can be considered to be composed of mean values (P_{im}, V_{am}) and pulsations (P_{ip}, V_{ap}), which are

$$P_i = P_{im} + P_{ip} \qquad (3.3.17)$$

$$V_a = V_{am} + V_{ap} \tag{3.3.18}$$

and

$$P_{ip} << P_{im} \quad (P_{ip}: 1 - 2 \text{ mmHg}, P_{im}: 15 - 20 \text{ mmHg}) \tag{3.3.19}$$

$$V_{ap} << V_{am} \quad (V_{ap}: 1 - 2 \ \mu l, V_{im}: 30 \ \mu l) \tag{3.3.20}$$

Therefore, the IOP can be approximated with the IOP mean value, P_{im}. It is also possible to assume aqueous volume change rate equal to zero [CoWe80] as the period of interest is short enough (1 sec). Based on these assumptions, Eq. 3.3.16 can be simplified as

$$\frac{dP_{ip}}{dt} = \frac{V_{am}(E\,P_{im} + f)}{V_{am}(E\,P_{im} + f) + K\alpha(P_a - P_{im})^{\alpha}} \frac{dP_a}{dt} \tag{3.3.21}$$

By integrating Eq. 3.3.21, the IOP pulsation can be obtained as

$$P_{ip} = \int_0^{P_a} \frac{V_{am}(E\,P_{im} + f)}{V_{am}(E\,P_{im} + f) + K\alpha(P_a - P_{im})^{\alpha}} dP_a \tag{3.3.22}$$

This equation is used to calculate the IOP variation due to the OBP. P_{im} and V_{im} can be determined through Eqs. 3.3.9 and 3.3.2 as follows.

Integral form of Eq. 3.3.9 is

$$\Delta V_{im} = \frac{1}{E} \ln \left(\frac{P_{im2} + f/E}{P_{im1} + f/E} \right) \tag{3.3.23}$$

where ΔV_{im} is the average intraocular volume change ($V_{1m} - V_{2m}$). Equality of ΔV_{im} to ΔV_{am} is also preserved here, assuming ΔV_{aq} is zero. So, the

equivalent form of 3.3.23 is

$$P_{im2} = (P_{im1} + f/E)\, e^{-E(V_{am1} - V_{am2})} - f/E \qquad (3.3.24)$$

Replacing variables in Eq. 3.3.2 with mean values, we can get

$$\frac{1}{1-\alpha}\left[(P_{am2} - P_{im2})^{1-\alpha} - (P_{am1} - P_{im1})^{1-\alpha}\right] = K\alpha \ln\left(\frac{V_{am2}}{V_{am1}}\right) \qquad (3.3.25)$$

Combining Eqs. 3.3.24 and 3.3.25, the P_{im2} and V_{am2} can be solved.

Referring P_a as the OBP, the relationship between IOP (mean and pulsation part) and OBP has been achieved so that OBP variation can be directly transformed into the IOP pulsation. By assigning the OBP without stenosis in the CVS as state1 and the OBP with stenosis in the CVS as state 2, the IOP mean value and pulsation part with respect to blood supply from the OBP bearing certain (10-90%) level of stenosis severity can be obtained by solving Eqs. 3.3.24, 3.3.25, and 3.3.22. This relationship can be demonstrated by the case that stenosis is presented in segment 8 of the CVS. The OBP mean values have been calculated from the 10 curves in Fig. 3.2.2. The OBP mean value without stenosis is 55.5 mmHg, which makes the transmural pressure equal to 40.5 Hg. IOP and ocular vascular volume has been chosen to be 15 mmHg and 32.37 μl respectively. All these data values are similar with previous published results for man [CoWe80]. Corresponding to each of 10 reduced OBP mean values, the mean values of IOP and ocular blood volume are solved numerically through Eqs. 3.3.24 and 3.3.25, and listed in Table 3.3.1. The IOP mean value is reduced along with the OBP reduction, and ocular vascular volume is also reduced as a result of the transmural pressure reduction with the increased stenosis severity. Furthermore, the

Table 3.3.1 Mean values of IOP and ocular vascular volume as a function of stenosis severity located in segment 8 of the CVS.

% Stenosis	IOP [mmHg]	Volume [µl]
0	15.00	32.37
10	14.99	30.34
20	14.95	32.27
30	14.94	32.08
40	14.63	31.67
50	14.22	30.90
60	13.50	29.48
70	12.24	26.92
80	10.02	22.03
90	6.10	11.81

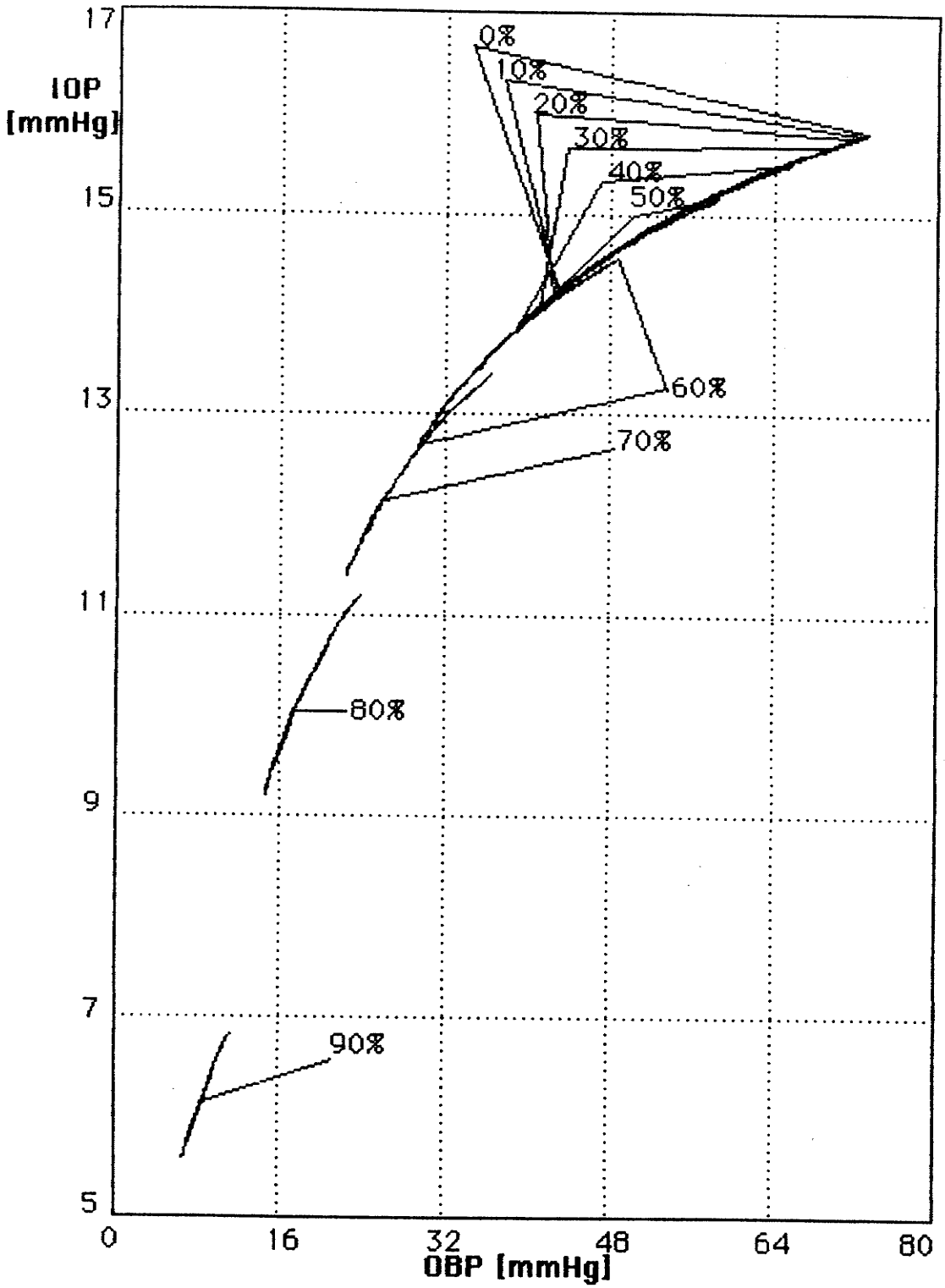

Fig. 3.3.2. OBP-IOP relationship as a function of stenosis severity located in segment 8 of the CVS.

relationship between IOP pulsation and OBP as a function of stenosis severity can also be obtained by Eq. 3.3.22, as plotted in Fig. 3.3.2. This result illustrates how the OBP variation (at a certain level of the mean value) is transformed to the IOP pulsation. The percent numbers indicate the corresponding stenosis severity, and IOP pulsation range with different OBP varying range are also marked. From this graph, it can be seen that OBP-IOP relationship is monotonic and highly linear, and the IOP pulsation range is between 1 and 2 mmHg which accords with the previous result [Adle65]. Such a relation between OBP and IOP will convey the OBPW, altered by the stenosis, to the ocular pulse waveform (OPW) which is directly related with the IOP pulsation. It is should be noted the IOP pulsation range does not change monotonicly with the stenosis severity progression due to the non-linear OBP-IOP relationship.

3.3.5 Ocular Pulse

The eyeball is assumed to be a perfectly elastic, thin walled sphere. Five layer sandwich structure of the corneal wall has been studied by Mow [Mow68], in which it is assumed that the cornea is elastic and linear. In his corneal model, the viscoelastic properties of the cornea was not considered. These properties can be reasonably neglected because the pulsation period of interest is short, compared with their larger time constant. The linearity of the cornea is supported by the fact that the deformation of cornea due to the IOP variations is small and falls into the linear portion of its long time displacement trend. Fig. 3.3.3 shows the cornea model, in which the corneal wall, supported by the ciliary muscles, is measured by three parameters for the core thickness, internal, and external surface thickness. The internal and

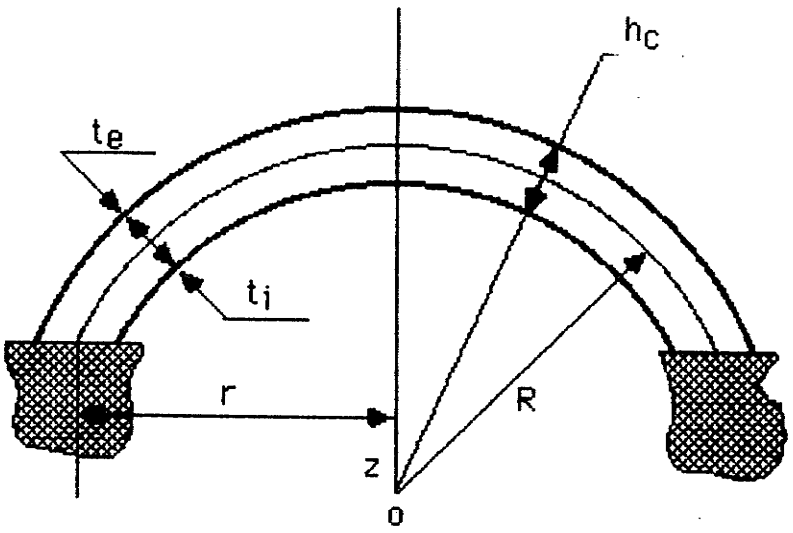

Fig. 3.3.3. Cornea model.

external surface thickness can be considered equal, denoted as t. The following dimensions have been used in this model:

Typical dimensions of the cornea

Symbol	Name	Value
R	Radius of corneal sphere	7.43 mm
t_e, t_i	Internal and external surface layer thickness	15 μm
h_c	Core layer thickness	700 μm
r	Half of the corneal width	6 mm

In the simplified form where the stress in the cornea due to the IOP variation is only considered, the model for the radial displacement of the cornea along the z coordinate is expressed as

$$\Delta H = \frac{(1-\nu)R^2}{4tE_f}\Delta P_i \qquad (3.3.26)$$

where ΔH is the radial displacement or ocular pulse, ΔP_i is the pulsation of IOP, ν is Poisson's ratio of cornea, equal to 0.3 [Jul184b], and E_f is Young's modulus of internal and external face layers of the shell. This approximation for the Young's modulus is justified since $E_f/E_c = 10^2-10^3$ [Jul184a], where E_c is Young's modulus of the shell core.

Now, the way has been established to obtain the OPW driven by the pulsation of IOP. Therefore, both stenosis beared from IOP as discribed

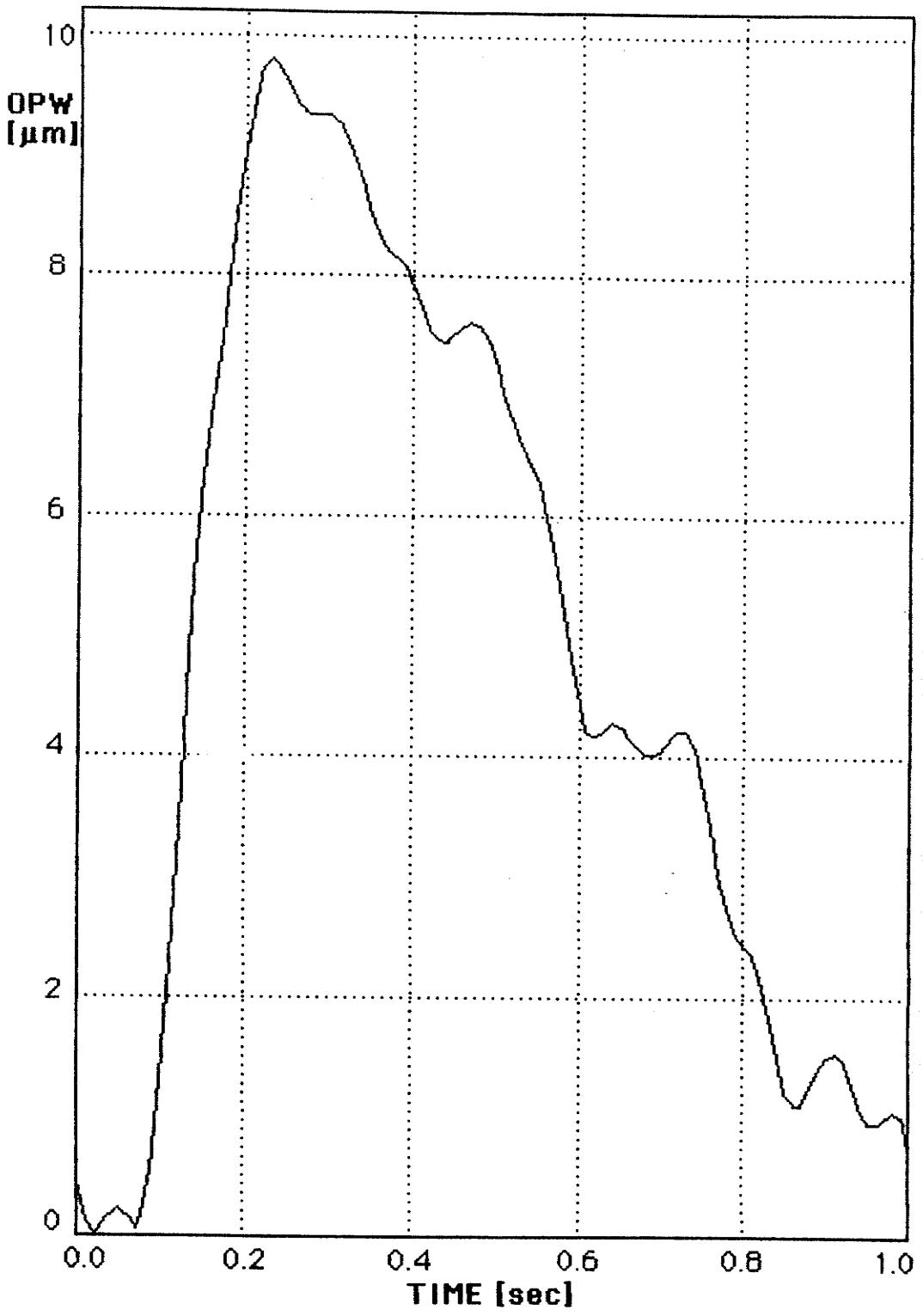

Fig. 3.3.4. OPW without stenosis.

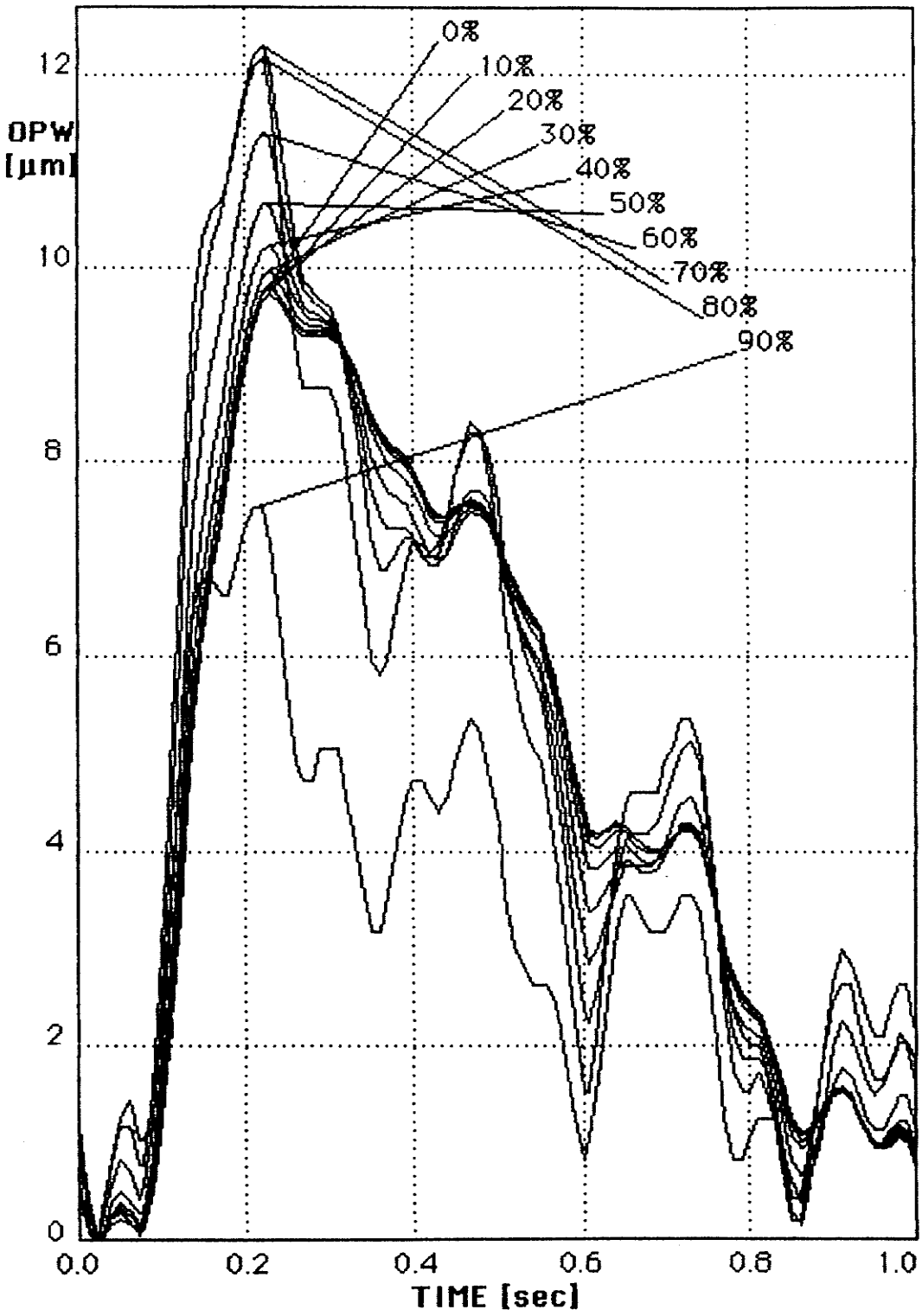

Fig. 3.3.5. OPWs as a function of stenosis severity located in segment 8 of the CVS.

earlier, and elevated IOP can be screened from the OPW to conform to the goal of this research.

As an example, Fig. 3.3.4 illustrates the OPW corresponding to the blood supply from the OBP as shown in Fig. 3.1.12. The two waveforms (Fig. 3.3.4 and 3.1.12) are very similar, indicating that the OPW directly reflects the OBP alteration as stated before. The amplitude of this OPW is about 10 μm, which is compatible with the published result in [Horv70]. Fig. 3.3.5 illustrates the OPW as a function of stenosis severity in segment 8 of the CVS. Associated OBPWs is Fig. 3.2.2. It can also be seen that the OBPWs are directly transformed to OPWs. Similarly, as discussed earlier, this set of waveforms presents a complicated pattern of OPW, in which the shape and phase (frequency content) are altered by the stenosis existence. All of these features can be traced in the frequency spectral analysis. It should be noted that the OPW amplitude does not change monotonicly with the stenosis severity progression due to non-linear dynamic range transformation from OBP to IOP as stated in last section. This is different from Best's result [Best71c] since the ocular pulse obtained in his test is controlled by the suction level and the OPW is compressed. Another reason for this difference is that the test subject was rabbit, which has physiological difference from man. From Fig. 3.3.5, it is clear that graphic analysis is not suitable for an accurate, non-contact screening method, and the OPW analysis with respect to stenosis effect will be pursued in the frequency spectral domain.

3.3.6 Summary

Based on the previous model describing the mechanism within the eye

[CoWe80], a model of the eye was developed [Jul184a]. for achieving the OBP-IOP relationship. This model is improved with respect to the OBP-IOP relationship as a function of either stenosis severity or levels of IOP. The present eye model can be incorporated through this relationship with the CVS model. The corneal model is also presented in this part based on the study in [Mow68], [Jul184a] so that the corresponding OPW as a function of either stenosis severity levels or levels of IOP can be obtained. Simulated results presented in this section are compared with the previous experimental data consistently. The OPW result from this study showed a much more complicated pattern bearing the effect from the carotid stenosis, which can be analyzed more precisely in frequency domain. This will be described in next chapter.

3.4 Description on the System Structure

The ocular pulse system, as described above, includes the models of CVS, stenosis and the eye. They are simulated using numerical methods. The actual computer program structure and listing are presented in Appendix C and D. The structure of this system containing all the interconnected models and units is shown in Fig. 3.4.1. Several specific signal , as well as others, can be obtained from this system. The ABP model produces ABPWs with different features, based on the basic typical ABP function. The CVS model takes an ABPW as an input. With the integrated stenosis model, the CVS model can produce not only the normal OBP output, but also the OBPWs bearing the effect from the stenosis. The OBP output provides blood supply to the ocular circulation within the eye. Based on the OBP–IOP relationship in the eye model, the OPW can be obtained, which contains features of either stenosis or elevated IOP. All of the results from different stages of the

system can be displayed and monitored for further analysis. All of the detailed descriptions of the models have been given in this chapter.

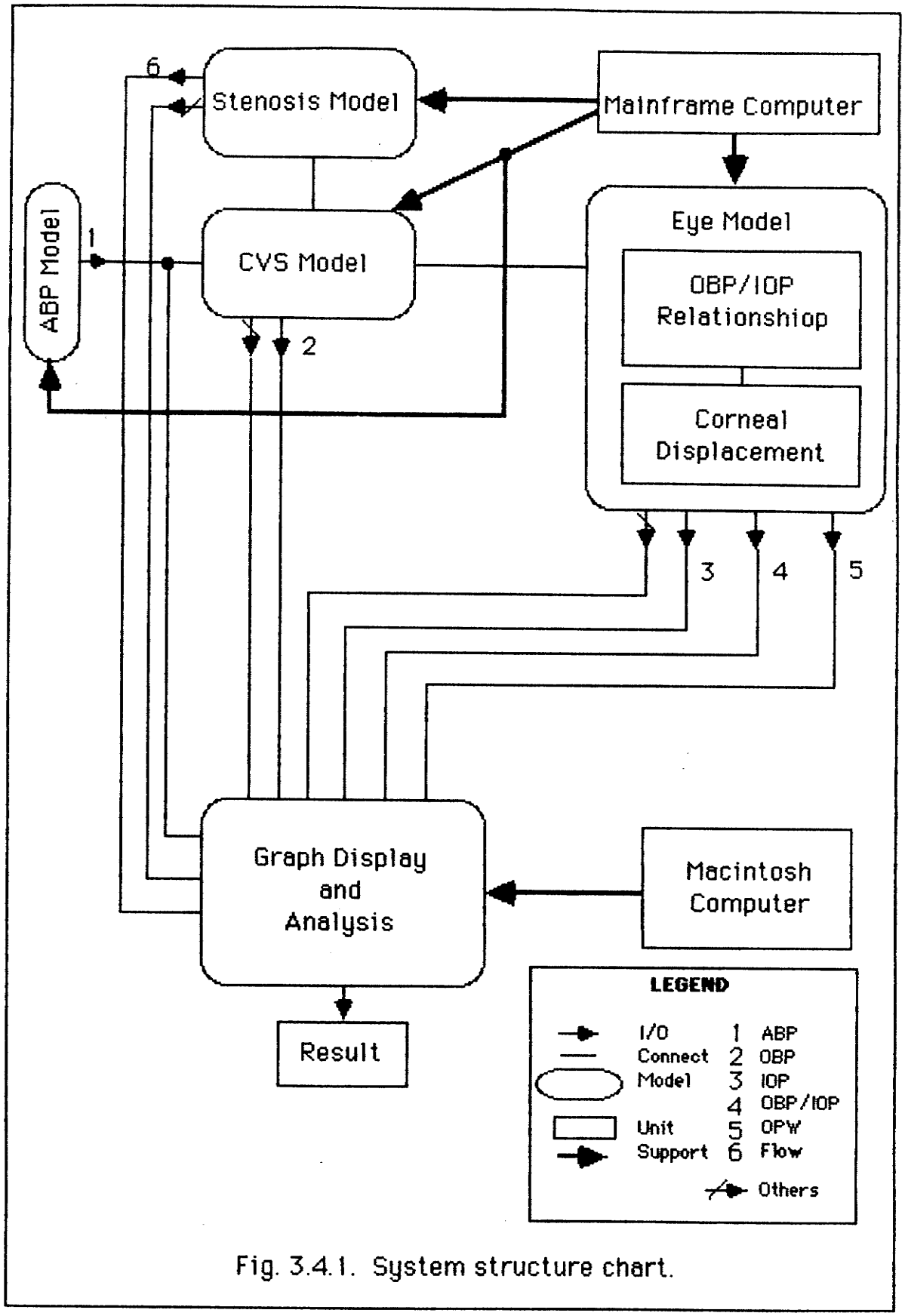

Fig. 3.4.1. System structure chart.

CHAPTER IV

A SENSITIVITY STUDY AND PATTERN EXPLORATION OF OCULAR PULSE

Based on the models described last chapter, variations of the ocular pulse system on stenosis change, ABPW change, vascular bed change, and geometric parameter change of the CVS can be established in order to study the sensitivity of OPW to either stenosis or elevated IOP. With these variations (all related to the 14th degree CVS model), methods for exploring the OPW pattern corresponding to severity levels and locations of stenosis in the CVS can be studied. These methods can also be used to analyze the OPW with respect to elevated IOP.

The variations for a study on stenosis are classified into 23 cases:

CASE1: The original case with stenosis located in segment 8 of the CVS.

Variations for stenosis displacement:

CASE2: Stenosis located in segment 1.

CASE3: Stenosis located in segment 2.

CASE4: Stenosis located in segment 3.

CASE5: Stenosis located in segment 5.

CASE6: Stenosis located in segment 6.

CASE7: Stenosis located in segment 9.

Variations from CASE1:

CASE8: Stenosis length, L_S, changed to 2 cm.

CASE9: Stenosis length, L_S, changed to 3 cm.

Note: Stretching stenosis length will increase the viscous and inertial loss, as described in the stenosis model.

CASE10: ABP diastolic amplitude decreased by 10%.

CASE11: ABP diastolic amplitude increased by 10%.

CASE12: ABP systolic amplitude decreased by 10%.

CASE13: ABP systolic amplitude increased by 10%.

Note: These are only linear expansions of the ABPW. No new frequency content is introduced by these four cases.

CASE14: IOP level decreased to 10 mmHg.

CASE15: IOP level increased to 20 mmHg.

Note: In these two cases, the OPW is altered.

CASE16: Ophthalmic terminal resistance R10 increased by 20%.

CASE17: R10 deceased by 10%.

Note: These two cases will increase or decrease the level of the CVS output, OBP, and also alter the transfer function of the system. The resistance bed R7 is also changed accordingly to keep the ratio R7/R10 unchanged.

CASE18: Radius, r, for each segment of the CVS increased by 20%, with corresponding artery wall thickness, h, increased proportionally by 4% to keep the ratio r/h constant.

CASE19: r decreased by 20%, with h decreased proportionally by 4%.

CASE20: Length, Δz, for each segment of the CVS increased by 10%.

CASE21: Δz decreased by 10%.

Note: These four cases will change the component values in the electric model of CVS accordingly.

CASE22: ABP duration changed to 0.4 sec with systolic portion 0.25 sec and diastolic portion 0.15 sec.

CASE23: ABP duration changed to 1.5 sec with systolic portion 0.35 sec and

diastolic portion 1.15 sec.

Note: In these two cases, the ABP frequency content has been changed so that new frequency content will be introduced into the CVS model.

All of concrete values for parameters changed in each case from CASE1 are listed in Appendix B.

4.1 Stenosis

In this part, the variations are applied to analyze how stenosis presented in the CVS affects the system outputs both in spatial and frequency domain. Study in spatial domain gives the general analysis of the system behavior with respect to the stenosis, while in frequency domain, the methods on finding the OPW patterns for screening stenosis (severity and location) are described. In section 4.2, the same analysis methods will be applied to the study on the effect of elevated IOP levels to OPW.

4.1.1 Spatial Analysis

CASE1 is the original as used in last chapter. The derivatives of CASE1, (CASE2 to CASE7) can be studied for the stenosis location. The method for stenosis displacement along the CVS tree has been presented in section 3.2. Stenosis coefficients (K_v) are listed in Appendix B, modified from that in Table 3.2.1 for stenosis located in different segments. Since 7 segments of the CVS can be grouped to present the common carotid (Segment 1–3), the external carotid (segment 5 and 6), and the internal carotid (segment 8 and 9), most of testing results will be presented here only for segment 2, 5 and 8

Table 4.1.1 Three index numbers for stenosis in segment 2, 5, and 8 of the CVS

% Stenosis	Segment								
	2			5			8		
	lv	lt	li	lv	lt	li	lv	lt	li
0%	0.019	0.0	0.0	0.084	0.0	0.0	0.031	0.0	0.0
10%	0.021	0.007	0.097	0.090	0.007	0.035	0.034	0.007	0.014
20%	0.022	0.038	0.092	0.095	0.038	0.035	0.036	0.038	0.015
30%	0.025	0.124	0.036	0.108	0.124	0.036	0.042	0.124	0.015
40%	0.029	0.331	0.103	0.123	0.331	0.038	0.049	0.331	0.017
50%	0.033	0.815	0.107	0.146	0.815	0.040	0.062	0.815	0.019
60%	0.046	1.980	0.118	0.205	1.980	0.043	0.096	1.980	0.025
70%	0.079	5.172	0.130	0.372	5.172	0.052	0.195	5.172	0.035
80%	0.016	16.320	0.145	0.841	16.320	0.077	0.491	16.320	0.058
90%	0.693	88.290	0.182	4.16	88.290	0.154	2.652	88.290	0.135

without losing any meaning for each segment.

Table 4.1.1 lists the three index numbers achieved for stenosis located in segment 2, 5 and 8. It shows, as in Table 3.2.2, the dominant effect from turbulent term, I_t which remains constant as stenosis moves to different segments because it only depends on the levels of the arterial occlusion. The inertial effect, I_i, is still relatively small and constant as expected in the development of the stenosis model. The viscous effect, I_v, is significant at low level of stenosis whereas it is gradually reduced at higher levels, compared with values of I_t. Values of I_v are different as stenosis moves to different segments. I_v values for stenosis in segment 5 are larger that those for stenosis in segment 2 and segment 8. This is because the arterial radius of segment 5 is smaller, which increases the viscous coefficient, K_v, and reduces the Reynolds number. All of these results are similar to those in [YoCR75].

Fig. 4.1.1 and 4.1.2, together with Fig. 3.2.2, are the OBPW outputs from the CVS for stenosis located in segment 2, 5, and 8 respectively. Stenosis in the common or internal carotid (segment 2 or 8) reduces the OBP amplitude and variation as it is on the path of blood flow to the ophthalmic artery. As stenosis moves to the external carotid (segment 5), the blood flow in the internal carotid is enhanced, as a result of which the OBP (amplitude and variation) output at the ophthalmic terminal is slightly increased along with the stenosis severity level progression. More and faster amplitude reduction of OBP can be seen when stenosis is located in the internal carotid (segment 8) than in any other places (e.g., segment 2) because the internal carotid is directly connected to the ophthalmic artery.

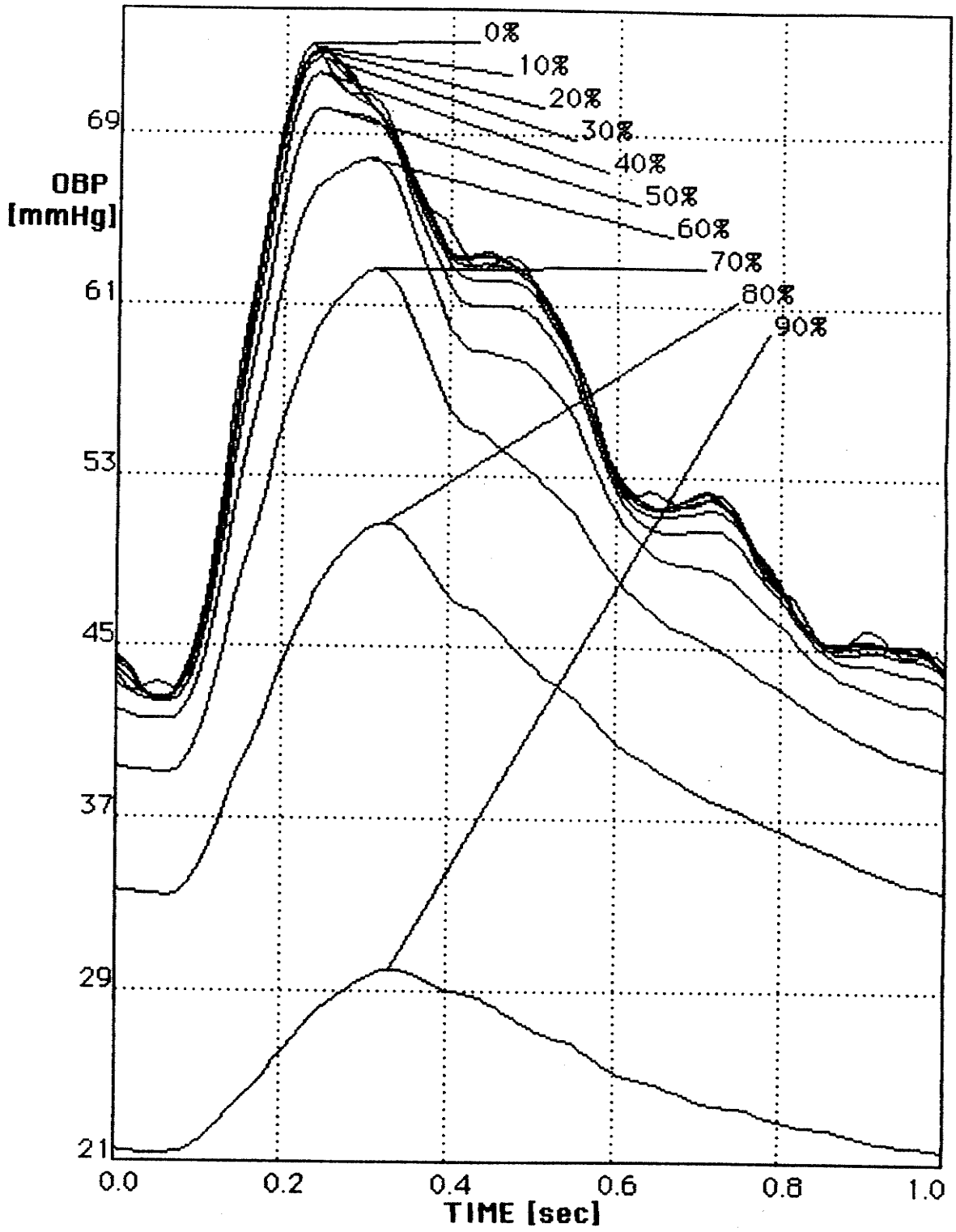

Fig. 4.1.1. OBPWs as a function of stenosis severity in segment 2 of the CVS.

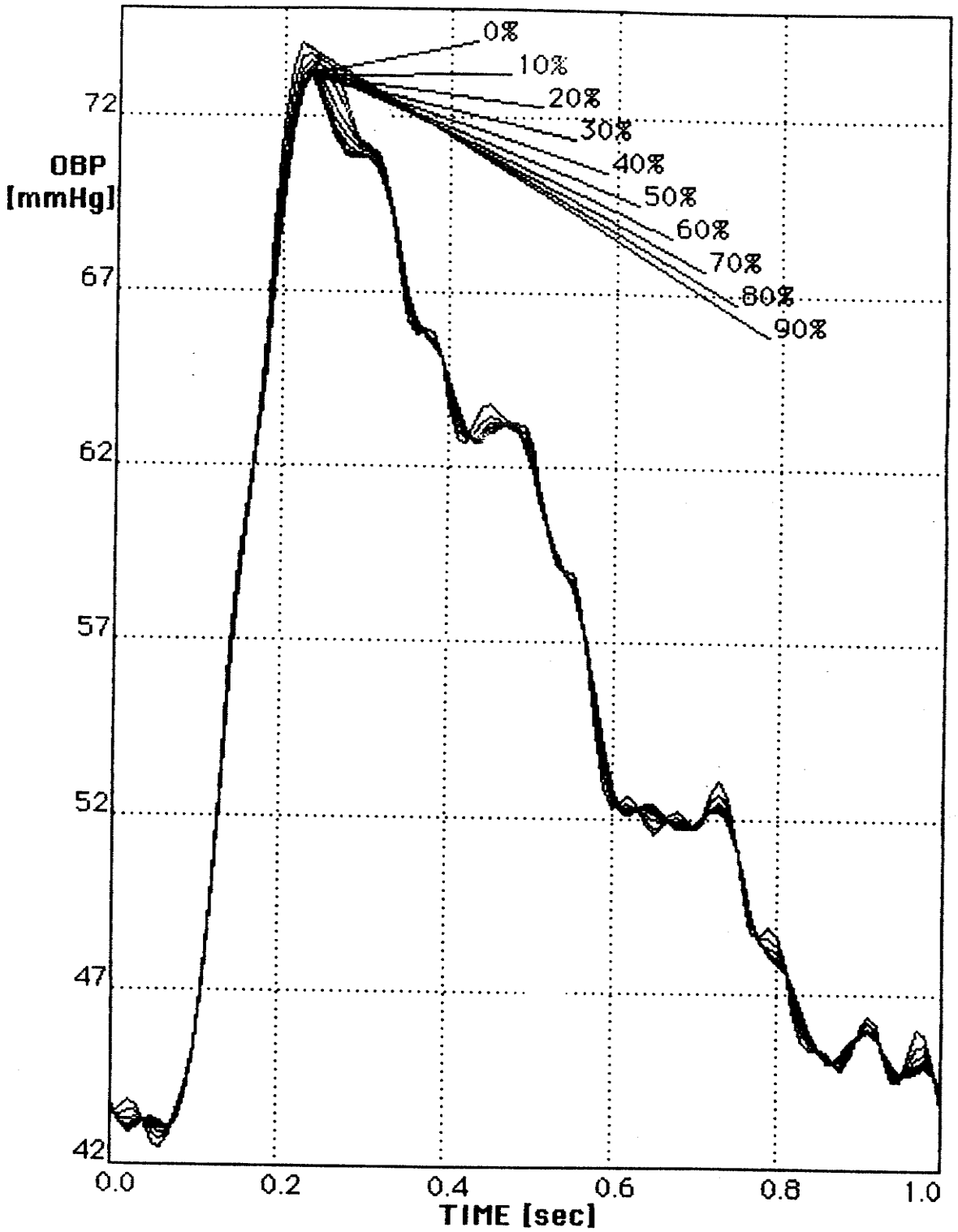

Fig. 4.1.2. OBPWs as a function of stenosis severity in segment 5 of the CVS.

The same effect can be seen from Fig. 4.1.3, which shows mean values of IOP as a function of stenosis severity located in different segments of the CVS. For stenosis in segment 5 and 6, mean values of IOP keeps almost constant (a slight increase). It has a slow reduction as stenosis moves to segment 1, 2, and 3, and the reduction grows faster when stenosis moves closer to the ophthalmic artery (segment 8 and 9).

Corresponding to the OBP supply to the eye shown in Fig. 4.1.1, 4.1.2 and 3.2.2, the OPW results were achieved (Fig 4.1.4, 4.1.5, and 3.3.5) for stenosis in segment 2, 5, and 8 respectively. Although the OPW result does not show the clear stenosis severity progression pattern, as explained in last chapter, it still exhibits that OPWs are altered differently by the carotid stenosis in different locations. The OPWs are so complex that it is difficult to apply graphic analysis methods as used for other peripheral signal studies in medical research. However, the frequency content for each set of OPWs is different, indicating that frequency analysis methods can be applied for screening both stenosis location and severity through analysis of OPW in frequency domain.

Variations from CASE8 to CASE21 are all based on CASE1 which has the stenosis located in segment 8. These variations include stenosis length change (CASE8 and CASE9), linear amplitude expansions of ABPW (CASE10–CASE13), IOP level changes (CASE14 and CASE15), ophthalmic peripheral resistance changes (CASE16 and CASE17) and geometric parameter changes (CASE18-CASE21). They are treated as one group since these variations are only linear expansions of certain parameters of the system in a small range,

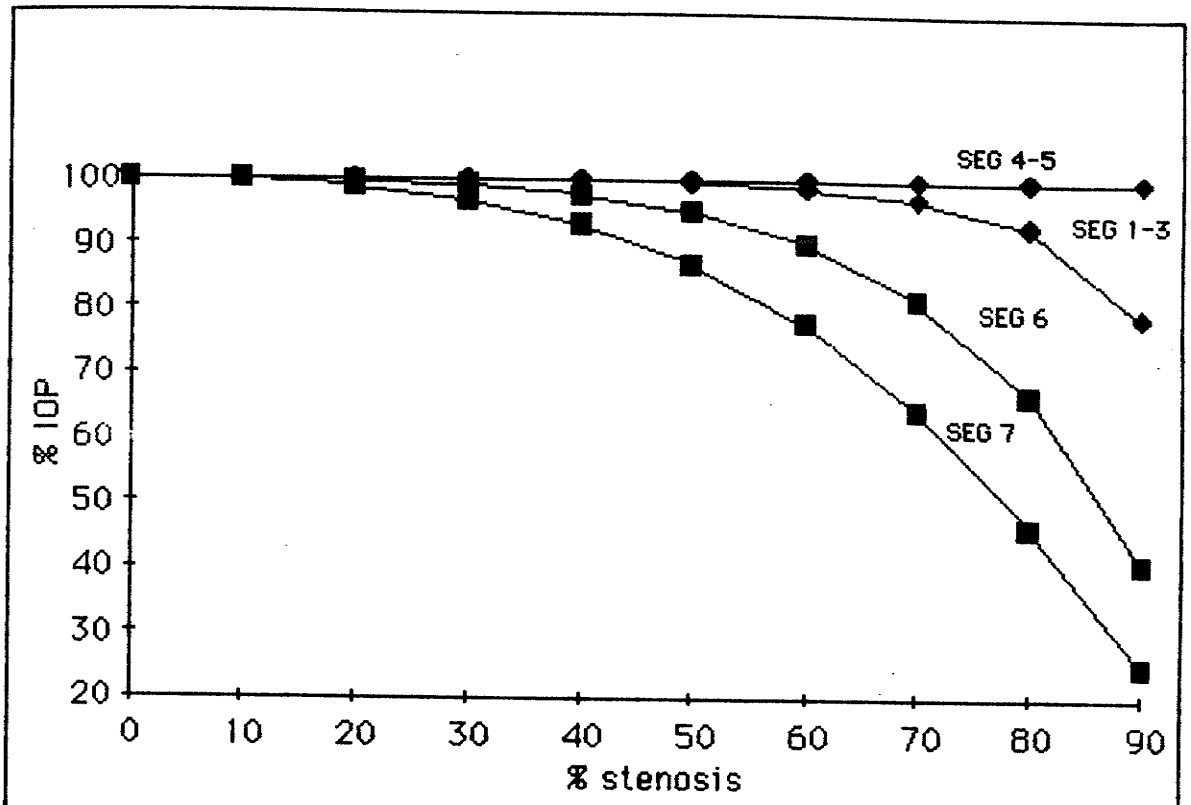

Fig. 4.1.3. Mean values of IOP as a function of stenosis severity, location of stenosis is marked above each curve, the IOP values are percent against the normal IOP level 15 mmHg.

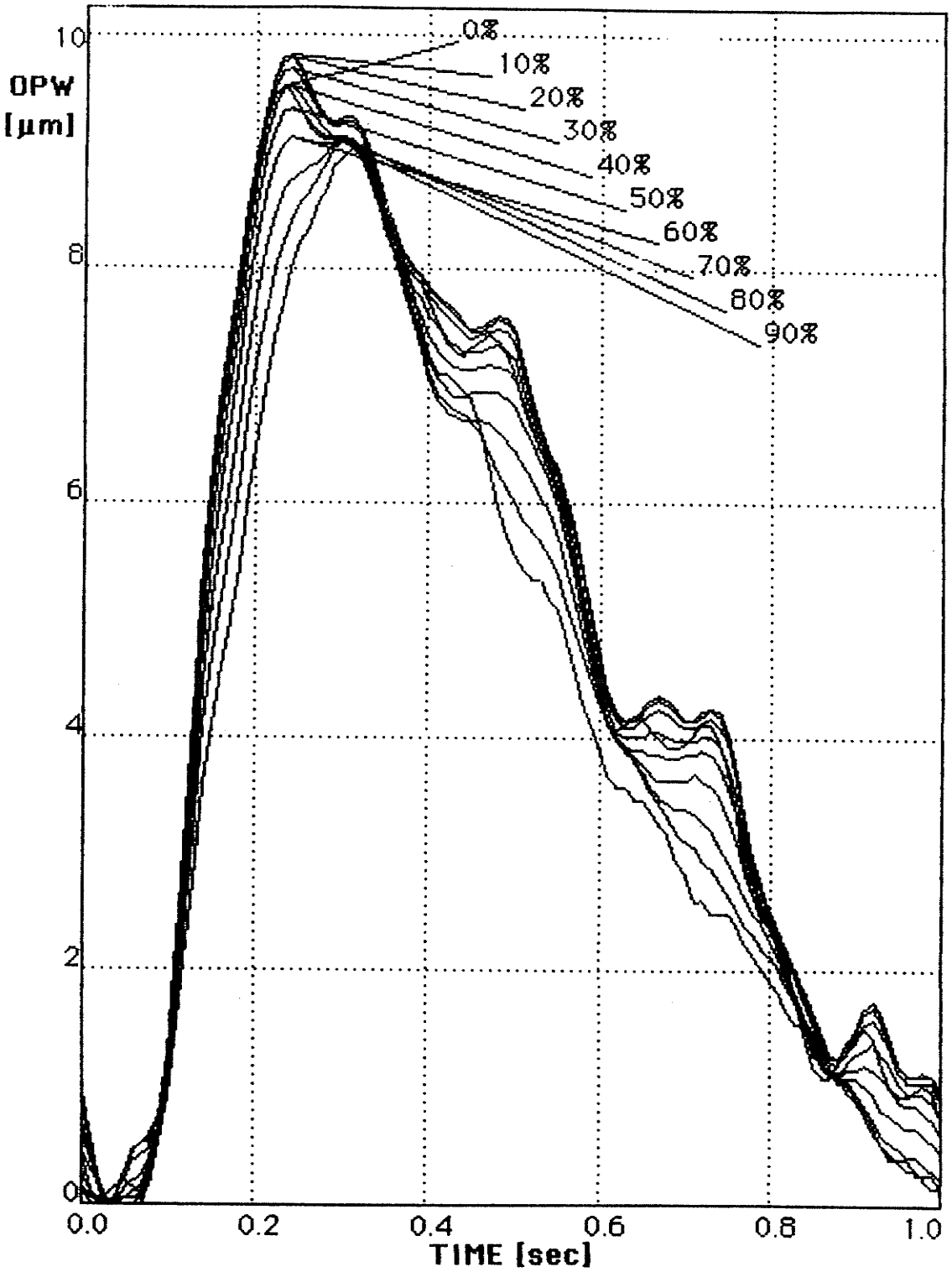

Fig. 4.1.4. OPWs as a function of stenosis severity in segment 2 of the CVS.

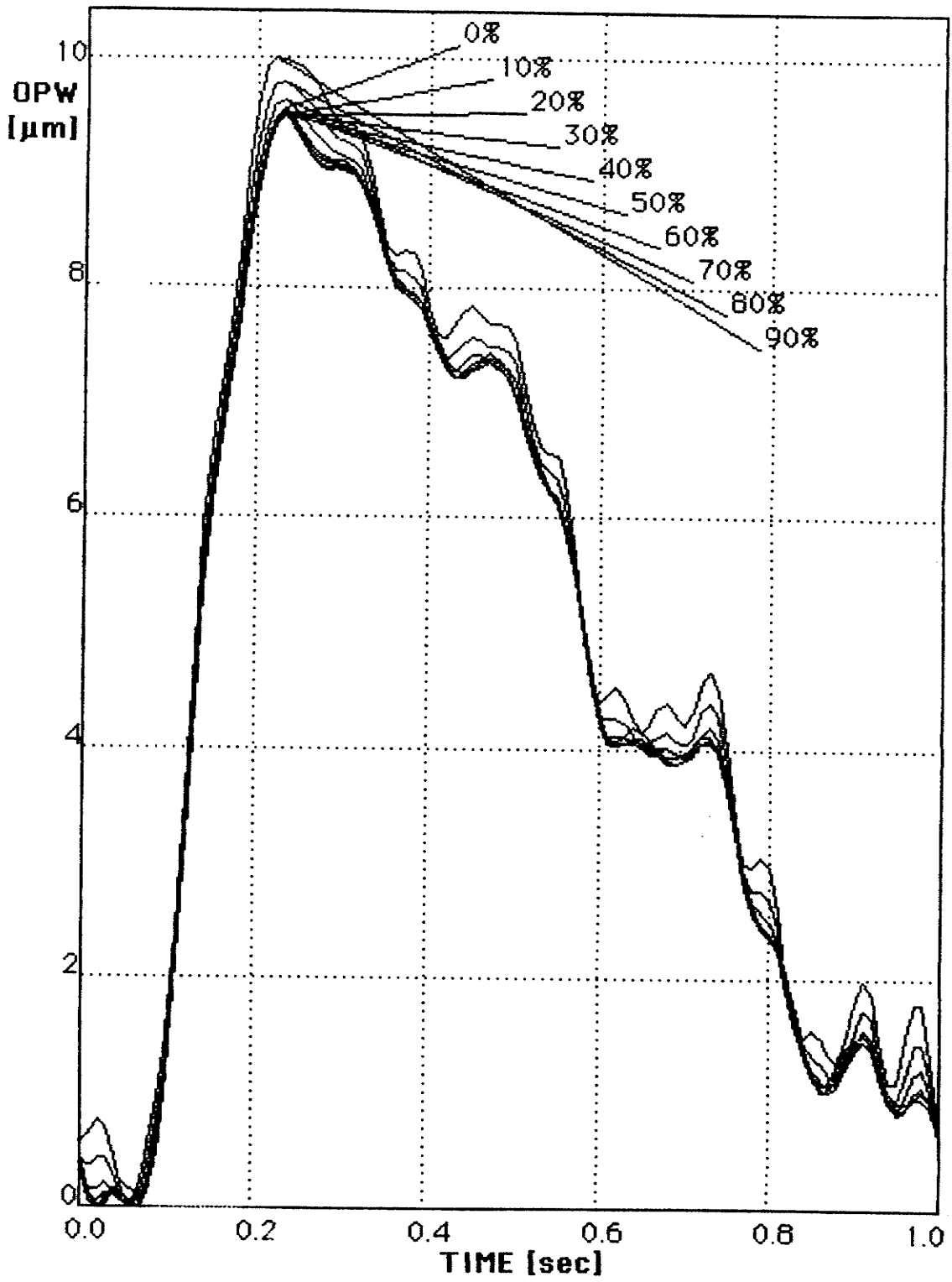

Fig. 4.1.5. OPWs as a function of stenosis severity in segment 5 of the CVS.

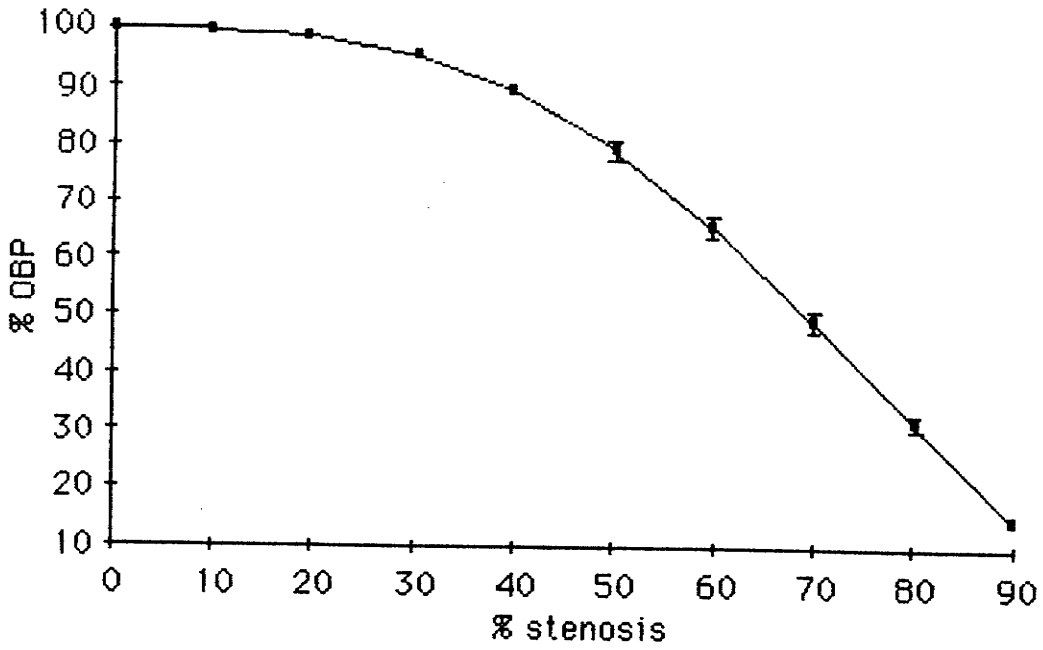

Fig. 4.1.6 Mean values of OBP as a function of stenosis severity in segment 8 of the CVS for CASE1 and CASE8–CASE21, the values are percent against the normal OBP mean value 55.5 mmHg, standard deviation is marked.

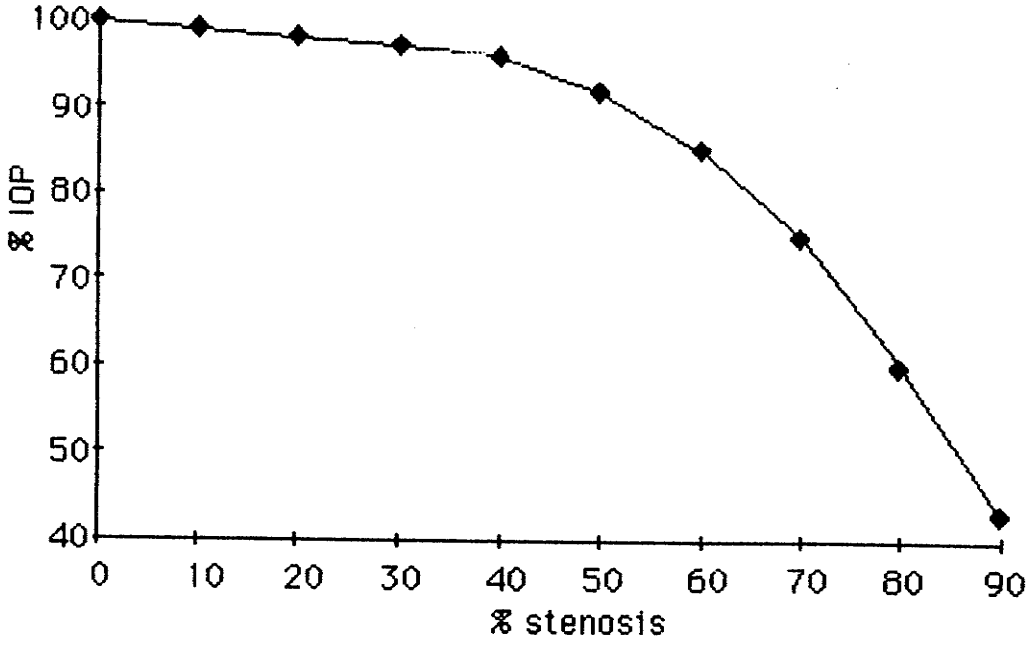

Fig. 4.1.7. Mean values of IOP corresponding to mean values of OBP in Fig. 4.1.6, the normal IOP level is 15 mmHg.

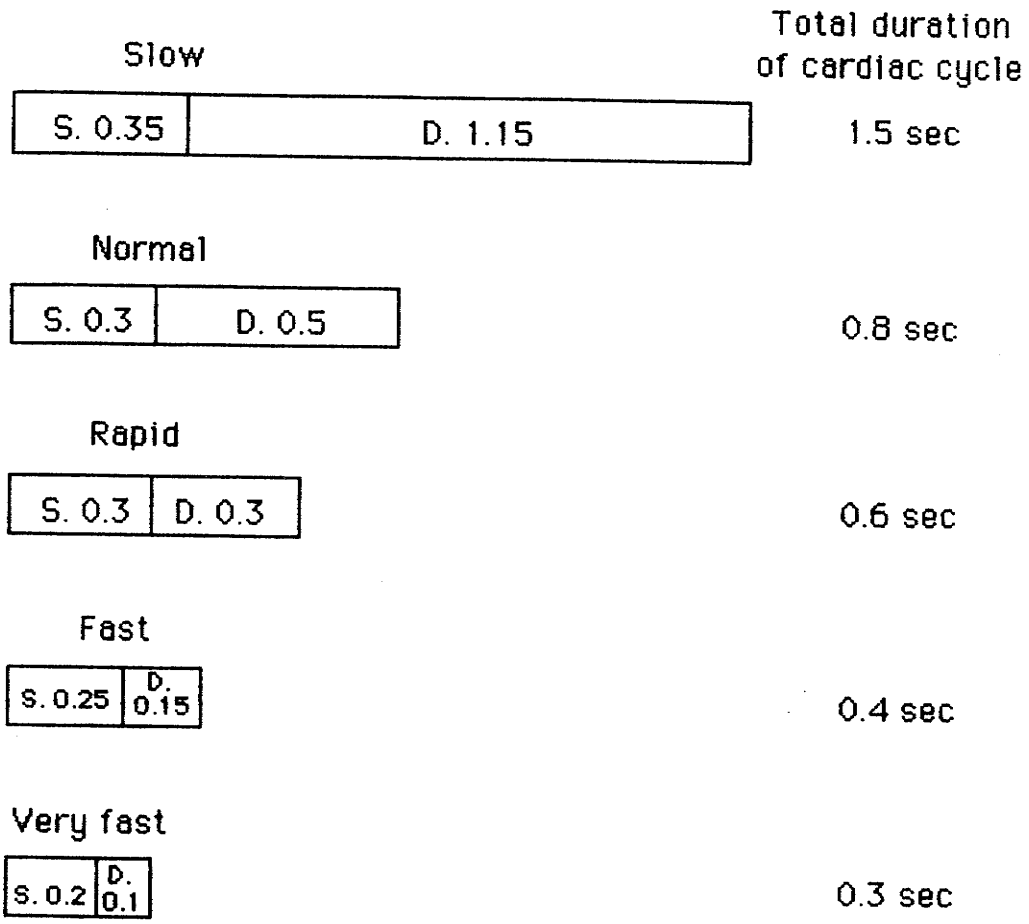

Fig. 4.1.8. Spectrum of human heart beat cycle with systolic (S) and diastolic (D) portions. [From [Gree78]]

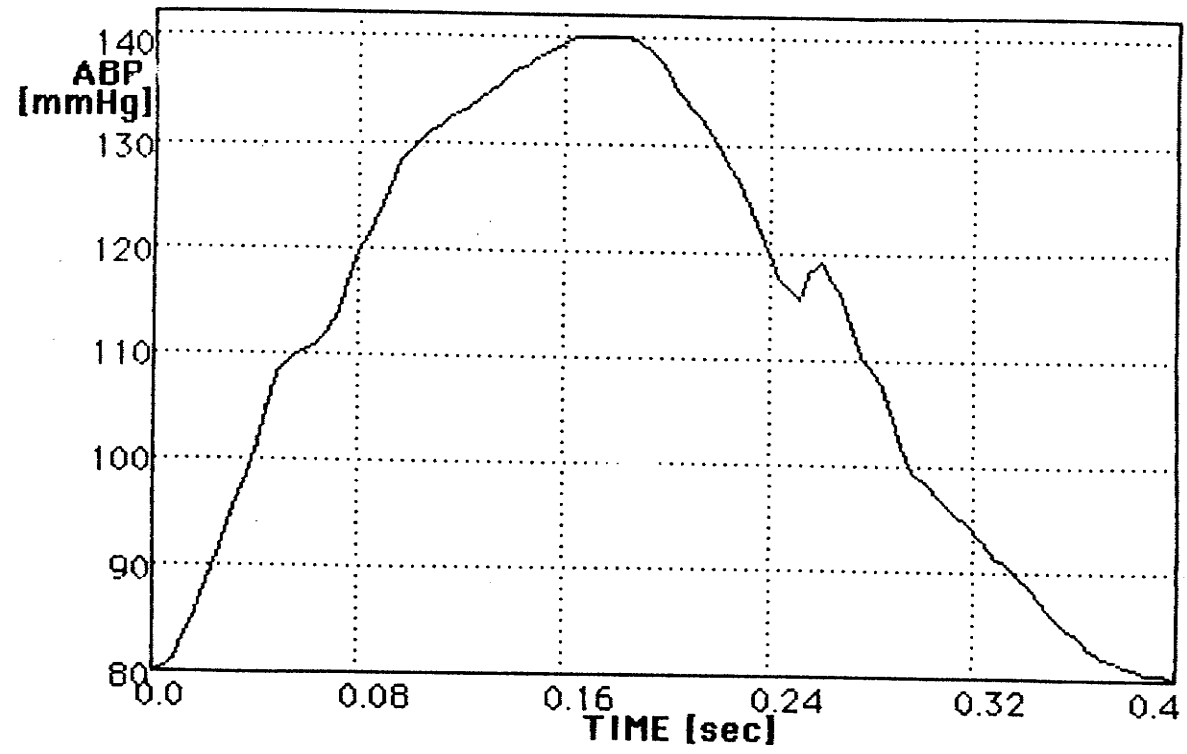

(a)

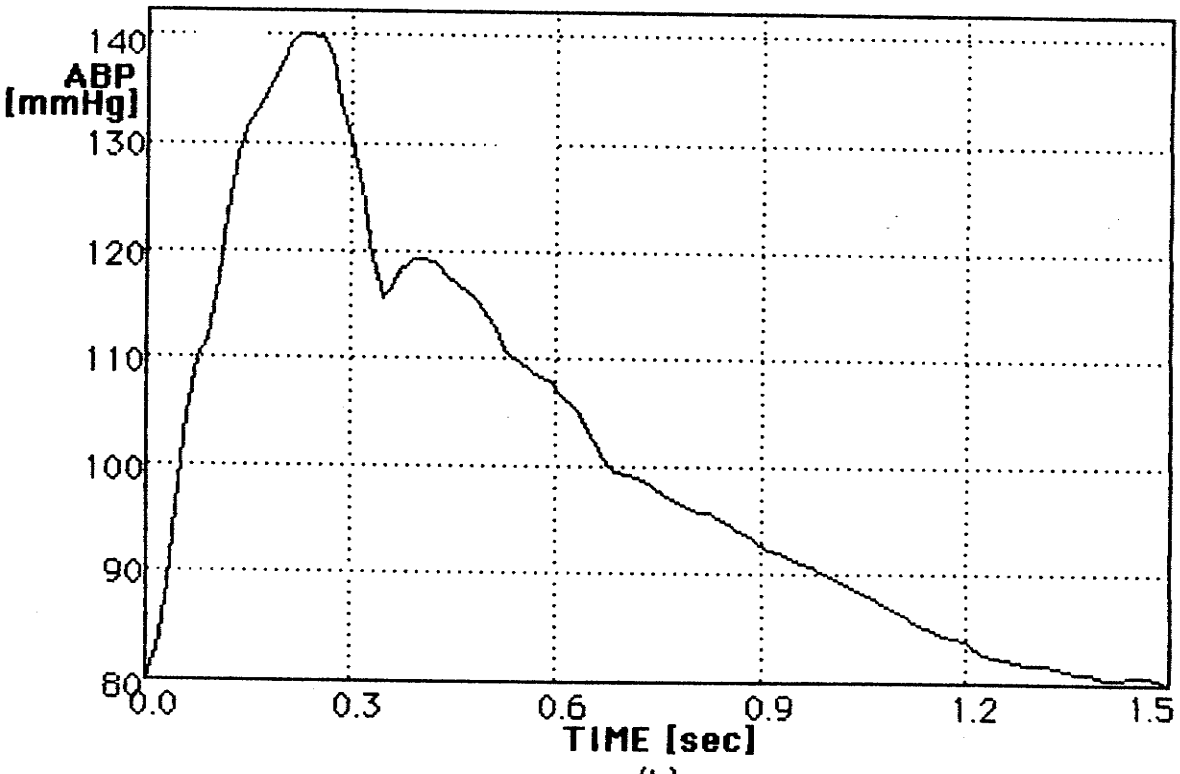

(b)

Fig. 4.1.9. ABPWs with (a) cycle 0.4 sec, systolic portion 0.25, diastolic portion 0.15, (b) cycle 1.5 sec, systolic portion 0.35 sec, diastolic portion 1.15 sec.

and have the stenosis all in segment 8 of the CVS. These changes will not make significant spectral pattern changes, as will be confirmed in the following spectral analysis. They are discussed in preparation for studying the spectral pattern of OPWs in the next section.

Fig. 4.1.6 and 4.1.7 show the OBP mean values and corresponding IOP mean values reduced by the growing stenosis severity. As can be seen, all the cases fall into the same pattern with very small standard deviations. The OBPWs and OPWs of these cases, as a function of stenosis severity, have also been obtained, which are similar with Fig. 3.3.2 and 3.3.5. Therefore, they can be indeed identified with the same group.

The last part of the variation cases are CASE22 and CASE23, where the ABPW is modified. The modification is based on the published result [Gree78] on human heart rate for the ABP duration adjustment, and the ABPW shown in Fig. 3.1.7 for the amplitude expansion. The human heart rate spectrum has been classified into five averaged groups [Gree78] as shown in Fig. 4.1.8. For this study, two extreme cases were chosen with heart durations 0.4 and 1.5 sec respectively. Due to the duration change (systole and diastole), the ABP frequency spectral pattern for each group will be different, which causes the system output OPW to have new spectral patterns. The methods of finding spectral patterns for these two cases also apply to other groups. In the clinical test, it is feasible to divide subjects into different groups, having different spectral patterns.

The ABP amplitude of these two cases was chosen to be the standard as in Fig. 3.1.7. By the linear alignment with this standard ABPW, two new

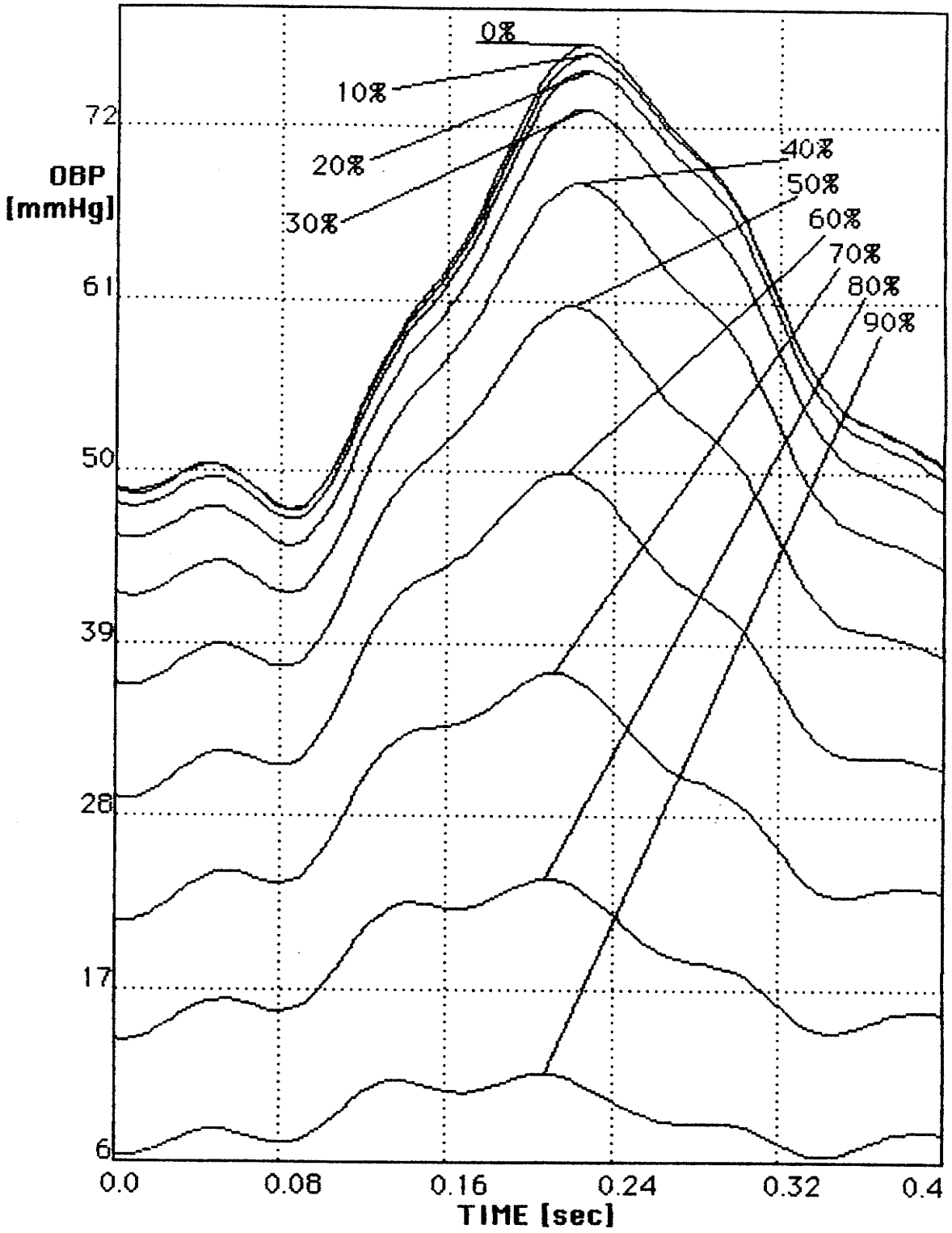

Fig. 4.1.10 OBPWs as a function of stenosis severity in segment 8 of the CVS with the input ABP shown in Fig. 4.1.9a.

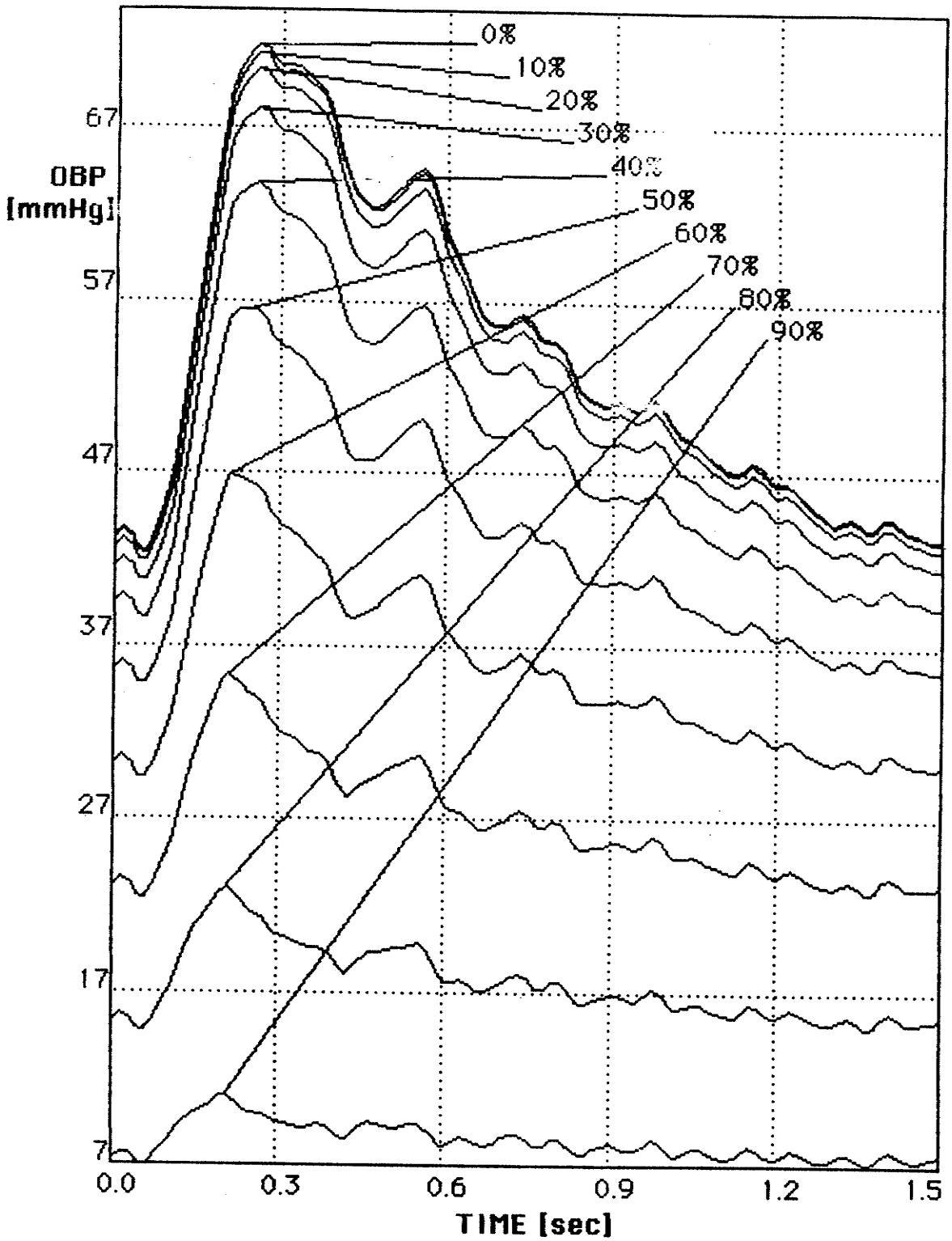

Fig. 4.1.11. OBPWs as aa function of stenosis severity in segment 8 of the CVS with the input ABP shown in Fig. 4.1.9b.

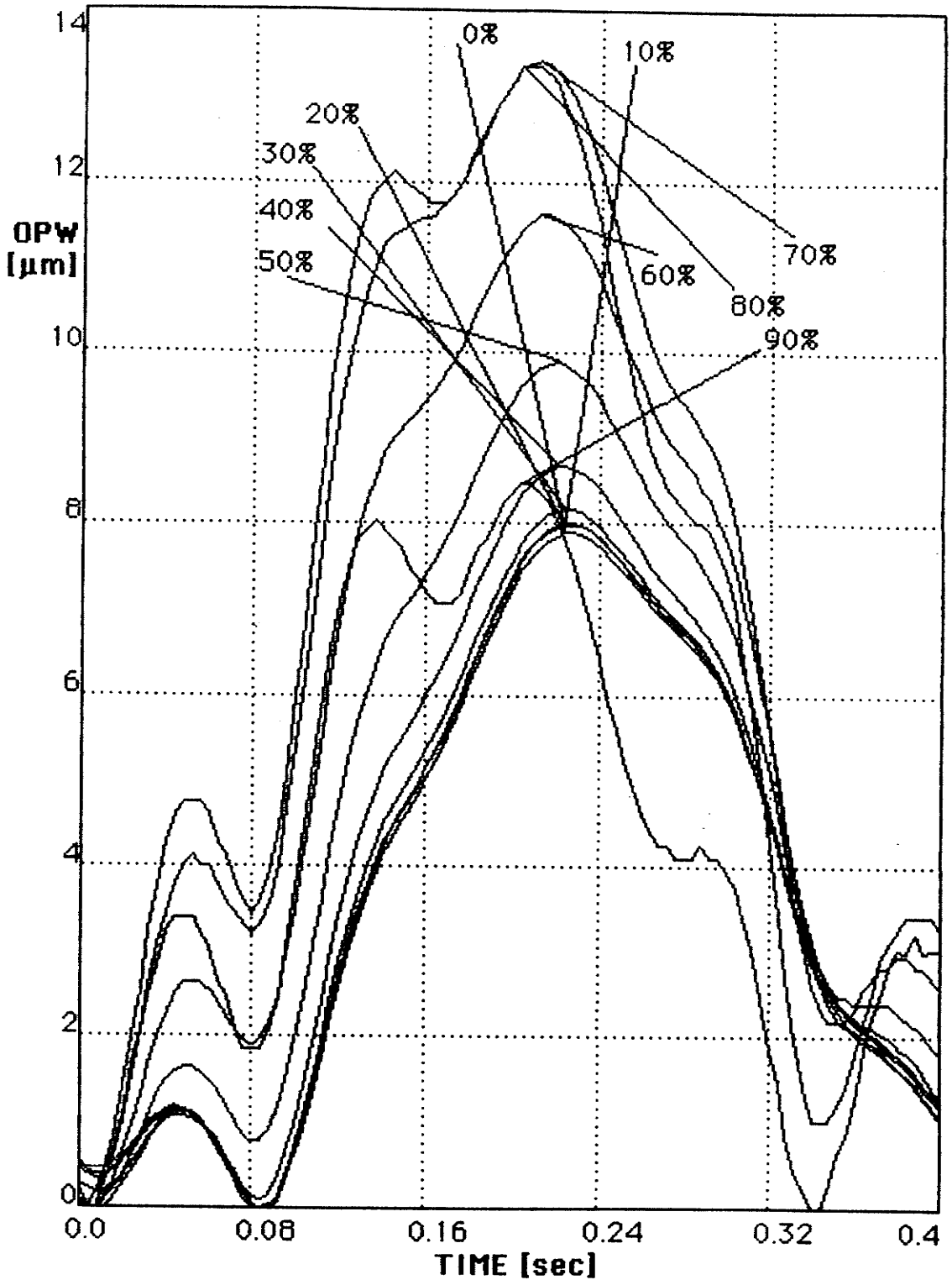

Fig. 4.1.12. OPWs as a function of stenosis severity in segment 8 of the CVS with the input ABP shown in Fig. 4.1.9a.

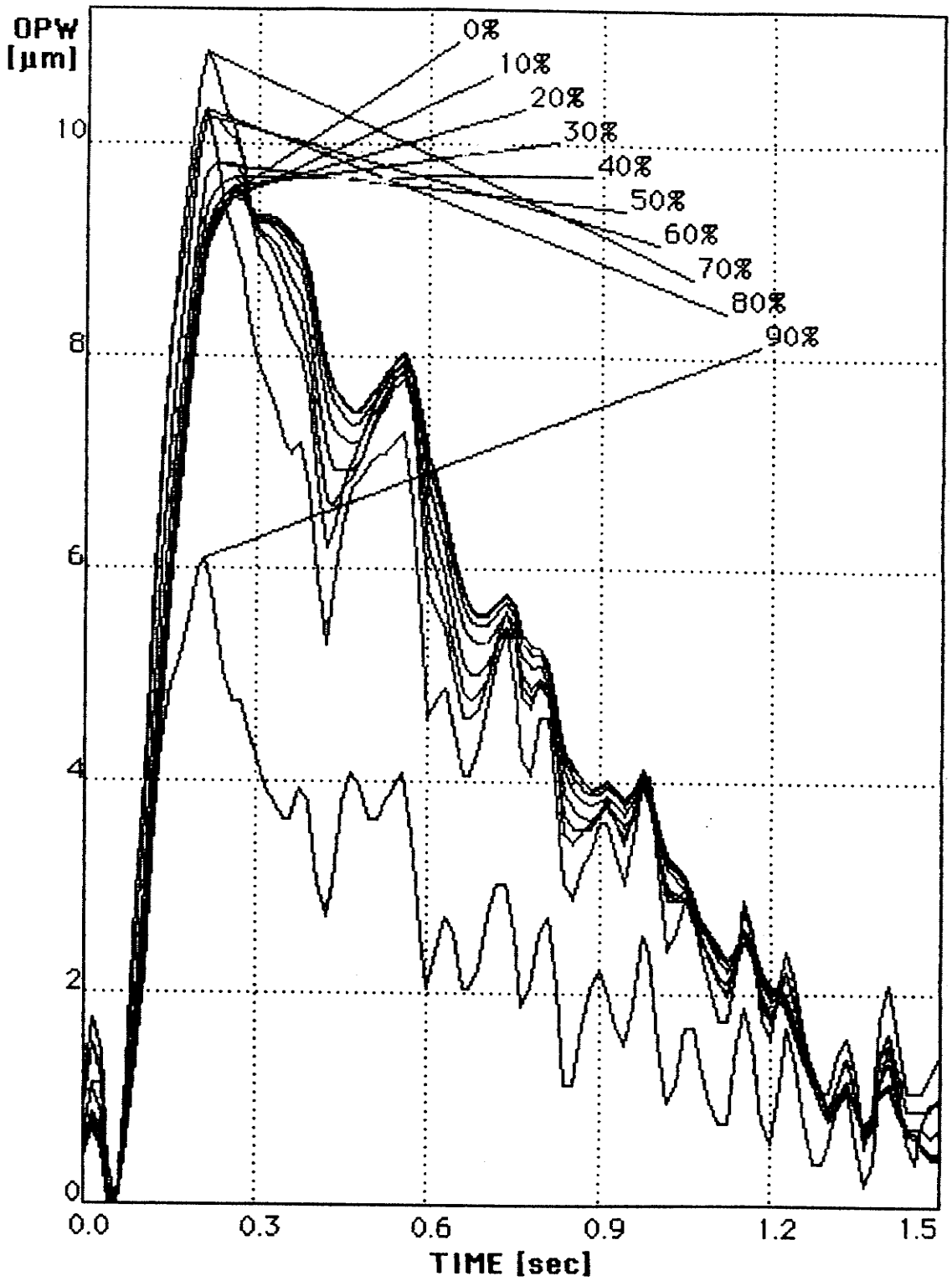

Fig. 4.1.13. OPWs as a function of stenosis severity in segment 8 of the CVS with the input ABP shown in Fig. 4.1.9b.

ABPWs were obtained (Fig. 4.1.9a and 4.1.9b). Both ABPWs have obvious frequency content change from the standard one. Systolic portion in Fig. 4.1.9a is stretched with anacrotic and catacrotic slope in this portion certainly reduced and catacrotic slope in diastolic portion increased. The opposite changing effect is shown in Fig. 4.1.9b. These apparent frequency content changes will make them have different spectral patterns, which is to be discussed in the next section.

With the two ABPWs as inputs to the system, corresponding OBPWs and OPW as outputs are shown in Fig. 4.1.10–4.1.13. As can be seen, the similar shape patterns as the ABPWs are shown in these graphs with more ripples occurring on the longer slopes as predicted.

4.1.2 Spectral Analysis of OPW

Due to the non-linear distortion from OBP to IOP and the direct relation between the ocular pulse and pulsation of IOP, the OPW amplitude does not have a clear progression pattern in order of the increasing severity levels of stenosis, and the graphic pattern of the OPW, as displayed in last section, is very complicated. This fact indicates that screening the stenosis from OPW cannot be accomplished by using graphic analysis. As mentioned before, carotid occlusion alters OPW to such a extent that spectral content in frequency domain has been changed as a function of stenosis locations and severity levels. Therefore, it is reasonable to think that frequency spectral analysis, which is more sensitive to the waveform change, could be useful to screen the stenosis.

In order to tell the difference that the carotid stenosis makes on OPW, the spectrum of OPW without stenosis was chosen as reference to be compared with other OPWs bearing the stenosis effect. In the clinical test on human subjects where the normal OPW may not be available for a particular patient, this reference can be shifted to the OPW obtained from another eye because the carotid occlusion at a single side of CVS (usually the case) is not supposed to change the OPW from another eye so that this OPW will keep unchanged throughout the stenosis development. Therefore, even although OPWs from both eyes may be different (they actually appear similar in shape [Best71c]) for the healthy CVS, the reference spectrum can still be derived from the OPW at the side of CVS without stenosis. Thus, it is practical to take, in this study, the OPW without stenosis as a reference and analyze only its difference with other OPWs bearing some level of stenosis at the same side of CVS. By using this differencing method, the obtained spectral patterns of OPWs will be more stable, not be affected by infinite variations from different patients, and therefore, universally applicable to all patients.

Since the OPW amplitude and varying range do not have a clear order in terms of their correspondence to the increasing levels of stenosis, a simple difference between magnitude spectra of the OPW with stenosis and reference (without stenosis) will not be able to reveal the true spectral difference brought in by the induced stenosis. The scaled spectrum by the relative difference of adjacent frequency points is needed to normalize all the spectra for uniform classification. The phase spectrum cannot be changed by amplitude changes of waveforms so that the simple difference between the phase spectra will be sufficient to derive patterns reflecting stenosis presence in the CVS.

Based on all these reasons explained above, a differential differencing frequency spectrum for an OPW as a function of certain level of stenosis is defined in this study, and denoted as DIF_X. For the magnitude spectrum ($MAGDIF_X(i)$), it is expressed as

$$MAGDIF_X(i) = \frac{[F_0(i) - F_0(i-1)]}{F_0(i-1)} - \frac{[F_X(i) - F_X(i-1)]}{F_X(i-1)} \qquad (4.1)$$

where F(i) is the magnitude of the discrete Fourier transform at frequency point i (or ith harmonic), Subscript "o" indicates the reference spectrum, or the transform of the OPW without stenosis, subscript "x", to be substituted for one of 9 levels of stenosis severity from 10% to 90%, indicates the spectrum of the OPW with certain level stenosis. The magnitude of the $MAGDIF_X(i)$ will truly reflect the spectrum difference between OPW with certain level of stenosis in certain segment of the CVS and the reference OPW without stenosis regardless of how the amplitudes of different individual OPWs vary within the same level of stenosis. In this way, this spectrum difference is able to indicate the different presence of stenosis in the CVS.

The differencing method can also be applied on the phase spectrum. The definition for the phase spectrum difference ($PHADIF_X(i)$) is

$$PHADIF_X(i) = P_0(i) - P_X(i) \qquad (4.2)$$

where P is the phase spectral value. With these two spectrum differences, the spectral pattern for a certain OPW can be studied for screening the carotid stenosis from OPW. This method can be further applied to all the waveforms to search for the spectrum difference.

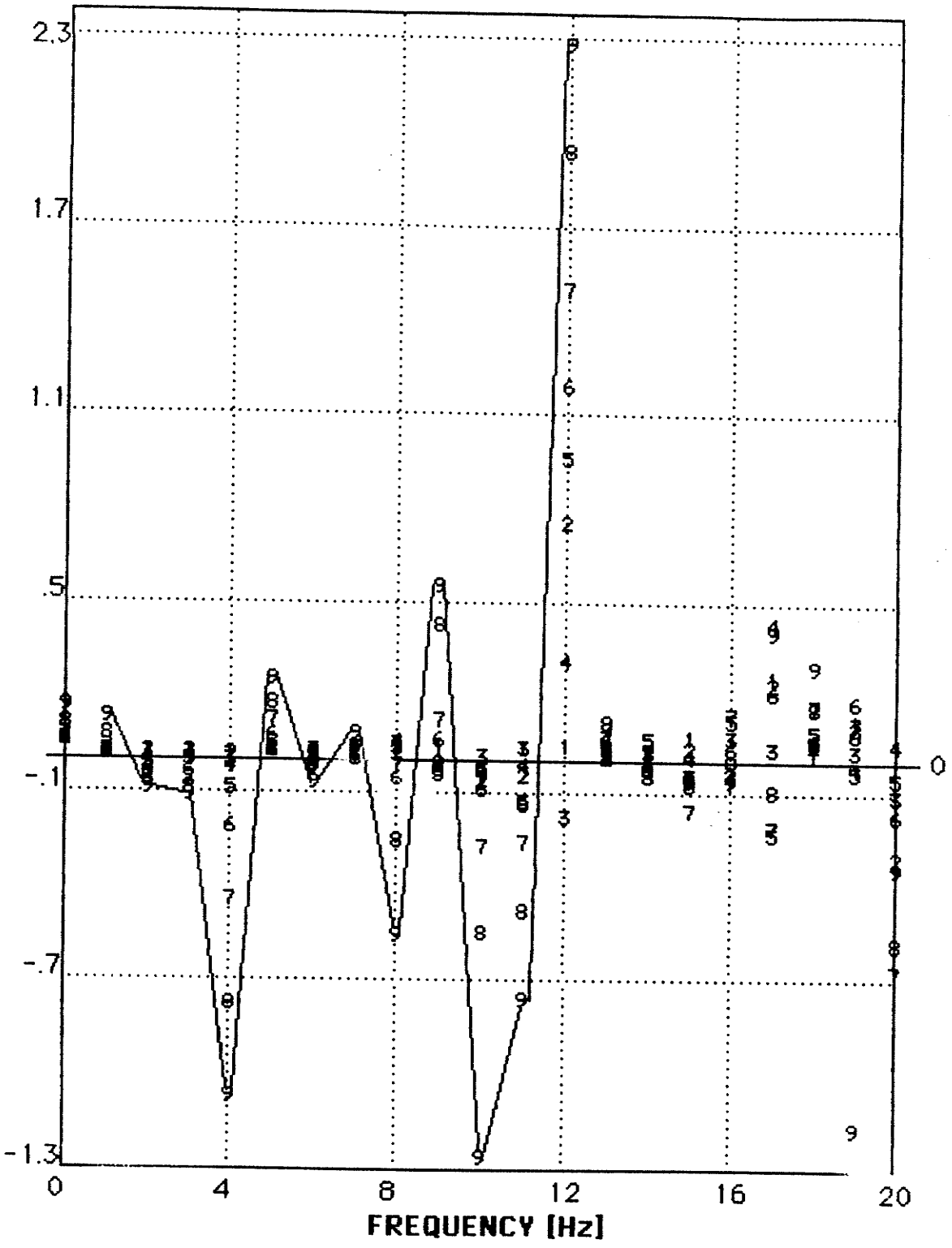

Fig. 4.1.14 MAGDIF spectrum of the OPW for CASE1, spectral points are denoted by 9 numbers corresponding to 9 levels of stenosis severity from 10% to 90%.

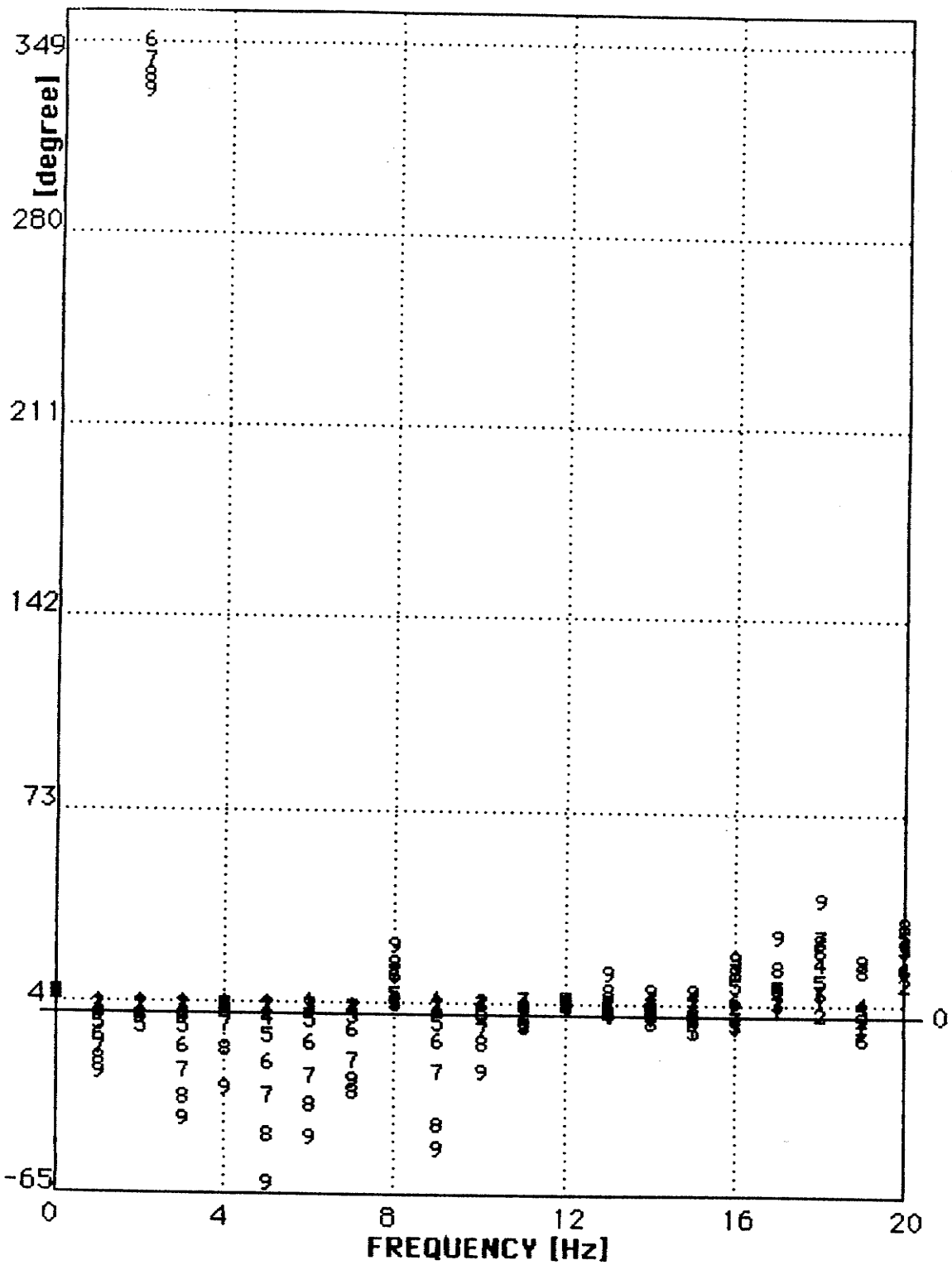

Fig. 4.1.15. PHADIF spectrum of the OPW for CASE1, spectral points are denoted by 9 numbers corresponding to 9 levels of stenosis severity from 10% to 90%.

As studied in last section, frequency spectral patterns of OPWs can be grouped in different categories: (i) 7 patterns (CASE1–CASE7) for each stenosis location in 7 segments of the CVS for stenosis displacement study. CASE8–CASE21 can be grouped with the pattern for stenosis located in segment 8, (ii) and (iii) CASE22 and CASE23 are set to two different categories due to the new frequency content introduced by ABP duration changes. Each category corresponds to each set of patterns for screening the stenosis with 10 level severity and 7 locations.

The method for finding all the patterns are developed by studying the pattern for CASE1. The $DIF_X(i)$ spectra of OPW in CASE1 are shown in Fig. 4.1.14 and Fig. 4.1.15 for both magnitude and phase spectra up to 20 Hz (or the 20th harmonic). From these two spectra, it can be seen that the frequency spectrum change as a function of stenosis severity progression. Very sensitive difference value can be traced with respect to the level of stenosis in that some frequency component is increased and others is reduced. Corresponding phase spectrum is also altered by the different level of stenosis. From these two spectra, the patterns of OPW for a specific stenosis can be investigated.

The same spectra for each cases have also been studied for the pattern exploration. By connecting the lines through each frequency point for certain spectrum (as connected lines shown in Fig. 4.1.14 for 90% stenosis) the $MAGDIF_X$ changing trend pattern for ocular pulse in each category can be obtained (Fig. 4.1.16) without considering the $MAGDIF_X$ values. The trend patterns are only examined for up to the 12th harmonic because the

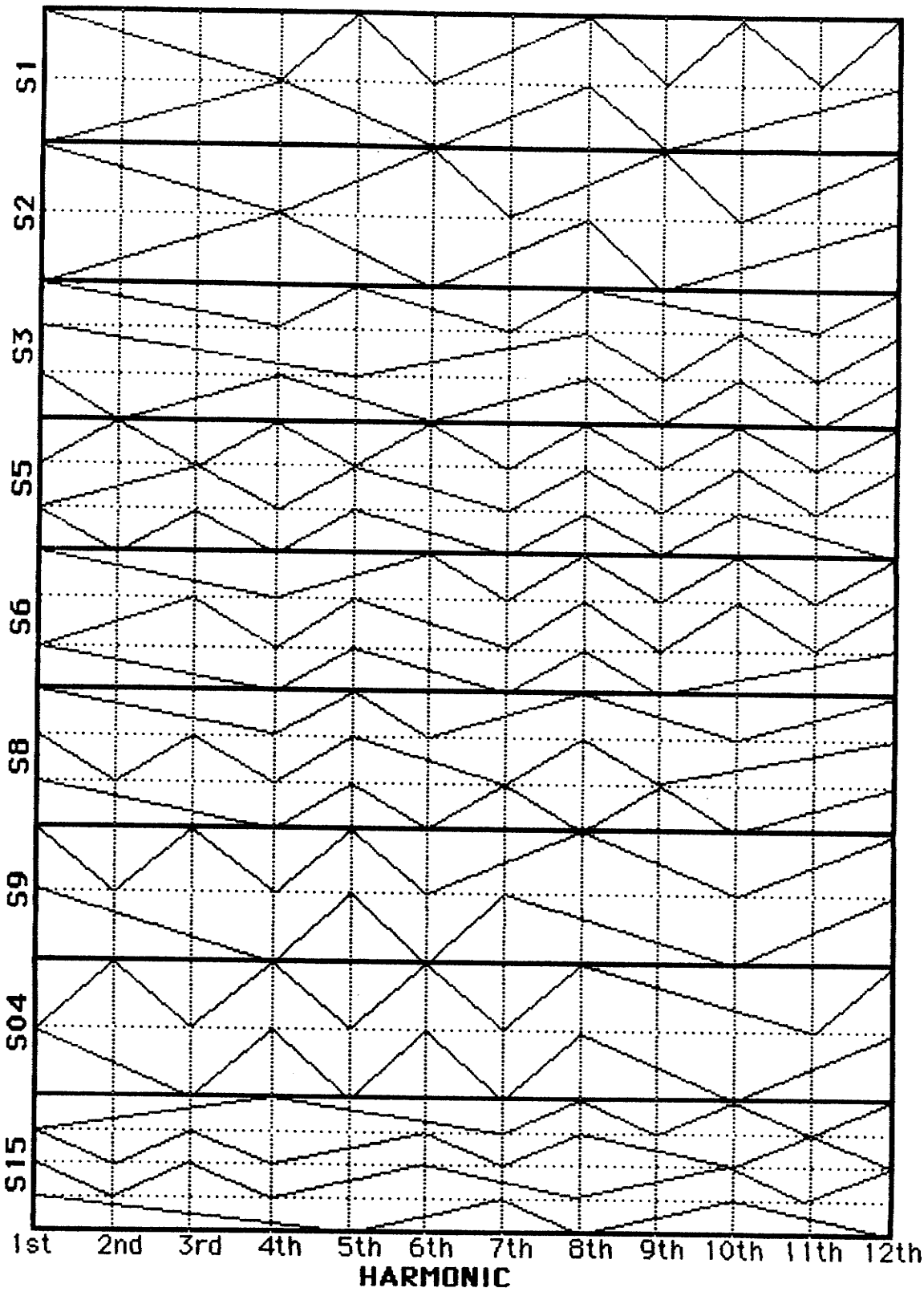

Fig. 4.1.16 Trend patterns from MAGDIF spectra for different slots.

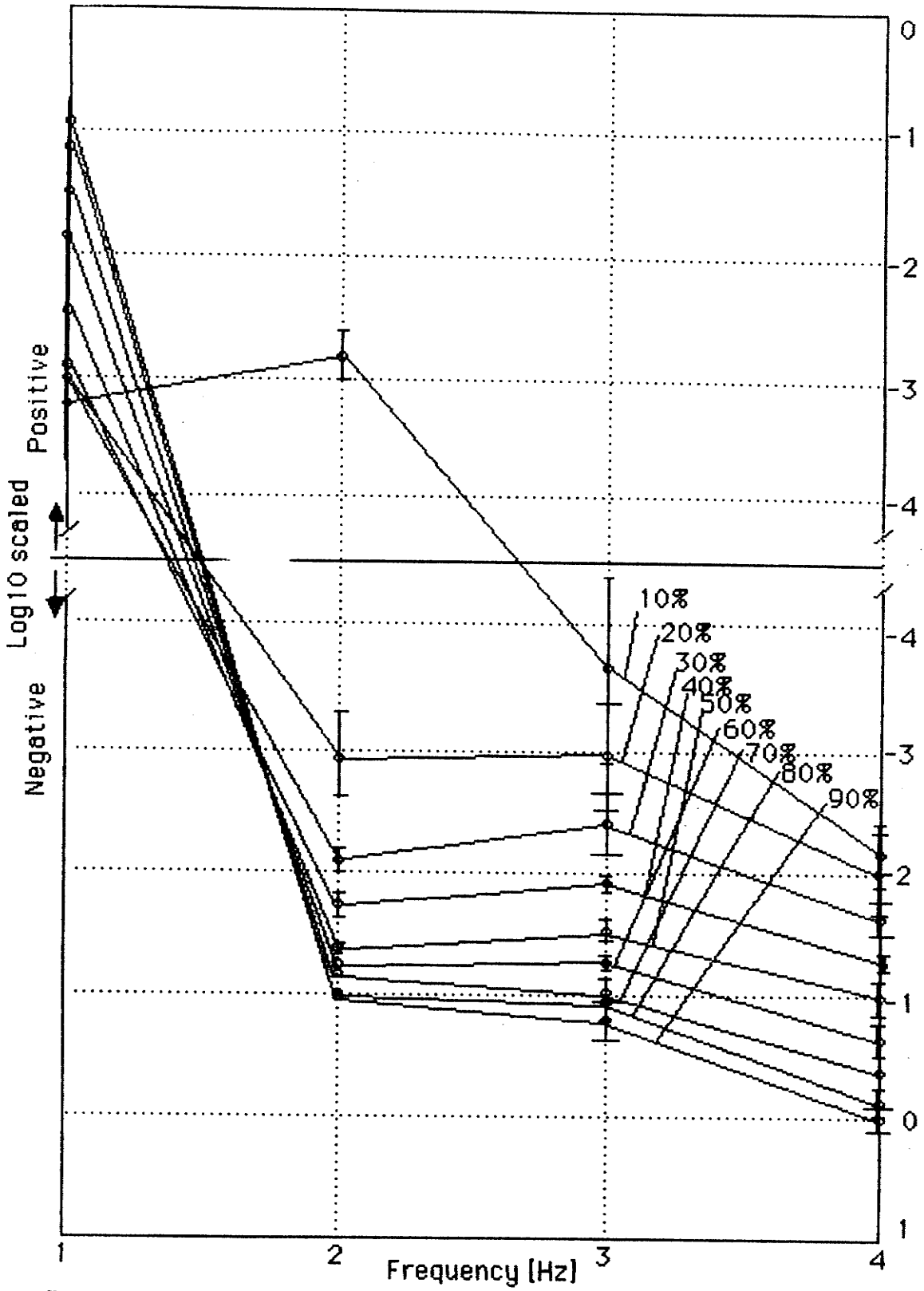

Fig. 4.1.17. MAGDIF pattern of the OPW as a function of stenosis severity for CASE1 and CASE8–CASE21, level of stenosis severity and SD for each point are marked.

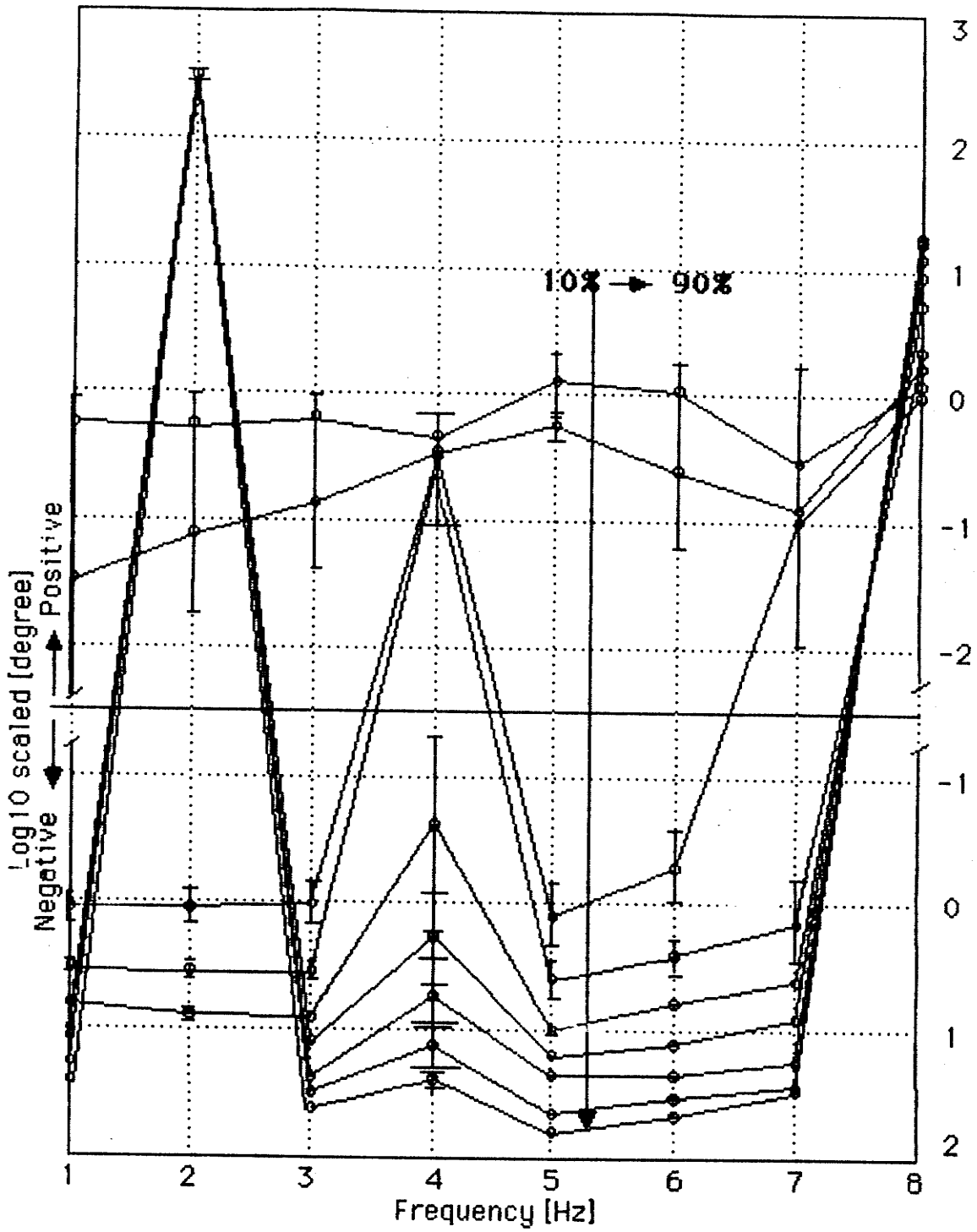

Fig. 4.1.18 PHADIF pattern of the OPW as a function of stenosis severity (progression direction marked) for CASE1 and CASE8–CASE18, SD is marked for each point.

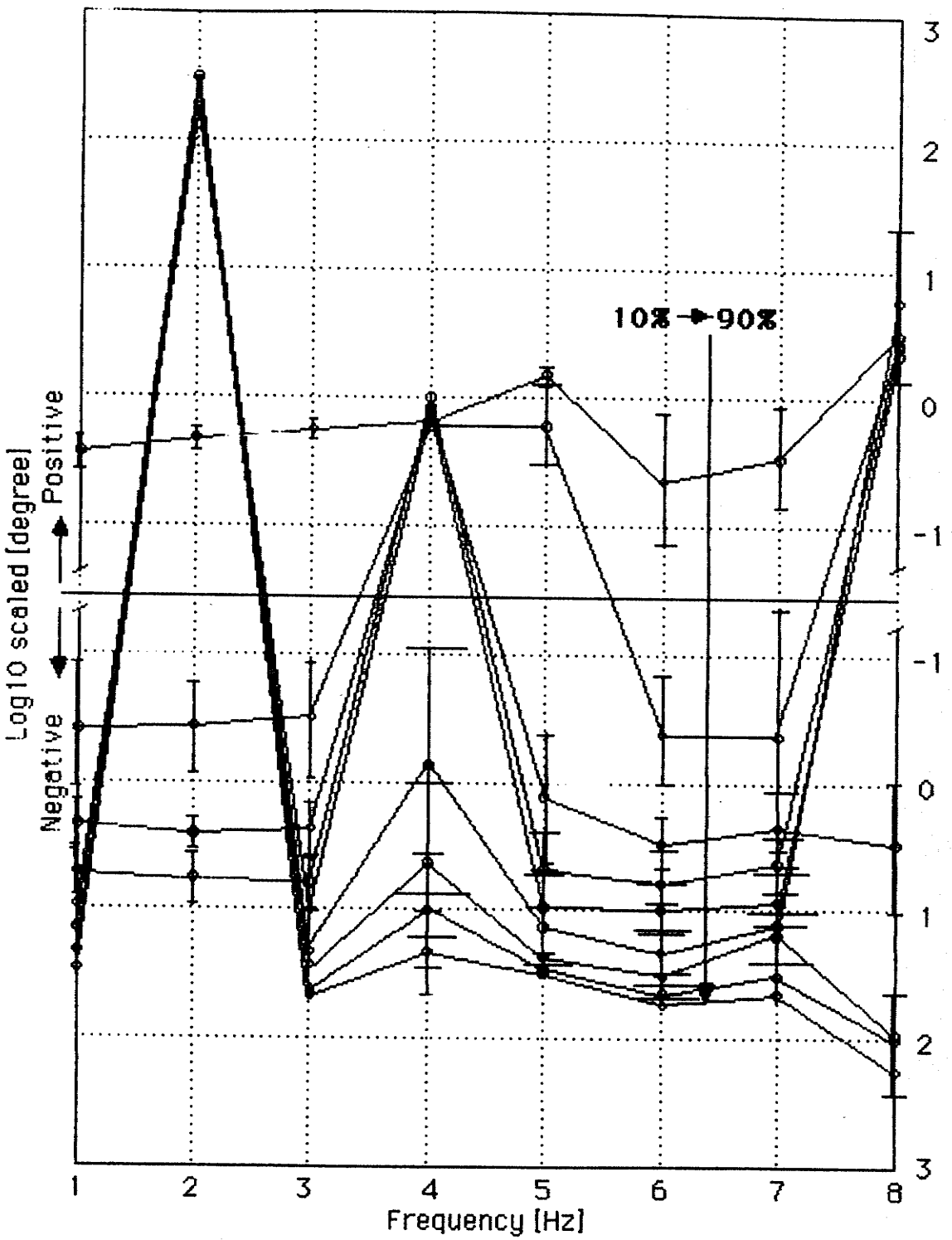

Fig. 4.1.19. PHADIF pattern of the OPW as a function of stenosis severity (progression direction marked) for CASE7 and CASE19–CASE21, SD is marked

consistency within the trends for CASE1 and CASE8–CASE21 can only be found in this frequency range. Study on these $MAGDIF_X$ changing trend patterns reveals 5 different groups with at least 4 point difference between groups and less than 3 point difference within a group. These five groups are (i) S1–S3, the common carotid stenosis, (ii) S5 and S6. the external carotid stenosis, (iii) S8 and S9, the internal carotid stenosis, (iv) and (v) S04, S15 present the internal carotid stenosis with different ABP patterns as shown in Fig. 4.1.9.

The same kind of patterns of the OPWs for CASE8–CASE21 fall into the pattern group (iii) with, at most, two different points. Pattern groups (i), (ii), and (iii) can be used to roughly classify the stenosis location as a pre-step. This pattern search method for stenosis location study can also apply to the derivative cases from CASE22 and CASE23 as the way used for CASE1–CASE21.

Patterns of the DIF_X spectra of CASE1 and its derivatives, CASE8–CASE21, have also been studied for more precise classification of stenosis with respect to its severity levels and locations. The consistency for spectrum values of these cases was found up to 4 Hz for $MAGDIF_X$ and 12 Hz for $PHADIF_X$. For the $PHADIF_X$, the patterns for CASE19, CASE20, and CASE21 fell very close to the pattern for CASE7.

To show how the DIF_X patterns of OPW are derived to classify levels and locations of the carotid stenosis, the $MAGDIF_X$ pattern for CASE1 and CASE8–CASE21, the $PHADIF_X$ patterns for CASE1 including CASE8–CASE18 and CASE7 including CASE19–CASE21 are given in Fig. 4.1.17, 4.1.18, and 4.1.19

respectively. The standard deviations (SD) are marked with a dash designating the limit for each SD. For overlaped SD, the longer dash corresponds to the spectrum for the higher stenosis. A exception is that only one bold line connecting all the spectrum points at 1 Hz of Fig. 4.1.17 without dashed limit is used to mark the SD for all the spectra due to their severe overlapping. From these spectra as a function of stenosis severity, it can be seen that the different stenosis makes pronounced difference on OPW in frequency domain. For each level of stenosis, the patterns of both $MAGDIF_X$ and $PHADIF_X$ values give a specific correspondence. Although there are SD overlapping for variation cases, the precision of classifying the stenosis severity level by these patterns can still be within the level difference of 20%, as it can be traced from these three graphs.

The DIF_X patterns for CASE1 and CASE7 may be grouped together as one to represent a pattern for stenosis located in the internal carotid of the CVS because the pattern in Fig. 4.1.18, as can be seen, is very similar to that in Fig. 4.1.19, and the $PHADIF_X$ patterns for CASE19–CASE21, as mentioned above, already fell into that for CASE7.

Now, the method has been established for exploring the OPW spectral patterns for classifying stenosis located in the internal carotid with precision of the severity level difference of 20%. The same method applies to studying on other patterns for other cases. Since results from study on other cases have also shown the same precision, the patterns presented in the following will only show the three middle level stenoses, i.e., 20%, 50%, 80%. These three levels are sufficient to cover the stenosis severity span from 10% to 90% with the established precision of the level difference of 20%.

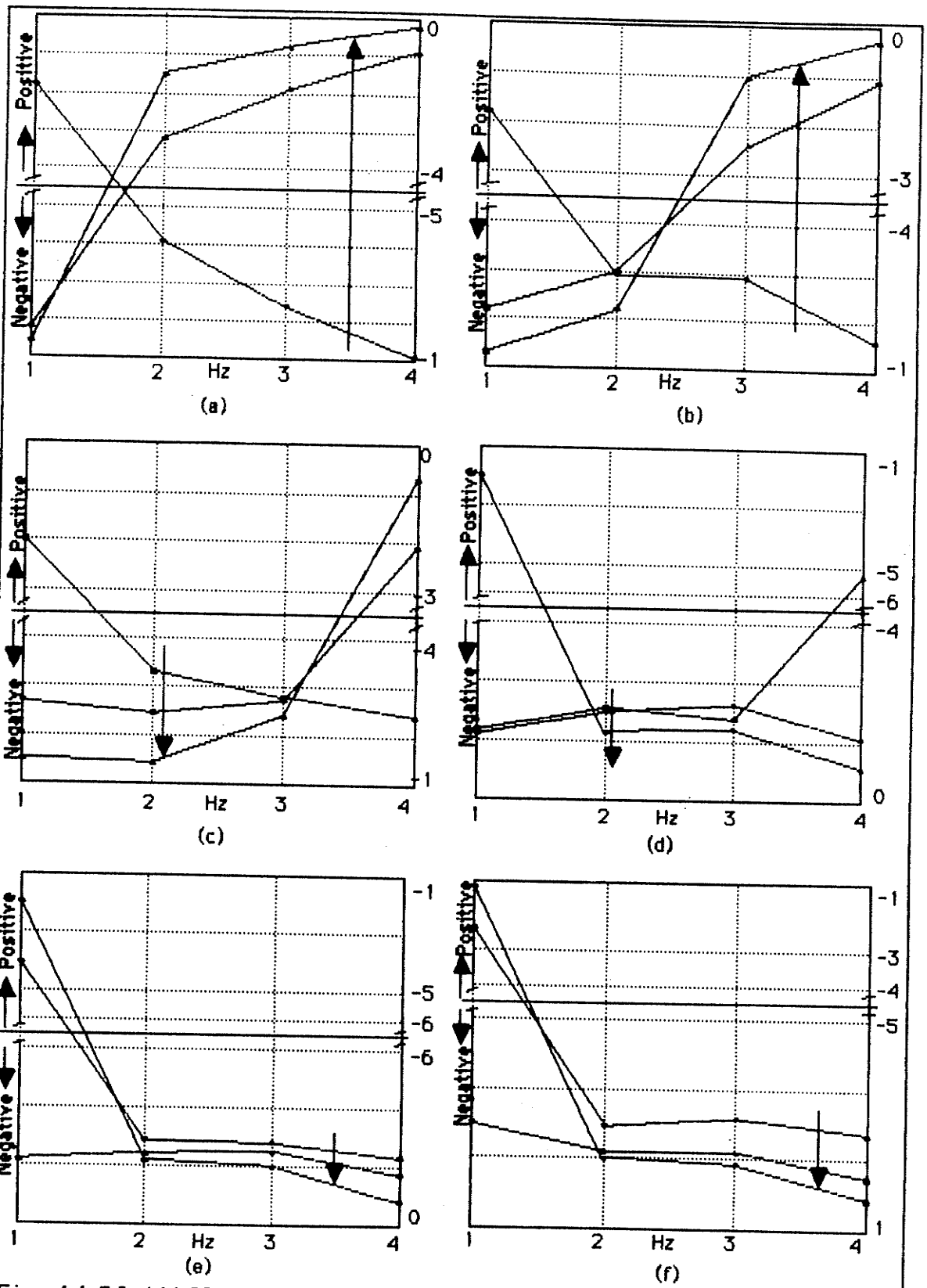

Fig. 4.1.20 MAGDIF patterns of the OPW as a function of stenosis severity in different locations, all values are log10 scaled.

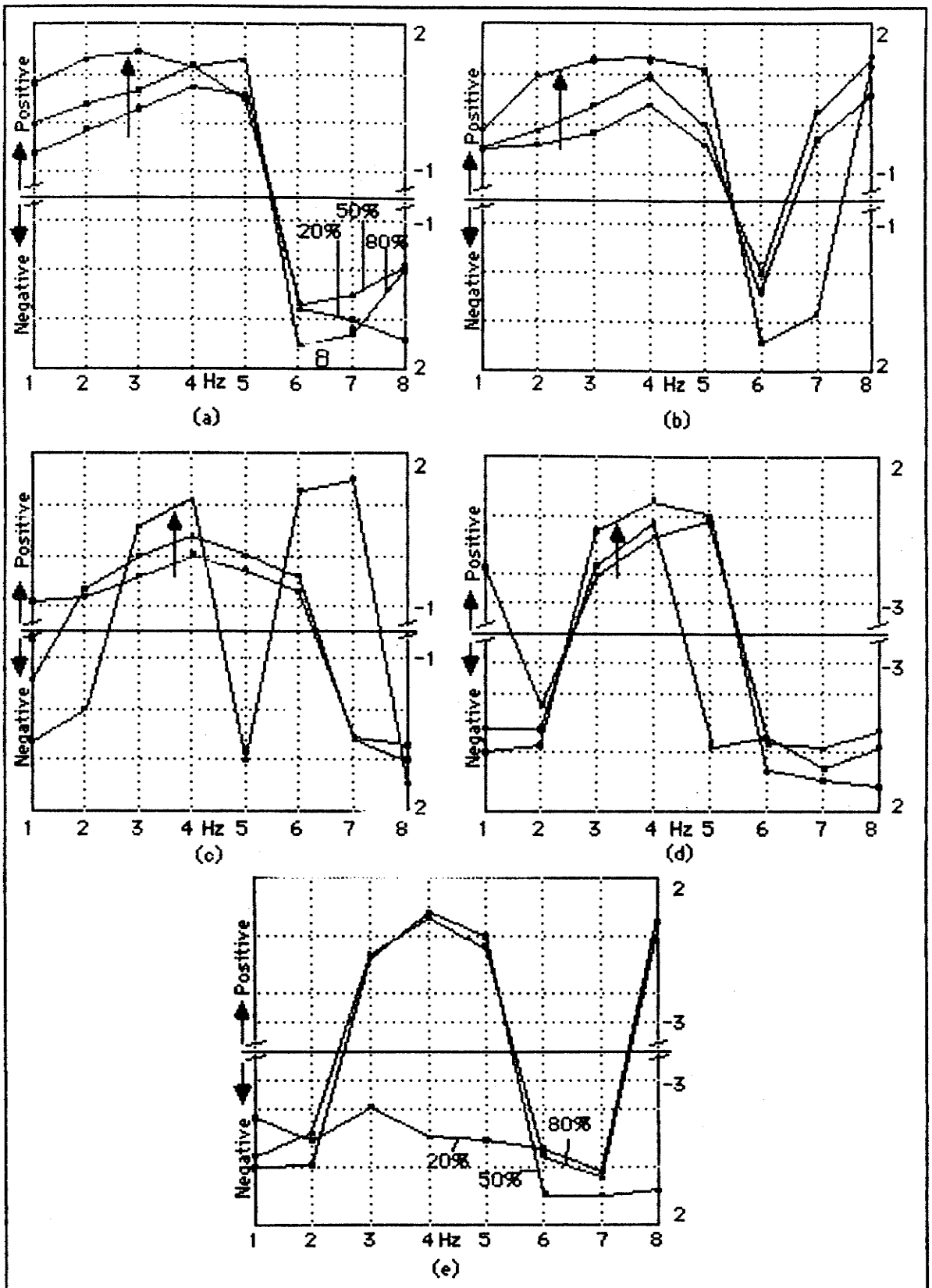

Fig. 4.1.21. PHADIF patterns of OPW as a function of stenosis severity in different locations, all values are log10 scaled.

Fig. 4.1.20 and 4.1.21 show the $MAGDIF_X$ and $PHADIF_X$ patterns of OPWs for stenosis located in segment 1 (a), segment 2 (b), segment 3 (c), segment 5 (d), segment 6 (e), and segment 9 (f). These patterns, together with patterns in Fig. 4.1.17, 4.1.18 and 4.1.19, cover all the locations where the carotid stenosis can be presented in the CVS. They clearly show the spectrum difference progression due to different stenosis severity levels (20%, 50%, and 80%). By using the DIF_X pattern (with concrete values as a function of frequency) for each stenosis severity level located in certain segment of the CVS, the severity levels and locations of the carotid stenosis can be screened from the OPWs.

It can be inspected from these patterns that some patterns appear similar both in shape and values because they represent the stenosis in adjacent segment. These patterns ($MAGDIF_X$ and $PHADIF_X$) can be classified into three groups within which the patterns are largely similar. These three groups are (i) patterns for stenosis in segment 1, 2, and 3, representing the common carotid, (ii) patterns for stenosis in segment 5, 6, representing the external carotid, (iii) patterns for stenosis in segment 8, 9, representing the internal carotid. Although similarities between $MAGDIF_X$ patterns for stenosis in segment 3 and segment 4 and 5, and between $MAGDIF_X$ patterns for segment 8 and segment 5 also exist, these similarities are eliminated in the corresponding $PHADIF_X$ patterns. Therefore, combined patterns ($MAGDIF_X$ and $PHADIF_X$) have very strong specificity for classifying certain level of stenosis (with precision of the severity level difference of 20%) located in certain part of the carotid artery (the common carotid, the external carotid, and the internal carotid).

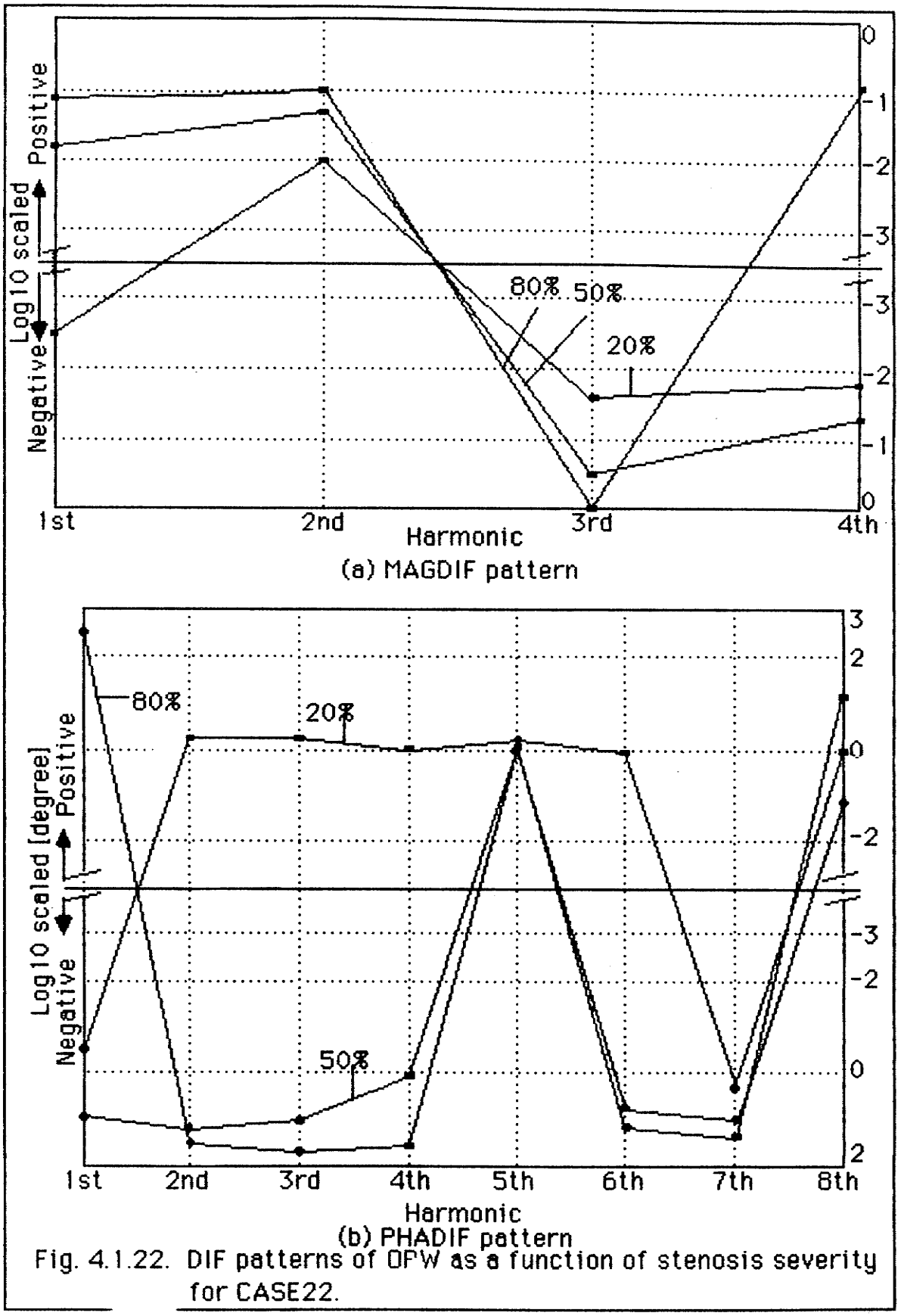

Fig. 4.1.22. DIF patterns of OPW as a function of stenosis severity for CASE22.

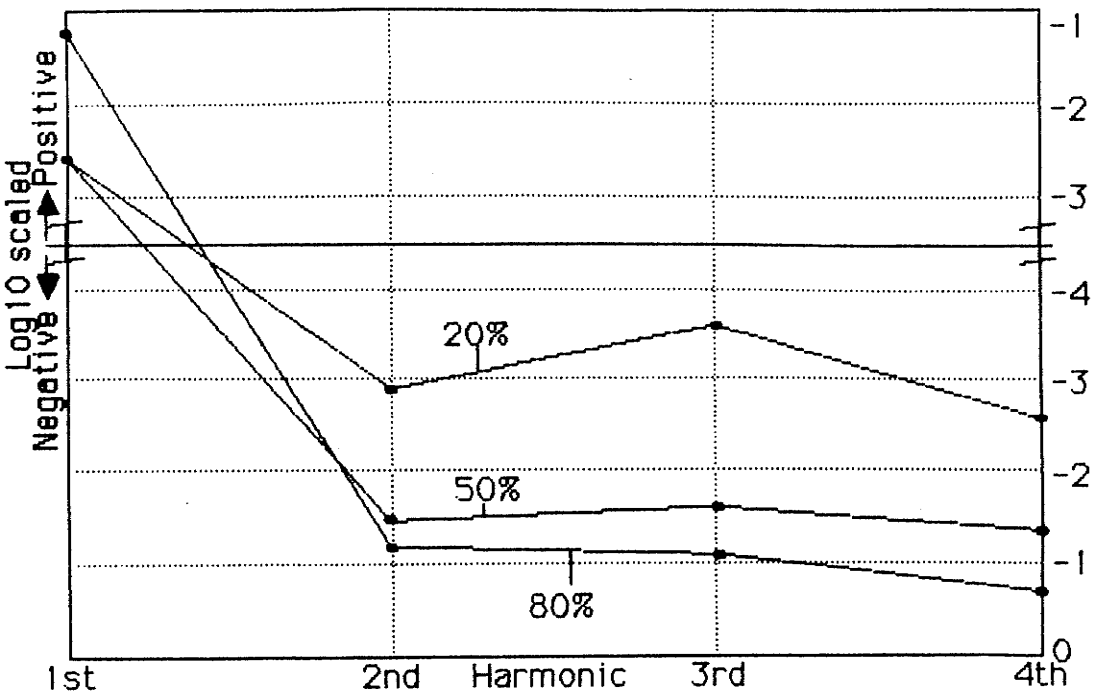

(a) MAGDIF pattern

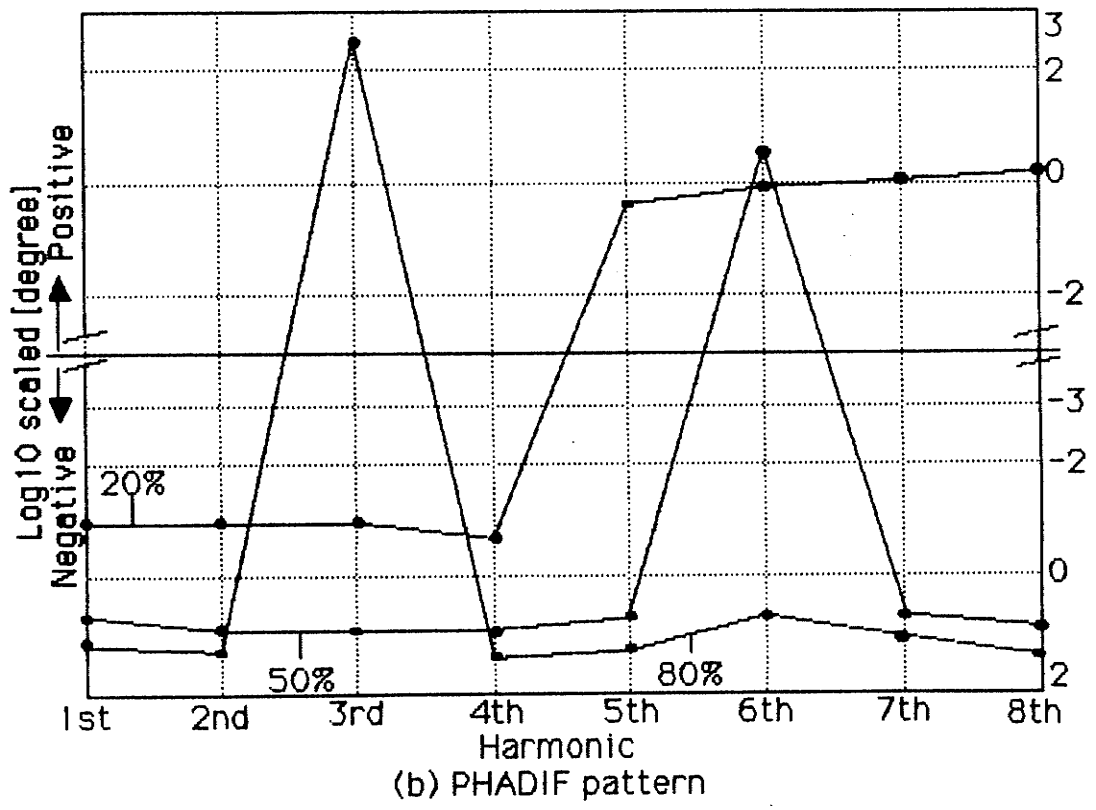

(b) PHADIF pattern

Fig. 4.1.23 DIF patterns of OPW as a function of stenosis severity for CASE23.

For the other two different categories of the patterns, Fig. 4.1.22 and 4.1.23 show the $MAGDIF_X$ and $PHADIF_X$ patterns for CASE22 and CASE23 respectively. These patterns are indeed different from any of those shown above, indicating CASE22 and CASE23 really belong to different categories. As explained earlier, the reason for the existence of different categories of patterns is that the frequency content is totally changed due to the duration pattern change of ABPWs. Therefore, for each category, the same set of patterns of OPW as in CASE1–CASE21 covering stenosis with varying levels from 10% to 90% and its location in one of the segments of the CVS can be investigated based on the patterns shown in Fig. 4.1.22 or 4.1.23. In the clinical study, the subjects should be first identified for certain category of patterns and then, screened by the patterns established for that specific category.

Finally, it should be noted that the patterns for the variation cases, expressed in CASE8–CASE21, are very similar and can be treated as one pattern, as exhibited in Fig. 4.1.17, 4.1.18, and 4.1.19. This result indicates that variations in a small range on stenosis length (CASE8 and CASE9), amplitude of ABPW (CASE10–CASE13), IOP level (CASE14 and CASE15), ophthalmic peripheral resistance (CASE16 and CASE17), and geometric parameter (CASE18–CASE21) do not make pronounced difference to the DIF_X patterns of OPW with respect to stenosis so that the patterns are quite generalized and stable for variations. This finding is expected by this pattern study which is to search for finite patterns from an infinite number of variations.

4.2 Elevated IOP

Glaucoma is characterized by abnormally high IOP, or elevated IOP. In the equilibrium state of the eye, the intraocular pressure is maintained at a nearly constant level 15–20 mmHg with variation 1–2 mmHg [CoWe80], as shown earlier. Abnormally elevated IOP may result in an inadequate blood supply to the nerve fiber in the retina, causing collapse of the corresponding blood vessels, or blindness. Visual loss resulting from glaucoma cannot be restored. Present therapy is to maintain the IOP at a level which does not cause further damage to the optic nerve [CoWe80]. Therefore, outpatient screening of elevated IOP is specially important in preventing the disease, glaucoma. Although the elevated IOP is not always sufficient for impairment of blood supply to the nerve fiber, screening the elevated IOP is still helpful and plays an major role in diagnosing the potential glaucoma with other clinical conditions [ChKu73].

For examining the sensitivity of OPW to the IOP levels, the mean IOP (P_{im}) in the eye model is forced to be elevated from 15 to 40 mmHg (Table 4.2.1). Corresponding vascular volume is calculated through Eq. 3.3.25 with the standard OBP as shown in Fig. 3.1.12. As can be seen, the ocular vascular volume is reduced with the increasing levels of the mean IOP because the elevated IOP reduces the transmural pressure ($P_a - P_i$). This corresponding relationship can be examined through the vascular rigidity function as stated in Eq. 3.3.3. According to the IOP and vascular volume (Va) values in Table 4.2.1 with the mean value of OBP (P_a) in Fig. 3.1.12 equal to 55.5 mmHg, the relationship between transmural pressure ($P_a - P_i$) and ocular vascular volume (V_a) is plotted in Fig. 4.2.1. This relationship is very consistent with

Table 4.2.1 IOP level and ocular vascular volume

IOP [mmHg]	Volume [µl]
15	32.37
20	30.00
25	27.85
30	25.18
35	22.06
40	18.38

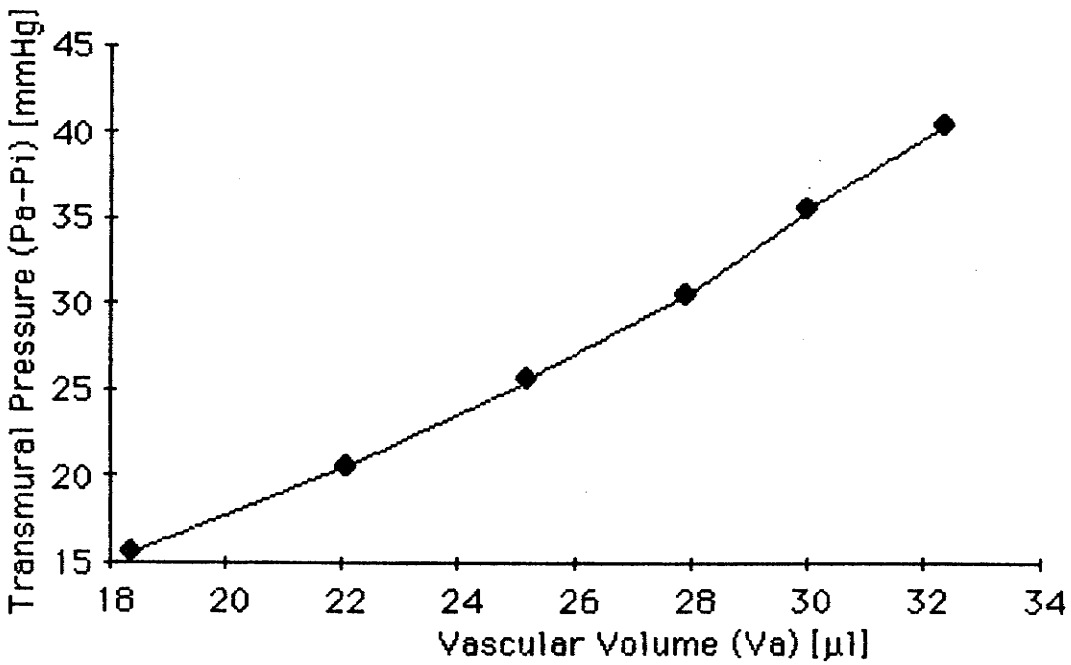

Fig. 4.2.1 Relationship between transmural pressure and ocular vascualr volume.

previously published result in [Best71d], where the vascular rigidity function (VR) was studied.

To examine the pulsation of IOP, the OBP–IOP relationship for the elevated IOP has also been investigated, shown in Fig. 4.2.2 in which the IOP level is elevated with the constant level of OBP and pulsation from about 2 mmHg for normal IOP to about 8 mmHg for high level of IOP. The OPW corresponding to each level of the elevated IOP is given in Fig. 4.2.3, in which the effect of elevated IOP on OPW is clearly reflected. As the IOP level is elevated from 15 to 40 mmHg, the ocular pulse amplitude is increased from about 10 to about 50 μm. Previous study in [Horv70] has shown that the ocular pulse amplitude was increased to 28 μm after the IOP level was elevated to 30 mmHg. Similar result can be found in Fig. 4.2.3, where the ocular pulse amplitude is 25 μm at the IOP level of 30 mmHg.

Although the OPWs in Fig. 4.2.3 show a clear amplitude progression as a function of elevated IOP, it may be still necessary to investigate the spectral patterns for each OPW in frequency domain for a more precise and better classification. The method for exploring DIF_X pattern of OPW, used in last section in studying the effect of stenosis, also applies to exploring the DIF_X pattern of OPW with respect to the elevated IOP levels.

Fig 4.2.4 and 4.2.5 show the $MAGDIF_X$ and $PHADIF_X$ spectra of OPW as a function of IOP levels. They demonstrate clearly that the elevated IOP levels have the pronounced effect on the OPW spectrum, the clear progression as a function of elevated IOP levels for each frequency component. Therefore, it is very possible to extract a clear pattern from these spectra for screening

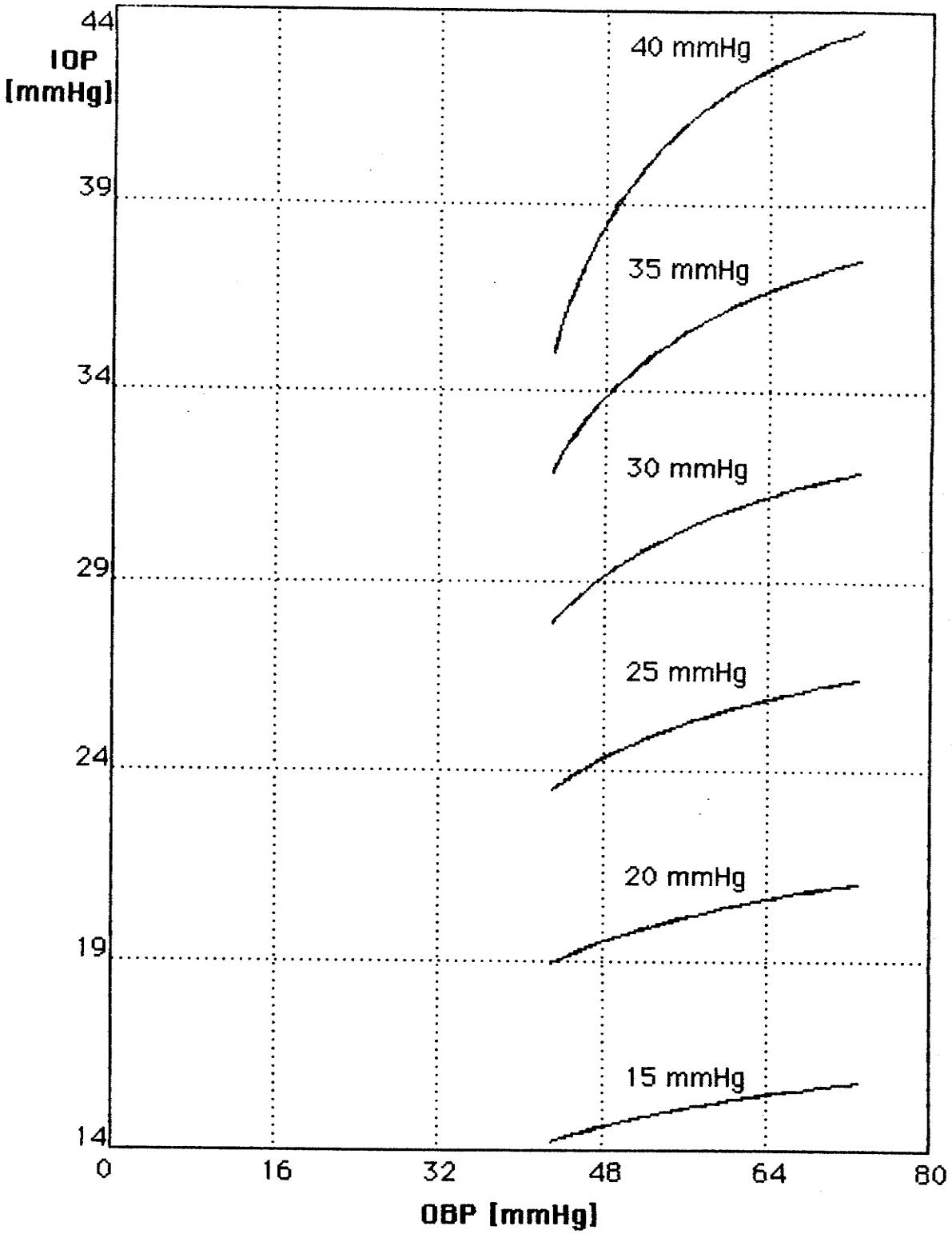

Fig. 4.2.2. OBP-IOP relationship as a function of the elevated IOP, a constant level of OBP is 55.5 mmHg, and the elevated IOP levels marked above each curve.

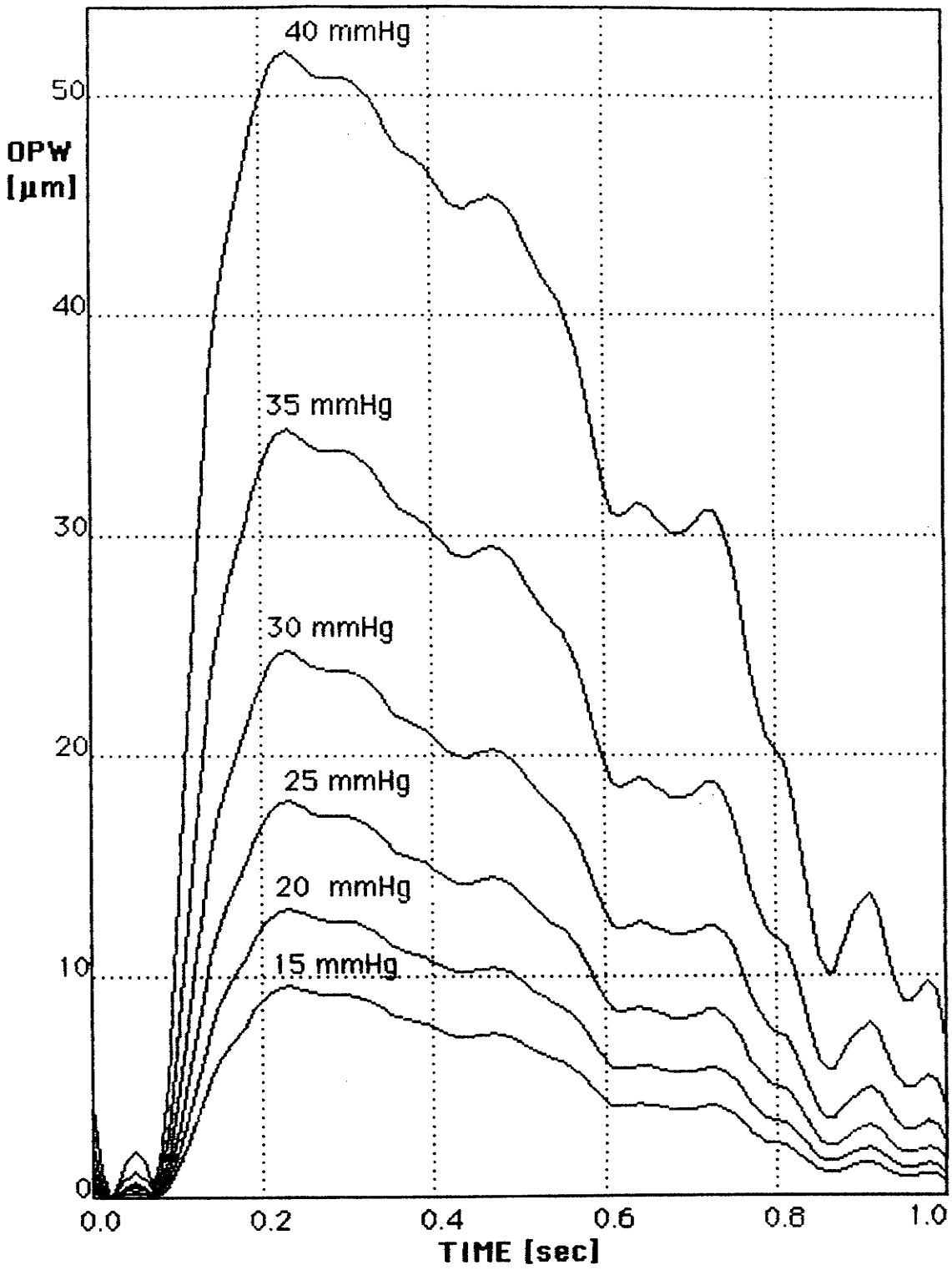

Fig. 4.2.3. OPWs as a function of IOP levels, marked above each curve.

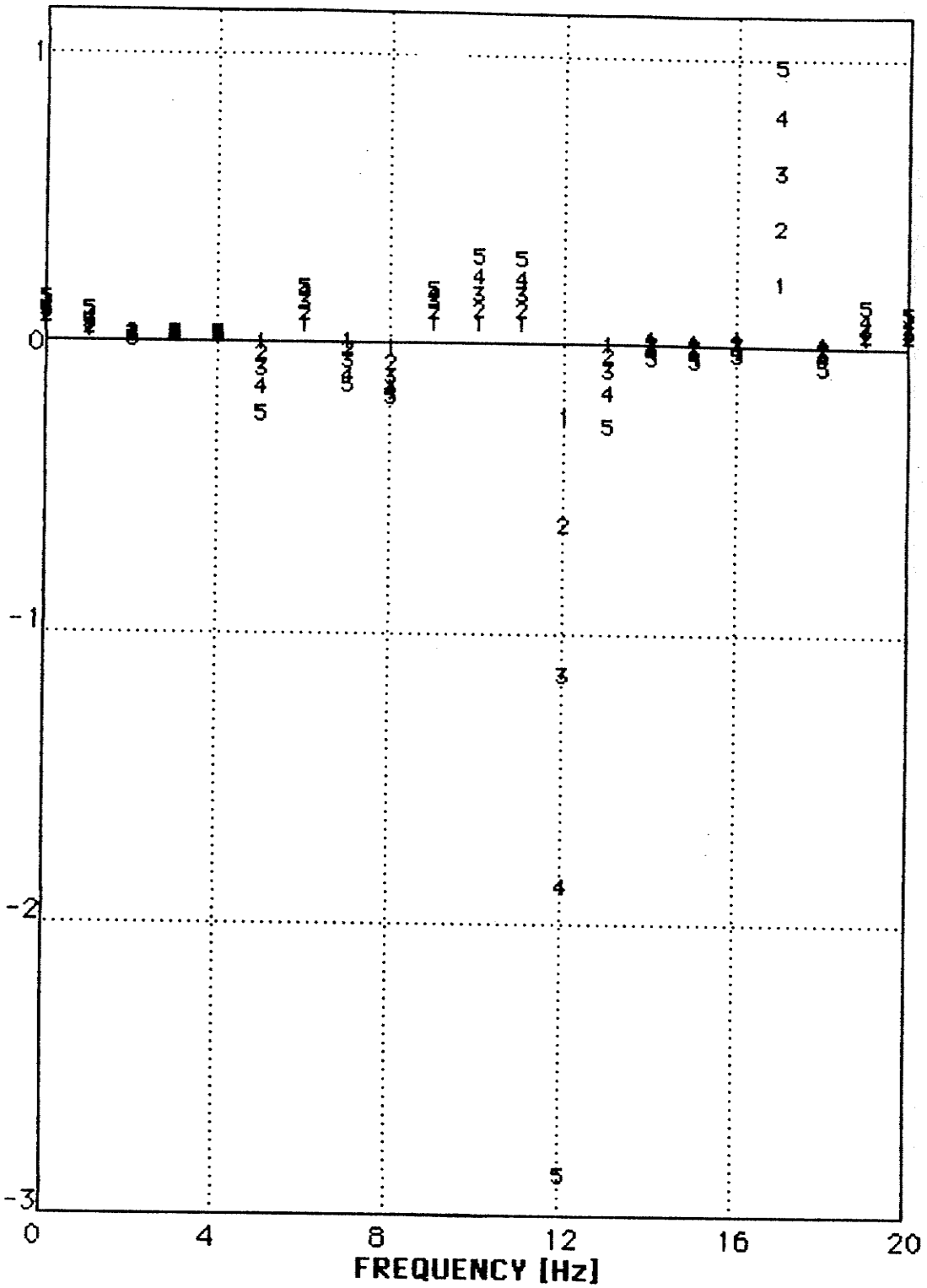

Fig. 4.2.4 MAGDIF spectrum of the OPW as a function of IOP levels, spectral points are denoted by 5 numbers corresponding to 5 elevated IOP levels from 20 to 40 mmHg.

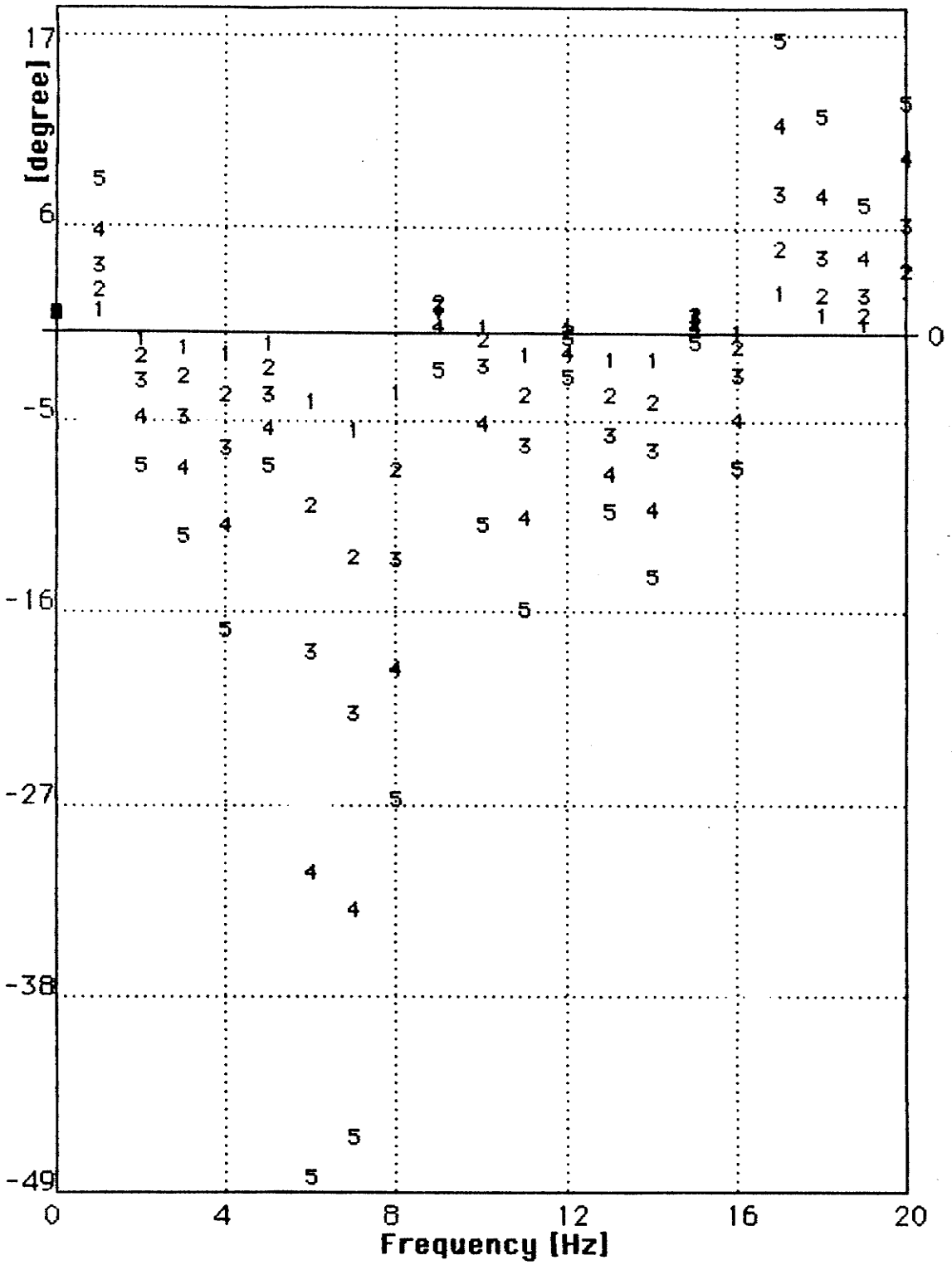

Fig. 4.2.5 PHADIF spectrum of the OPW as a function of IOP levels, spectral points are denoted by 5 numbers corresponding 5 elevated IOP levels from 20 to 40 mmHg.

the elevated IOP from OPW.

4.3 Summary

Based on the ocular pulse system model described in last chapter, the sensitivity study with respect to both stenosis and elevated IOP levels is proceeded in this chapter. Spatial analysis of OBP, IOP, OPW shows that results from this system are largely comparable with previous published results, while revealing new patterns of OBP and OPW with respect to both stenosis and IOP levels. The OPW can be effectively analyzed and described by the spectral pattern in frequency domain. A new differential differencing method (DIF_X) based on the spectrum of OPW is defined and implemented in the OPW pattern exploration with respect to both stenosis and elevated IOP levels. The results showed that the stenosis severity level from 10% to 90% with precision of the level difference of 20% can be screened from DIF_X pattern of OPW with its location in one of sections (the common, external, internal carotid) of the CVS. The IOP level may also be analyzed from OPW both in spatial and frequency domain based on the same method used in studying on stenosis.

CHAPTER V

CONCLUSIONS AND RECOMMENDATIONS

Stroke and glaucoma are of major concern to preventive medicine. Screening the plausible causes of the two diseases, stenosis and elevated IOP, is of great importance for preventing the development of the diseases. It is possible to find a single screening technique through an analysis of OPW for screening both the carotid stenosis and elevated IOP within the eye because the previous studies have shown their interrelationships with the OPW [Best], [Mow68]. Previous techniques and methods for screening the blood vessel narrowing (a stenosis) and measuring the IOP and OPW from the eye have proved to be either inaccurate or not reliable and simple enough to apply to the outpatient screening. A new accurate technique, based on a non-contact laser interferometry method [JuKi84b], suitable for outpatient screening, has been selected as the one to measure the OPW with the resolution less than 0.1 μm. The ultimate goal of this research work is to establish a non-contact, non-invasive, reproducible, economical, outpatient method for early screening of the stenosis and the elevated IOP.

Following the selected methodology to the goal of this research, the model of the overall ocular pulse system has been developed [JuKi84a, Jul184a] and improved in this thesis work, including the models of the CVS, stenosis, and the eye. The method of achieving the OPW analysis in this thesis with respect to the stenosis and IOP is: (i) modelling of the CVS to obtain the output of OBP, (ii) integrating a stenosis model to achieve OBPWs bearing the information on both locations and severity level of stenosis for stenosis study, and then, (iii) by embedding the eye model with the CVS, OPW

is analyzed with respect to either the carotid stenosis or the IOP levels.

Results from this study have revealed that:

1. The present CVS model is of different specificity from the previous models for systemic arterial tree. This model is specially intended to clearly exhibit the OBP regulation, and has the explicit expression (state equations) for its behavior so that the system modification and incorporation of both stenosis and eye models can be easily proceeded.

2. The validity of the CVS model is shown through its stability, accuracy, sensitivity to degrees of the model, and linearity of the system. The eigenvalues (Table 3.1.4 or 3.1.5) and step response (Fig. 3.1.9 or 3.1.10) of the CVS have been studied to confirm that the CVS model is stable, and the numerical solution converges after 5 sec to a expected output OBP level at 75 mmHg with an error of less than 1 mmHg. Since repeated solutions of the CVS are required in the study of the overall ocular pulse system, and computation with the 22nd degree CVS model is time-consuming, the 22nd degree has been reduced to the 14th degree. The 14th degree model preserves the same structure and frequency response bandwidth of the CVS as the 22nd degree model. The corresponding eigenvalues and step responses of the two models are similar, indicating that the 14th degree model contains most of the fundamental frequency components of the 22nd degree model. The OBP spectral difference in Fig. 3.1.15 shows that the difference between frequency components of the OBP outputs from the two models is mostly less than 10^{-1}. It has also been proved that the numerical method for the solution of the CVS does not introduce nonlinearity because the

difference between the impedance transfer function and its numerically obtained counterpart (Fig. 3.1.16) is less than 0.078 for each frequency component.

3. The stenosis model can be integrated into a certain segment of the CVS model. The relationship between the OBP output of the CVS and the IOP (level and pulsation) within the eye can be obtained from the eye model. According to the cornea model, the ocular pulse is driven by the pulsation of IOP so that the OPW can be analyzed with respect to its relationship with either the stenosis (severity levels) located in a certain place (the common carotid, the external carotid, the internal carotid) of the CVS, or the elevated IOP levels. The results about the stenosis effects, OBP, IOP, and OPW amplitudes are comparable with the previously published results.

4. The OBP and IOP levels are systematically reduced by the stenosis severity progression located in different parts of the CVS. The results for the OPW analysis have also shown that OPW is very sensitive to both stenosis (severity and location) and IOP levels in a complicated fashion.

5. The OPW is altered by either stenosis (severity and location) or IOP level to such an extent that the analysis of its sensitivity to these two effects has to be fulfilled in its frequency spectral domain by a differential differencing method.

6. Spectral analysis based on the differential differencing method has shown that (i) the OPW is sensitive to the severity level of carotid

stenosis from 10% to 90% with precision of level difference of 20%, (ii) locations of the carotid stenosis (the common carotid, the external carotid, and the internal carotid) can also be traced from the spectrum of the OPW, (iii) the different levels of IOP from 15 to 40 mmHg can be displayed from analysis of OPW both in spatial and frequency domains.

The key contributions of this thesis are:

(i) Studied the previous models for the systemic arterial tree, and improved the presently used CVS model for the OBP regulation, which was shown to have more proper specificity and easier ability for incorporation of models for both stenosis and eye.

(ii) Clarified and confirmed the validity of the CVS model in terms of its stability, accuracy, sensitivity to degrees of the model, and linearity of the system.

(iii) Established standard ways for the system analysis, and largely compared the basic system outputs (e.g., OBP, IOP, OPW) with previous reported results so that it can be shown that the system performs closely to reality.

(iv) Further developed and improved the present stenosis model for its coefficient modification, integration in the CVS, and study on either its own analysis (index numbers) or the displacement along the CVS.

(v) Further developed and improved the present eye model for its formulation and OBP-IOP relationship with respect to the different

stenosis severity levels.

(vi) Defined a differential differencing method for the OPW spectral analysis which is able to reveal the sensitivity of OPW to either stenosis (severity and location) or levels of IOP. This is specially important for future screening of stenosis and elevated IOP.

(vii) Extensive spectral analysis of the OPW in this study provides a basis for implementing other techniques used in signal analysis. The developed pattern recognition methods and artificial intelligence (AI) technologies can be merged with the results of this work to facilitate the further clinical study.

Further work required for this research topic is recommended as follows:

(a) Open-loop nature of the present model can be considered as a major limitation of the model. The future work should concentrate on a closed-loop model which includes the influence of the stenosis and IOP back on the CVS and ABP.

(b) Other than its severity levels and locations, the stenosis should be further studied with respect to kinds of deposits and relationship between the shape of stenosis and the blood flow past the stenosis.

(c) Detection of simultaneous existence of the stenosis and elevated IOP should be studied.

(d) Other techniques of signal analysis, pattern recognition methods, and AI technologies should be further studied to establish a intelligent information system for the ocular pulse screening of stenosis and elevated IOP.

(e) Development of an accurate, non-contact screening apparatus based on a laser interferometry method for measurement of OPW to be used in a clinical study for the early screening of both stenosis and elevated IOP.

REFERENCES

[Adle65] Francis H. Adler, Physiology of the Eye. Saint Louis: The C. V. Mosby Company, Fourth Ed., 1965.

[Best70] M. Best, T. A. Kelly, and M. A. Galin, "The ocular pulse-technical features," Acta Ophthalmol., vol. 48, pp. 357-368, 1970.

[Best71a] M. Best, R. Pola, G. Plechaty, S. Masket, and M. A. Galin, "Ocular pulse studies in carotid stenosis: Relationship to carotid hemodynamics," Arch. Ophthalmol., vol. 85, pp. 730 - 737,1971.

[Best71b] M. Best, "Carotid hemodynamics and the ocular pulse in carotid stenosis", Neurology, vol. 21, pp. 982-990,1971.

[Best71c] M. Best, M. Keyes, and G. Plechaty, "Graphic analysis of the ocular pulse in carotid occlusion," Arch. Ophthalmol., vol. 85, pp. 315-319,1971.

[Best71d] M. Best, A. Z. Rabinovitz, R. Pola, and S. Masket, "Vascular distensibility in the eye," Arch. Ophthalmol., vol. 86, July 1971.

[Best73] M. Best, D. Gerstein, N. Wald, A. Z. Rabinovitz, and G. J. Hiller, "Autoregulation of ocular blood flow," Arch. Ophthalmol., vol. 89, pp. 143–148, 1973.

[Best74] M. Best and R. Roger, "Techniques of ocular analysis in carotid stenosis," Arch. Ophthalmol., vol. 92, pp. 54-58, July 1974.

[BhMG82a] B. K. Bharadvaj, R. F. Mabon and D. P. Giddens, "Steady flow in a model of the human carotid bifurcation. Part I – Flow visualization," J. Biomechanics, vol. 15, No. 5, pp. 349–362, 1982.

[BhMG82b] ___, "Steady flow in a model of the human carotid bifurcation. Part II – Laser Doppler anemometer measurements," J. Biomechanics, vol. 15, No. 5, pp. 363–378, 1982.

[Bill75] A. Bill, "Blood circulation and fluid dynamics in the eye," Physiol. Rev., vol. 55, pp. 383–417, 1975.

[Bron86] Joseph D. Bronzino, Biomedical Engineering and Instrumentation - Basic Concepts and Applications., Boston, Mass.: PWS Publishers, 1986, p. 79.

[Chen83] Wai-Kai Chen, Linear Networks and Systems. New York: Brooks/Cole, 1983, pp. 41-124.

[ChKu73] S. Chokhani and C. A. Kulikowski, "Process control model for the regulation of intraocular pressure and for glaucoma," in Proceeding of Int. Conf. on Cybern. and Soc. (Boston, Mass, Nov. 5-7, 1973), pp. 305–310.

[CKKJ81] U. J. Chaput, J. Kinsner, W. Kinsner, and M. Jullian, Presentation of a Research Proposal For Ocular Pulse Measurement and Diagnosis Method to Mrs. James A. Richardson Foundation and the Winnipeg

Foundation. Manitoba, Canada: IAMC Publication, June 16, 1981.

[CoWe80] Richard Collins and Terry J. Van der Werff, Mathematical Models of the Dynamics of the Human Eye. Berlin, Germany: Springer-Verlag Berlin Heidelberg, 1980.

[FoMc78] R. W. Fox and A. T. McDonald, Introduction to Fluid Mechanics. New York: John Wiley and Sons, 1978.

[Gree78] J. H. Green, Basic Clinical Physiology. New York and Toronto: Oxford University Press, Third Ed., 1978, p. 5.

[Horv70] I. Horven, "Dynamic tonometry – the corneal indentation pulse in normal and glaucomatous eyes," Acta. Ophthalmol., vol. 48, pp. 39–58, 1970.

[Jage65] G. N. Jager, Electrical Model of the Human Systemic Arterial Tree. Ph.D. Thesis, Univ. of Utrecht, Holland, 1965.

[JuKi84a] M. Jullian and W. Kinsner, "Carotid steosis and ocular blood pressure modelling," in Proc. Computer Applis. Medical Care, IEEE 84CH2090-9, 1984, pp. 120-127.

[JuKi84b] ____, "Divergence calculations of an incident laser beam on the cornea," Technical Report, MC84-1, Microelectronics Center and Dept. Electrical Eng., University of Manitoba, Manitoba, Canada, July 1984.

[Jull84a] M. Jullian, Modelling of the Carotid Vascular System with Stenosis For Ocular Pulse Analysis. Ph.D Dissertation, University of Manitoba, Manitoba, Canada, 1984.

[Jull84b] ____, "Structure and implementation of the carotid vascular system model," Technical Report, MC84–2, Aug. 1984.

[Kins79] J. Kinsner and W. Kinsner, "Non-contact microprocessor-based ocular pulse monitoring system," Computer in Ophthalmology Conf. Proc., (St. Louis, MI: Apr. 5-6, 1979), pp. 211-219.

[Kins87] ____, "A method for early detection of stroke and glaucoma," A Presentation of the Paper in Proc. Ninth Annual Conf. IEEE Engineering in Medicine and Biology Society (Boston, Mass., Nov., 1987), pp. 1397 - 1398.

[LaSe86] J. R. Lacourse, D. A. Sekel, "A contact method of ocular pulse detection for studies of carotid occlusions," IEEE Trans. on Biomedical Engineering, vol. BME–33, pp. 381–385, No. 4, April, 1986.

[McHe65] W. K. McEWEN and R. ST. Helen, "Rheology of the human sclera. Unifying formulation of ocular rigidity," Ophthalmologica, vol. 150, pp. 321–346, 1965.

[Mow68] C. C. Mow, "A theoretical model of the cornea for use in studies of tonometry," Bulletin of Mathematical Biophysics, vol. 28, pp. 585-

634, 1966.

[Noor60] A. Noordergraaf, H. B. K. Boom, and P. D. Verdouw, "A human systemic analog computer," in Proc. 1st Congr. Soc. for Ballistocardiographic Res., 1960, pp. 23.

[Noor63] ___, "The use of an analog computer in a circulation model," Prog. Cardiovasc. Dis., vol. 5, pp. 419-439, 1963.

[PaVa64] L. De Pater and J. W. Van den gerg, "An electrical analogue of the entire human circulatory system," Med. Electrn. Biol. Eng., vol. 2, pp. 161-166, 1964.

[ReWo56] J. W. Remington and Earl H. Wood, "Formation of peripheral pulse contour in man," J. App. Physiol. vol. 9, pp. 433-442, 1956.

[RiDi67] V. C. Ridout and D. E. Dick, "Difference differential equations for fluid flow in distensible tubes," IEEE Trans. on Biomed. Eng., vol. BME-14, no. 3, pp. 171-177, July, 1967.

[ScAl69] Harold G. Scheie and Daniel M. Albert, Adler's Textbook of Ophthalmology. Toronto, Canada: W. B. Sanders Company, 1969, pp. 336.

[SnRi68] M. F. Snyder, V. C. Rideout, and R. J. Hillestad, "Computer modelling of the human systemic arterial tree," J. Biomechanics, vol. 1, pp. 341-353, 1968.

[Warn57] H. R. Warner, "A study of the mechanism of pressure wave distortion by arterial walls using an electrical analog," Circ. Res., vol. 5, pp. 79-84, Jan. 1957.

[Weit73a] J. J. Weiter, R. A. Schachar and J. T. Ernest, "Control of intraocular blood flow, I. Intraocular pressure," Invest. Ophth., vol. 12, pp. 327-331, 1973.

[Weit73b] ___, "Control of intraocular blood flow, II. Effects of sympathetic tone," Invest. Ophth., vol. 12, pp. 332-334, 1973.

[West69] N. Westerhof, F. Bosman, C. J. De Vries, and A. Noordergraaf, "Analog study of the human systemic arterial tree," J. Biomechanics, vol. 2, pp. 121-143, 1969.

[Wolf77] P. A. Wolf, T. R. Dawber, H. E. Thomas, T. Colton, and W. B. Kannel, "Epidemiology of stroke," Advance in Neurology, New York: Raven Press, vol. 16, pp. 5-19, 1977.

[YoTs73a] Donald F. Young and Frank Y. Tsai, "Flow characteristics in models of arterial stenosis- I. steady flow," J. Biomechanics, vol. 6, pp. 395-410,1973.

[YoTs73b] ___, " Flow characteristics in models of arterial stenosis - II unsteady flow," J. Biomechanics, vol. 6, pp. 547-559, 1973.

[YoCR75] D. F. Young, N. R. Cholvin, and A. C. Roth, "Pressure across artificially induced stenoses in the femocal arteries of dogs,"

Circ. Res., vol. 36, pp. 735-743, June 1975.

[ZaGB83] C. K. Zarins, D. P. Giddens, B. K. Bharadvaj, V. S. Souttiurai, R. F. Mabon, and S. Glagov, "Carotid bifurcation atherosclerosis – quantitative correlation of plaque localization with flow velocity profiles and wall shear stress," Circ. Res., vol. 53, No. 4, pp. 502–514, Oct. 1983.

APPENDIX A

Elements of State Equations of the CVS

For the 22nd degree model [After [Jul184b]]:

$x(t) = [\, I1, V3, I5, V7, I9, V11, I13, V15, I17, V19, I21, V23, I25, V27, I30,$
$V32, I34, V36, I38, V40, I43, V45\,]^T.$

V45 is OBP.

$C = [\, 0, 0, \ldots, 0, 1].$

$D = 0.$

$B = [1/L1, 0, \ldots, 0]^T.$

$A(1,1) = -R1/L1,\ A(1,2) = -1/L1,$

$A(2,1) = 1/C1,\ A(2,3) = -1/C1,$

$A(3,2) = 1/L2,\ A(3,3) = -R2/L2,\ A(3,4) = -1/L2,$

$A(4,3) = 1/C2,\ A(4,5) = -1/C2,$

$A(5,4) = 1/L3,\ A(5,5) = -R3/L3,\ A(5,6) = -1/L3,$

$A(6,5) = 1/C3,\ A(6,7) = -1/C3$

$A(7,6) = 1/L4,\ A(7,7) = -R4/L4,\ A(7,8) = -1/L4,$

$A(8,7) = 1/C4,\ A(8,9) = -1/C4,\ A(8,15) = -1/C4,$

$A(9,8) = 1/L5,\ A(9,9) = -R5/L5,\ A(9,10) = -1/L5,$

$A(10,9) = 1/C5,\ A(10,11) = -1/C5,$

$A(11,10) = 1/L6,\ A(11,11) = -R6/L6,\ A(11,12) = -1/L6,$

$A(12,11) = 1/C6,\ A(12,13) = -1/C6,$

$A(13,12) = 1/L7,\ A(13,13) = -R7/L7,\ A(13,14) = -1/L7,$

$A(14,13) = 1/C7,\ A(14,14) = -1/(C7R12),$

$A(15,8) = 1/L8,\ A(15,15) = -R8/L8,\ A(15,16) = -1/L8,$

$A(16,15) = 1/C8,\ A(16,17) = -1/C8,$

A(17,16) = 1/L9, A(17,17) = -R9/L9, A(17,18) = -1/L9,

A(18,17) = 1/C9, A(18,19) = -1/C9, A(18,21) = -1/C9,

A(19,18) = 1/L10, A(19,19) = -R10/L10, A(19,20) = -1/L10,

A(20,19) = 1/C10, A(20,20) = - 1/(C10R14),

A(21,18) = 1/L11, A(21,21) = -R11/L11, A(21,22) = -1/L11,

A(22,21) = 1/C11, A(22,22) = -1 /(C11R13),

Other elements of A[1:22,1:22] are zero.

For the 14th degree model (similarly using the same method):

$x(t) = [\ I1, V3, I5, V7, I13, V15, I17, V19, I25, V27, I34, V36, I38, V40\ ]^T$.

v40 is OBP.

B, C, D are not changed.

A(1,1) = -R1/L1, A(1,2) = -1/L1,

A(2,1) = 1/C1, A(2,3) = -1/C1,

A(3,2) = 1/L2, A(3,3) = -R2/L2, A(3,4) = -1/L2,

A(4,3) = 1/C2, A(4,5) = -1/C2,

A(5,4) = 1/L3, A(5,5) = -R3/L3, A(5,6) = -1/L3,

A(6,5) = 1/C3, A(6,7) = -1/C3, A(6,11) = -1/C3,

A(7,6) = 1/L5, A(7,7) = -R5/L5, A(7,8) = -1/L5,

A(8,7) = 1/C5, A(8,9) = -1/C5,

A(9,8) = 1/L6, A(9,9) = -R6/L6, A(9,10) = -1/L6,

A(10,9) = 1/C6, A(10,10) = -1/(C6R7),

A(11,6) = 1/L8, A(11,11) = -R8/L8, A(11,12) = -1/L8,

A(12,11) = 1/C8, A(12,13) = -1/C8,

A(13,12) = 1/L9, A(13,13) = -R9/L9, A(13,14) = -1/L9,

A(14,13) = 1/C9, A(14,14) = -1/(C9R10),

Other elements of A[1:14,1:14] are zero.

APPENDIX B
PARAMETER CHANGES IN VARIATION CASES OF CHAPTER IV

(Changes in all cases are based on CASE1.)

CASE2, CASE3, CASE4:

(coefficients of stenosis changed: only K_v changed, K_t, K_i unchanged.)

% stenosis	0%	10%	20%	30%	40%	50%	60%	70%	80%	90%
K_v	51	54	57	64	71	80	103	156	255	655

CASE5:

(coefficients of stenosis changed: only K_v changed, K_t, K_i unchanged.)

% stenosis	0%	10%	20%	30%	40%	50%	60%	70%	80%	90%
K_v	135	144	151	170	188	212	274	415	679	1747

CASE6:

(coefficients of stenosis changed: only K_v changed, K_t, K_i unchanged.)

% stenosis	0%	10%	20%	30%	40%	50%	60%	70%	80%	90%
K_v	202	216	226	256	283	319	410	623	1018	2620

CASE7:

(coefficients of stenosis changed: only K_v changed, K_t, K_i unchanged.)

% stenosis	0%	10%	20%	30%	40%	50%	60%	70%	80%	90%
K_v	156	166	174	196	217	245	316	479	784	2015

CASE8:

(coefficients of stenosis changed: only K_v changed, K_t, K_i unchanged.)

% stenosis	0%	10%	20%	30%	40%	50%	60%	70%	80%	90%
K_v	225	240	252	284	314	354	456	692	1132	2911

CASE9:

(coefficients of stenosis changed: only K_v changed, K_t, K_i unchanged.)

% stenosis	0%	10%	20%	30%	40%	50%	60%	70%	80%	90%
K_v	337	360	378	426	471	531	684	1038	1698	4368

CASE10:

Diastolic amplitude of ABP is changed to 72 mmHg.

CASE11:

Diastolic amplitude of ABP is changed to 88 mmHg.

CASE12:

Systolic amplitude of ABP is changed to 126 mmHg.

CASE13:

Diastolic amplitude is changed to 154 mmHg.

CASE16:

(Corresponding R7 also changed to keep the ratio R7/R10 unchanged.)

R10 = 3856.079 g cm^{-4} s^{-1} , R7 = 6426.719 g cm^{-4} s^{-1}.

CASE17:

(Corresponding R7 also changed to keep the ratio R7/R10 unchanged.)

R10 = 2892.06 g cm^{-4} s^{-1} , R7 = 4820.039 g cm^{-4} s^{-1}.

CASE18:

Segment	1	2	3	5	6	8	9
r	0.48	0.48	0.48	0.18	0.12	0.216	0.156
h	0.0624	0.0624	0.0624	0.0468	0.026	0.0468	0.0416

(coefficients of stenosis also changed: only K_v changed, K_t, K_i unchanged.)

% stenosis	0%	10%	20%	30%	40%	50%	60%	70%	80%	90%
K_v	94	100	105	118	131	147	190	288	472	1213

CASE19:

Segment	1	2	3	5	6	8	9
r	0.32	0.32	0.32	0.12	0.078	0.144	0.104
h	0.0576	0.0576	0.0576	0.0432	0.024	0.0432	0.0384

(coefficients of stenosis also changed: only K_v changed, K_t, K_i unchanged.)

% stenosis	0%	10%	20%	30%	40%	50%	60%	70%	80%	90%
K_v	140	150	157	177	196	221	285	433	707	1820

CASE20:

Segment	1	2	3	5	6	8	9
Δz	7.7	7.7	7.7	9.9	9.9	6.6	6.6

CASE21:

Segment	1	2	3	5	6	8	9
Δz	6.3	6.3	6.3	8.1	8.1	5.4	5.4

APPENDIX C
SIMULATION PROGRAM STRUCTURE

(a) Structure of the CVS section

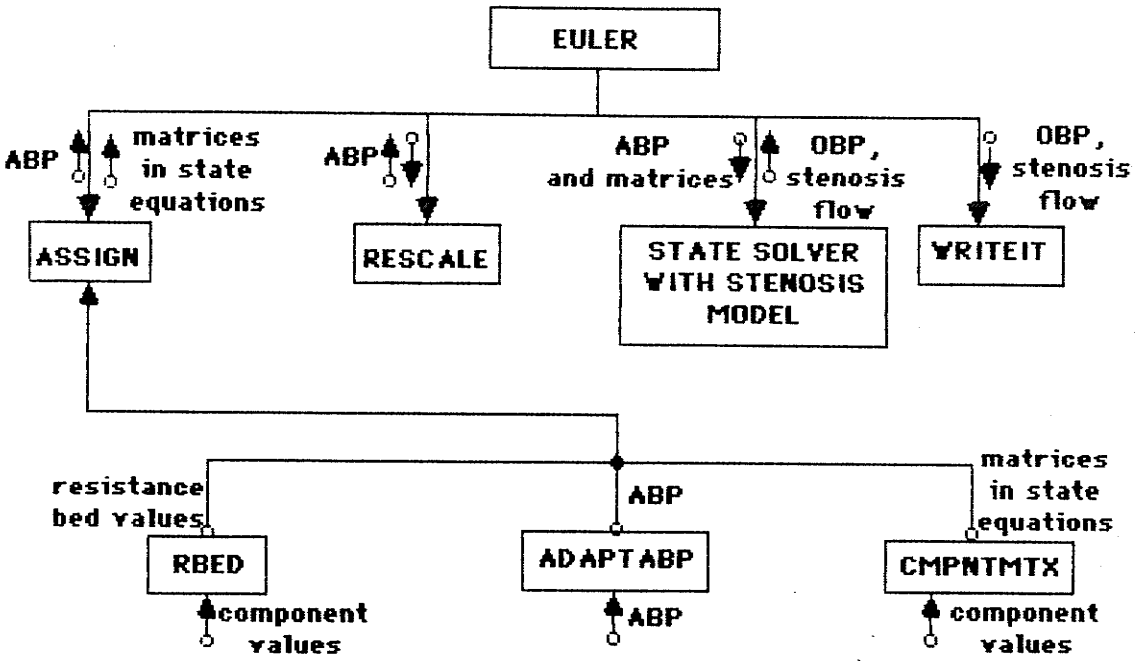

Fig. C1. Structure of the CVS process.

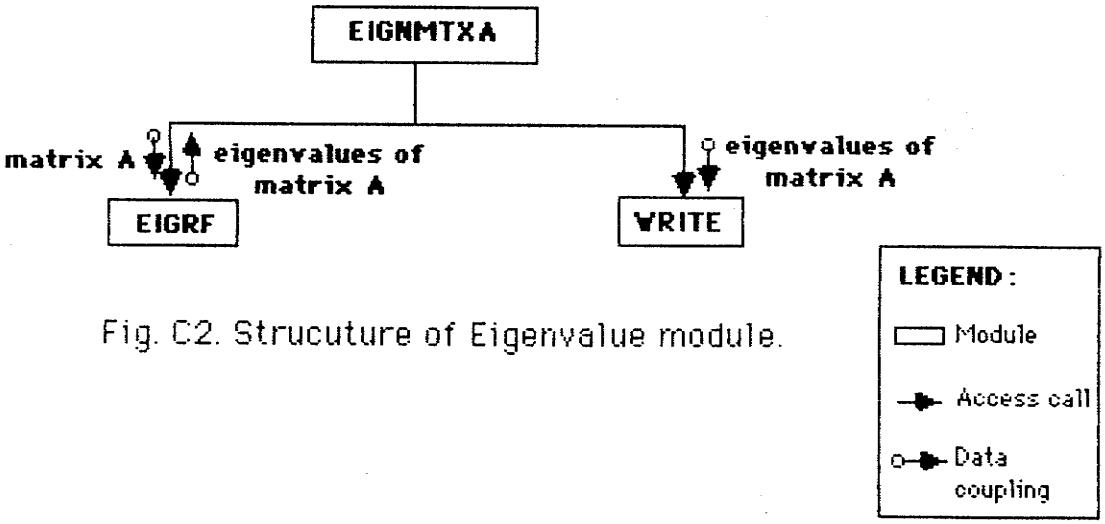

Fig. C2. Strucuture of Eigenvalue module.

(b) Sturcture of the eye section

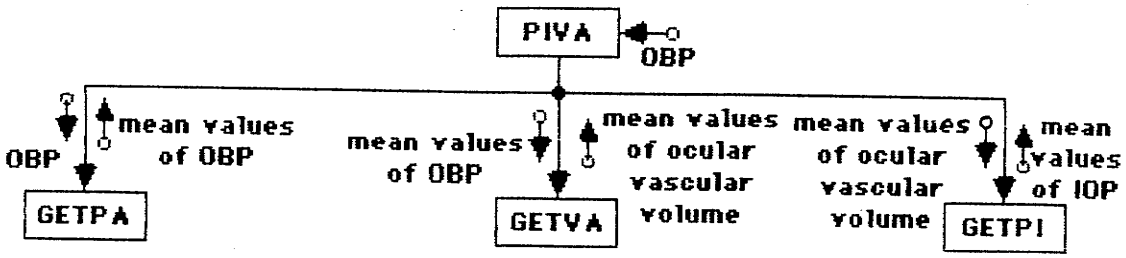

Fig. C3. Structure of mean values of IOP and vascular volume process.

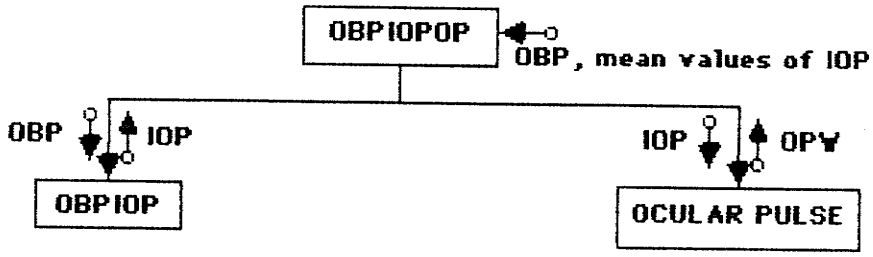

Fig. C4. Structure of OBP-IOP realtionship and OPW section.

(c) Structure of spectral analysis section

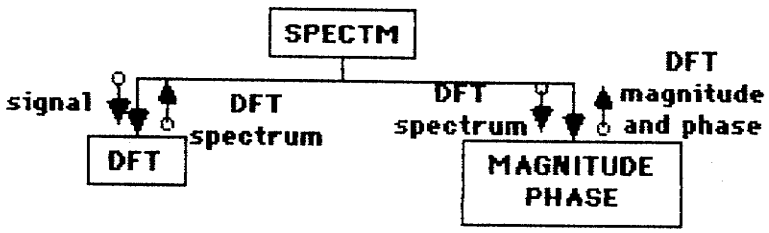

Fig. C5. structure of DFT spectrum process.

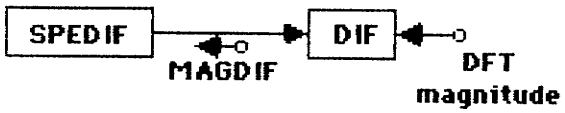

Fig. C6. Structure of MAGDIF spectrum process.

APPENDIX D
PROGRAM LISTING

(a) Simulation of the Models in WATFIV

```
//YAN JOB 'I=35,T=25M','EULER',MSGLEVEL=(1,1),CLASS=1
//STEP1 EXEC WATFIV,SIZE=768K
//SYSIN DD *
$JOB WATFIV  EULER,NOEXT,NOWARN
//*****************************************************************
//*                    MODULE NAME: EULER (modified from [Jul184b])
//*   THIS MODULE COMPUTES THE OBP FUNCTION USING THE STATE EQUATION
//*   REPRESENTATION OF THE CVS MODEL.
//*   (EULER2 IS THE CORRECTED VERSION OF THE EULER.)
//*   A NON-LINEAR ELEMENT OF STENOSIS IS A PART OF THE MODEL AND ITS
//* POSITION IS IDENTIFIED BY NE.
//*
//*   INPUT DATASET TYPE: ABP
//*   OUTPUT DATASET TYPE: OBP, STENOSIS FLOW, AND STENOSIS PRESSURE
//*                        DROP.
//*   VARIABLE DICTIONARY :
//*   A : THE STATE MATRIX REPRESENTATION OF THE CVS MODEL.
//*   B,C : CONSTANT MATRICES.
//*   WK  : THE INPUT DRIVING FUNCTION.
//*   VIN : THE EXPANDED INPUT DRIVING FUNCTION.
//*   XC1 : THE INITIAL CURRENT STATE VECTOR.
//*   Y   : THE OUTPUT VECTOR.
//*   KP  : THE NUMBER OF PERIODS OVER WHICH THE ITERATIVE SOLUTION
//*         IS TO BE APPROXIMATED.
//*   LOC : THE LOCATION OF THE STENOSIS WITHIN THE CVS MODEL.
//*   NE  : THE LOCATION OF THE NONLINEAR ELEMENT IN THE STATE MATRIX.
//*   N   : THE SIZE OF THE STATE MATRIX.
//*   NS  : THE NUMBER OF POINTS OVER ONE PERIOD ( USED TO DETERMINE
//*         THE STEP SIZE OF THE ITERATIONS ).
//*   ZZ  : LOOP COUNTER.
//*   LNE : THE INDUCTANCE OF THE SEGMENT IN WHICH THE STENOSIS IS
//*         PLACED.
//*   LSEG: THE LENGTH OF THE SEGMENT IN WHICH THE STENOSIS IS PLACED.
//*   RNE : THE RESISTANCE OF THE SEGMENT IN WHICH THE STENOSIS IS
//*         PLACED.
//*   RSEG: THE RADIUS OF THE SEGMENT IN WHICH THE STENOSIS IS PLACED.
//*   SF  : THE SCALING FACTOR FOR FLOW WITHIN THE STENOSIS.
//*   TABP: THE DURATION OF ABP CYCLE (SEC)
//*****************************************************************
      DOUBLE PRECISION A(20,20),B(20),C(20)
      DOUBLE PRECISION VIN(10001),XC1(20),Y(10001)
      DIMENSION WK(101)
      INTEGER KP,LOC,N,NE,NP,NR,NS,NS1,ZZ
      REAL LNE,LSEG,RNE,RSEG,SF,TABP
C     READ INPUT DATA AND ASSIGN EXECUTION-INDEPENDENT VARIABLES
      CALL ASSIGN(A,B,C,KP,LNE,LOC,LSEG,N,NE,NP,NS,RNE,RSEG,SF,
     *WK,XC1,TABP)
C     RESCALE AND EXPAND INPUT DRIVING FUNCTION
```

```
      CALL RESCALE(NP,NS,WK,NR,NS1,VIN)
      DO 999 ZZ=1,10
C       COMPUTE STATE VECTOR USING EULER METHOD
        CALL COMSTATE(A,B,C,KP,LNE,LSEG,NE,N,NS,NS1,RNE,RSEG,SF,
     *                VIN,XC1,ZZ,Y,TABP)
C       WRITE DATA TO DISK
        CALL WRITEIT(NR,NS1,Y)
  999 CONTINUE
      STOP
      END
C
      SUBROUTINE ASSIGN(A,B,C,KP,LNE,LOC,LSEG,N,NE,NP,NS,RNE,RSEG,
     CSF,WK,XC1,TABP)
C-----------------------------------------------------------------------
C     MODULE NAME : ASSIGN
C
C     PURPOSE : TO READ IN THE NECESSARY VARIABLES AND ASSIGN STARTING
C               VALUES TO EXECUTION-INDEPENDENT VARIABLES.
C
C     VARIABLES :
C               NE : LOCATION OF THE STENOSIS ELEMENT IN THE STATE
C                    MATRIX.
C               N  : SIZE OF THE STATE MATRIX.
C               NS : NUMBER OF POINTS OVER ONE PERIOD ( USED TO
C                    DETERMINE THE STEP SIZE OF THE ITERATIONS ).
C               KP : NUMBER OF PERIODS OVER WHICH THE ITERATIVE
C                    SOLUTION IS APPROXIMATED.
C               A  : THE STATE MATRIX.
C               B,C: CONSTANT MATRICES.
C               XC1: THE INITIAL CURRENT STATE VECTOR.
C               WK : THE INPUT DRIVING FUNCTION.
C               SF : THE SCALING FACTOR FOR FLOW WITHIN THE STENOSIS.
C               LNE: THE INDUCTANCE OF THE SEGMENT IN WHICH THE
C                    STENOSIS IS LOCATED.
C               ALNE: ARRAY OF LNE FOR 7 SEGMENTS
C               RNE: THE RESISTANCE OF THE SEGMENT IN WHICH THE
C                    STENOSIS IS LOCATED.
C               ARNE: ARRAY OF RNE
C               LSEG : THE LENGTH OF THE SEGMENT IN WHICH THE STENOSIS
C                      IS LOCATED.
C               RSEG : THE RADIUS OF THE SEGMENT IN WHICH THE STENOSIS
C                      IS LOCATED.
C               ARSEG: ARRAY OF RSEG.
C               DZ: THE LENGTH OF THE SEGMENT FOR 7 SEGMENT.
C               LOC: THE LOCATION OF THE STENOSIS IN THE CVS MODEL.
C               TABP: THE DURATION OF ABP CYCLE (SEC)
C
C-----------------------------------------------------------------------
      DOUBLE PRECISION A(20,20),B(20),C(20),XC1(20)
      DIMENSION WK(101),ALNE(7),ARNE(7),ARSEG(7),DZ(7)
      INTEGER KP,LOC,N,NE,NP,NS
      REAL LNE,LSEG,RNE,RSEG,SF,TABP
C     READ INPUT DATA
      READ (1,*) LOC,N,NS,TABP,NP,KP,LSEG
```

```
      READ (1,*) (B(I),I=1,N),(C(I),I=1,N),(XC1(I),I=1,N)
      N2=N/2
      READ(12,105)(ARNE(I),I=1,N2)
      READ(12,105)(ALNE(I),I=1,N2)
      READ(12,105)(ARSEG(I),I=1,N2)
      READ(12,105)(ARSEG(I),I=1,N2)
      READ(12,105)(DZ(I),I=1,N2)
      DO 52 I=1,N
        READ(13,82)(A(I,J),J=1,N)
52    CONTINUE
82     FORMAT(4D15.7)
      B(1)=1./ALNE(1)
      READ(4,105)(WK(I),I=1,101)
105    FORMAT(4E15.7)
      PRINT ,LOC,N,NS,N2
      PRINT ,A(1,1),B(1),C(1),XC1(1)
      PRINT 105,(ARNE(I),I=1,N2)
      PRINT 105,(ALNE(I),I=1,N2)
      PRINT 105,(ARSEG(I),I=1,N2)
      PRINT 105,(DZ(I),I=1,N2)
      DO 53 I=1,N
           PRINT 82,(A(I,J),J=1,N)
53    CONTINUE
C     ASSIGN STARTING VALUES
      SF=1.333E+5
      LNE=ALNE(LOC)
      RNE=ARNE(LOC)
      NE=LOC*2-1
      RSEG=ARSEG(LOC)
      RNE=((DZ(LOC)-LSEG)/DZ(LOC))*RNE
      PRINT ,LNE,RNE,NE,RSEG,LSEG
      RETURN
      END
      FUNCTION DMAX(N,X)
C-----------------------------------------------------------------------
C
C
C     SEARCH FOR THE MAXIMUM IN A ONE-DIMENSIONAL ARRAY OF NUMBERS.
C     N        - DIMENSION OF THE ARRAY
C     X        - THE ONE-DIMENSIONAL ARRAY
C
C-----------------------------------------------------------------------
      DOUBLE PRECISION X(101),DMAX
      DMAX=0.0
      DO 100 I=1,N
        IF (X(I).GT.DMAX) DMAX=X(I)
100   CONTINUE
      RETURN
      END
C
      SUBROUTINE RESCALE(NP,NS,WK,NR,NS1,VIN)
C-----------------------------------------------------------------------
C
C     MODULE NAME : RESCALE
C
```

```
C    PURPOSE : TO RESCALE AND EXPAND THE INPUT DRIVING FUNCTION.
C
C    VARIABLES :
C          WK : THE INPUT DRIVING FUNCTION.
C          NS : THE NUMBER OF POINTS OVER ONE PERIOD.
C          NP : UNKNOWN.
C          NP1,NR1,NS1 : DIMENSIONING VARIABLES.
C          VIN : THE RESCALED INPUT DRIVING FUNCTION.
C          VOMAX : THE MAXIMUM OF THE INPUT DRIVING FUNCTION.
C          V1 : THE INPUT DRIVING FUNCTION SCALED TO 80-140 MMHG.
C
C-----------------------------------------------------------------
      DOUBLE PRECISION VOMAX,DMAX,VIN(10001),V1(101),VO(101)
      DIMENSION WK(101)
C
C     RESCALE INPUT DRIVING FUNCTION
C     FOR 80 - 140 MMHG
C     FOR 100 - 180 MMHG
C     FOR 70 - 90 MMHG
      DO 120 I=1,101
120   VO(I)=WK(I)+80.0
C120   VO(I)=WK(I)+100.0
C120   VO(I)=WK(I)+70.0
      VOMAX=DMAX(101,VO)
      V1(1)=VO(1)
      DO 130 I=1,100
      RINC=(VO(I+1)-VO(I))*60.0/(VOMAX-80.0)
C     RINC=(VO(I+1)-VO(I))*80.0/(VOMAX-100.0)
C     RINC=(VO(I+1)-VO(I))*20.0/(VOMAX-70.0)
130   V1(I+1)=V1(I)+RINC
C     WRITE ABP
C     WRITE(3,555)(V1(I),I=1,101)
555   FORMAT(4E15.7)
C
C     EXPAND INPUT DRIVING FUNCTION TO NS PTS
C
      NR=NS/NP
      NP1=NP+1
      NR1=NR+1
      NS1=NS+1
C
C     SCALE INPUT DRIVING FUNCTION FOR 0.8 - 1.4 MMHG
C
      DO 110 I=1,NP1
110   V1(I)=V1(I)/1.0E2
      DO 10 I=1,NP1
      IF(I.EQ.NP1) GO TO 15
      RINC=(V1(I+1)-V1(I))/NR
      DO 20 J=1,NR
20    VIN(NR*(I-1)+J)=V1(I)+(J-1)*RINC
      GO TO 10
15    VIN(NR*(I-1)+1)=V1(I)
10    CONTINUE
C
```

```
      RETURN
      END
C
      SUBROUTINE COMSTATE(A,B,C,KP,LNE,LSEG,NE,N,NS,NS1,RNE,RSEG,SF,
     *VIN,XC1,ZZ,Y,TABP)
C-----------------------------------------------------------------
C
C     MODULE NAME : COMSTATE
C
C     PURPOSE : TO COMPUTE THE STATE VECTOR USING THE EULER METHOD.
C
C     VARIABLES :
C          ZZ : PERCENT STENOSIS ((ZZ-1)*10%) BEING CALCULATED.
C          SF : THE SCALING FACTOR FOR FLOW WITHIN THE STENOSIS.
C          LNE: THE INDUCTANCE OF THE SEGMENT IN WHICH THE
C             STENOSIS IS LOCATED.
C          RNE: THE RESISTANCE OF THE SEGMENT IN WHICH THE
C             STENOSIS IS LOCATED.
C          NE : THE LOCATION OF THE STENOSIS ELEMENT IN THE
C             STATE MATRIX.
C          XC1: THE INITIAL CURRENT STATE VECTOR.
C          XC : THE CURRENT STATE VECTOR.
C          A  : THE STATE MATRIX.
C          B,C: CONSTANT MATRICES.
C          VIN: THE INPUT DRIVING FUNCTION.
C          LSEG : THE LENGTH OF THE SEGMENT IN WHICH THE STENOSIS
C               IS LOCATED.
C          RSEG : THE RADIUS OF THE SEGMENT IN WHICH THE STENOSIS
C               IS LOCATED.
C          CV,CT,CI : COEFFICIENTS OF VISCOSITY,TURBULENCE, AND
C                INERTIA.
C          Y  : THE OUTPUT VECTOR.
C          TABP: THE DURATION OF THE ABP CYCLE (SEC)
C
C-----------------------------------------------------------------
C
      DIMENSION FFS1(101),FFS2(101),FFS3(101),Y2(101)
      DOUBLE PRECISION A(20,20),B(20),C(20),D(20),F(10001),DF,DABS
      DOUBLE PRECISION VIN(10001),XC(20),XC1(20),XN(20),Y(10001),YN
      DOUBLE PRECISION FS(10001),DFF(10001)
      INTEGER ZZ
      REAL LNE,RNE,LSEG,RSEG,KV,KT,KI,PIE,A0,A1,CV,CT,CI,TABP
      DF=0.D0
      DO 99 I=1,14
         XC(I)=XC1(I)
99    CONTINUE
C     ASSIGN VALUES DEPENDENT ON STENOSIS DEGREE
C     (BASED ON THE SEGMENT 8)
C
      DO CASE ZZ
      CASE 1
C          0% STENOSIS
      KV=112.5
      KT=0.0
```

```
      KI=0.0
C
      CASE 2
C          10% STENOSIS
      KV=120.0
      KT=1.07
      KI=1.2
C
      CASE 3
C          20% STENOSIS
      KV=126.0
      KT=1.21
      KI=1.2
C
      CASE 4
C          30% STENOSIS
      KV=142.0
      KT=1.35
      KI=1.2
C
      CASE 5
C          40% STENOSIS
      KV=157.0
      KT=1.49
      KI=1.2
C
      CASE 6
C          50% STENOSIS
      KV=177.0
      KT=1.63
      KI=1.2
C
      CASE 7
C          60% STENOSIS
      KV=228.0
      KT=1.76
      KI=1.2
C
      CASE 8
C          70% STENOSIS
      KV=346.0
      KT=1.9
      KI=1.2
C
      CASE 9
C          80% STENOSIS
      KV=566.0
      KT=2.04
      KI=1.2
C
      CASE 10
C          90% STENOSIS
      KV=1456.0
      KT=2.18
```

```
      KI=1.2
C
      END CASE
C     MODIFY THE KV FOR THE CURRENT STENOSIS SEGMENT
C     WITH RESPECT TO THE VALUE OF KV IN SEGMENT 8 AND LSEG8=1
      KV=(0.18*KV/RSEG)*LSEG
      PRINT ,' KV=',KV
C
C     CALCULATE CV,CT, AND CI
C
      PIE=3.14159
      CV=KV*0.031/(2*PIE*RSEG**3)
C
      A0=PIE*RSEG**2
      A1=A0*(1-(ZZ-1)*.1)
      CT=(KT*0.5*1.05*((A0/A1)-1)**2)/(PIE**2*RSEG**4)
C
      CI=(KI*LSEG*1.05)/(PIE*RSEG**2)
C
C
      DO 40 L=1,KP
      DO 50 K=1,NS1
C
C     COMPUTE NON-LINEAR ELEMENT OF A
C
C     DF IS THE DIFFERENTIAL SCALED FLOW USED TO COMPUTE
C     THE INERTIAL COEFFICIENT OF THE STENOSIS.
C
          IF(XC(NE).NE.0) GO TO 200
          A(NE,NE)=-(CV+RNE)/LNE
          FS(K)=0.0
          GO TO 250
  200     CU=(CI/(SF*XC(NE)))*DF
          RS=CV+(CT*SF*DABS(XC(NE)))+CU
          A(NE,NE)=-(RS+RNE)/LNE
          FS(K)=RS
          FS(K)=FS(K)*XC(NE)
C
C     COMPUTE NEW STATE VECTOR
C
  250     YN=0.D0
          DO 60 I=1,N
            D(I)=0.D0
            DO 70 J=1,N
  70          D(I)=D(I)+A(I,J)*XC(J)
            D(I)=D(I)+B(I)*VIN(K)
            XN(I)=XC(I)+D(I)*TABP/NS
C
C     COMPUTE DIFFERENTIAL SCALED FLOW FOR THIS STEP
            IF (I.EQ.NE) THEN DO
              DF=SF*D(I)
              DFF(K)=DF
            END IF
C     COMPUTE OUTPUT VECTOR
```

```
C
          YN=YN+C(I)*XC(I)
60      CONTINUE
        Y(K)=YN
        F(K)=XC(NE)*SF
        IF (K.NE.NS1) THEN DO
          DO 82 I=1,N
82          XC(I)=XN(I)
        END IF
50    CONTINUE
40    CONTINUE
      J=1
      DO 80 I=1,NS1,100
        FFS1(J)=FS(I)
        FFS2(J)=F(I)
        FFS3(J)=DFF(I)
80      J=J+1
      WRITE(9,81)(FFS1(J),J=1,101)
      WRITE(10,81)(FFS2(J),J=1,101)
      WRITE(11,81)(FFS3(J),J=1,101)
81    FORMAT(4E15.7)
      RETURN
      END
C
      SUBROUTINE WRITEIT(NR,NS1,Y)
C-----------------------------------------------------------------
C
C     MODULE NAME : WRITEIT
C
C     PURPOSE : TO WRITE THE OUTPUT OF THE EULER MODULE TO DISK.
C
C     VARIABLES :
C           VIN : THE INPUT DRIVING FUNCTION
C           XC  : THE CURRENT STATE VECTOR.
C           Y   : THE OCULAR BLOOD PRESSURE.
C-----------------------------------------------------------------
      DIMENSION Y2(101)
      DOUBLE PRECISION Y(10001)
C
C     SELECT POINTS TO BE WRITTEN
C
      J=1
      DO 80 I=1,NS1,NR
        Y2(J)=Y(I)
80      J=J+1
      WRITE(2,95)(Y2(I),I=1,101)
95    FORMAT(4E15.7)
C     PRINT 85,(I,Y2(I),I=1,101)
85    FORMAT (5(' Y2(',I3,')=',D13.5,2X))
      RETURN
      END
C
C THE FIRST NUMBER IN THE DATA LIST CAN RANGE BETWEEN 1 AND 7,
C AND CORRESPONDS TO THE SEGMENT OF THE CVS MODEL IN WHICH THE
C STENOSIS LIES.
```

```
C
$ENTRY
/*
//GO.FT01F001 DD *
6,14,10000,1.0,100,5,1.0
0.0,0.0,0.0,0.0,0.0,0.0,0.0,0.0,0.0,0.0,0.0,0.0,0.0,0.0,0.0
0.0,0.0,0.0,0.0,0.0,0.0,0.0,0.0,0.0,0.0,0.0,0.0,0.0,0.0,1.0
0.0,0.0,0.0,0.0,0.0,0.0,0.0,0.0,0.0,0.0,0.0,0.0,0.0,0.0,0.0
/*
//GO.FT02F001 DD DSN=YAN.AL2.OBP6,DISP=SHR
/*
//GO.FT04F001 DD DSN=YAN.ABP.JUN87,DISP=SHR
/*
//GO.FT12F001 DD DSN=YAN.A1.CPT,DISP=SHR
/*
//GO.FT13F001 DD DSN=YAN.A1.MTXA,DISP=SHR
/*
//GO.FT09F001 DD DSN=YAN.AL2.STEDRP6,DISP=SHR
/*
//GO.FT10F001 DD DSN=YAN.AL2.STEFLW6,DISP=SHR
/*
//GO.FT11F001 DD DSN=YAN.AL2.DSTEFLW6,DISP=SHR
/*

//YAN JOB 'I=10,T=5','RBED',MSGLEVEL=(1,1),CLASS=A
// EXEC WATFIV,SIZE=256K
//SYSIN DD *
$JOB  WATFIV  RBED,NOEXT,NOWARN
//*************************************************************
//*                  MODULE NAME: RBED
//*   PURPOSE : TO CALCULATE THE VASCULAR RESISTANCE BED VALUES
//*                  FOR THE CVS MODEL.
//*   INPUT DATASET TYPE: CPT
//*   OUTPUT DATASET TYPE: RBED VAUES.
//*************************************************************
   DIMENSION R(11)
   D=100.
   R13=1.0E+4
   N=11
   READ(1,81)(R(I),I=1,N)
81  FORMAT(4E15.7)
C
   V1=GETVA(R13,R,N)
   IF (ABS(V1) .LT. 0.0001) GO TO 1
4   R13S=R13
   R13 = R13 + D
   V2=GETVA(R13,R,N)
   IF (ABS(V2) .LT. 0.0001) GO TO 1
   IF ((V2 * V1) .GT. 0) GO TO 3
   D = -D/2
5   V1 = V2
   GO TO 4
3   IF (ABS(V2) .LT. ABS(V1)) GO TO 5
   D = -D
```

```
      GO TO 5
 1    CONTINUE
      PRINT ,'R13,R13S',R13,R13S
      R14=0.64*R13
      PRINT ,'R14,R12',R14
      STOP
      END
C
     FUNCTION GETVA(R13,R,N)
      DIMENSION R(N)
      REAL R14,R13,R12,R567,R89,R1234,RCE,ROP,REX,RS
      REAL V0,V2,VS
      V0=75.
      V2=140.
      R14=0.64*R13
      R12=R14
      R567=R(5)+R(6)+R(7)
      R89=R(8)+R(9)
      R1234=R(1)+R(2)+R(3)+R(4)
      ROP=R(11)+R13
      RCE=R(10)+R14
      REX=R567+R12
      VS=(V0/R13)*ROP
      RS=RCE*ROP/(RCE+ROP)
      VS=(VS/RS)*(R89+RS)
      RS=REX*(RS+R89)/(REX+RS+R89)
      VS=(VS/RS)*(RS+R1234)
      GETVA=VS-V2
      RETURN
      END
$ENTRY
/*
//GO.FT01F001 DD DSN=YAN.A22.CPT,DISP=SHR
/*

//YAN JOB 'I=10,T=5','ADAPTABP',MSGLEVEL=(1,1),CLASS=A
//STEP1 EXEC WATFIV,SIZE=256K
//SYSIN DD *
$JOB WATFIV ADAPTABP,NOEXT,NOWARN
//*************************************************
//*              MODULE NAME: ADAPTABP
//*    THIS MODULE WORKS FOR THE ADAPTATION OF ABP
//*    DURATION.
//*    INPUT DATASET TYPE : ABP.
//*    OUTPUT DATASET TYPE: ABP.
//*************************************************
     DIMENSION VA(101),V(101)
     READ(1,10)(VA(I),I=1,101)
10   FORMAT(4E15.7)
C----NA1: SYSTOLIC PORTION OF ABP(80-140)
C----NA2: DIATOLIC PORTION OF ABP(80-140)
C----N1:  SYSTOLIC PORTION OF ABP TO BE ADAPTED
C----N2:  DIATOLIC PORTION OF ABP TO BE ADAPTED
     NA1=32
     NA2=68
```

```
      N1=23
      N2=77
      V(1)=0.0
C     SYSTOLIC PROTION ADAPTATION:
      NI1=N1+1
      DO 20 I=2,NI1
         AI=FLOAT(I-1)*FLOAT(NA1)/FLOAT(N1)+1.
         IA1=INT(AI)
         IA2=IA1+1
         V(I)=VA(IA1)+(VA(IA2)-VA(IA1))*(AI-FLOAT(IA1))
20    CONTINUE
C     DIATOLIC PORTION ADAPTATION:
      NI1=NI1+1
      DO 30 I=NI1,101
       AI=FLOAT(I-N1-1)*FLOAT(NA2)/FLOAT(N2)+FLOAT(NA1+1)
       IA1=INT(AI)
       IA2=IA1+1
       IF (IA2.GT.101) THEN DO
        V(I)=VA(IA1)
       ELSE DO
        V(I)=VA(IA1)+(VA(IA2)-VA(IA1))*(AI-FLOAT(IA1))
       END IF
30    CONTINUE
C     OUTPUT:
      WRITE(2,10)(V(I),I=1,101)
      STOP
      END
$ENTRY
/*
//GO.FT01F001 DD DSN=YAN.ABP.JUN87,DISP=SHR
/*
//GO.FT02F001 DD DSN=YAN.A15.ABP,DISP=SHR
/*

//YAN JOB
//STEP1 EXEC WATFIV,SIZE=256K
//SYSIN DD *
$JOB  WATFIV  CMPNT,NOEXT,NOWARN
//*****************************************************************
//*                      MODULE NAME: CMPNTMTX
//*     THIS MODULE COMPUTE THE COMPONENT VALUES AND MATRIX A.
//*     OF THE CVS MODEL.
//*     OUTPUT DATASET TYPE: CPT; MTXA.
//*****************************************************************
      DIMENSION E(7),H(7),RD(7),Z(7),R(7),C(7)
      DIMENSION A(14,14)
      REAL PUAL,RAL,L(7),R7,R10
      N=7
      PUAL=0.031
      RAL=1.05
      PIE=3.141593
C     CALCULATE THE COMPONENT VALUES OF THE CVS MODEL
      READ(1,*)(E(I),I=1,N)
      READ(1,*)(H(I),I=1,N)
```

```
      READ(1,*)(RD(I),I=1,N)
      READ(1,*)(Z(I),I=1,N)
      READ(1,*)R7,R10
      DO 10 I=1,N
        E(I)=E(I)*1.E+6
   10 CONTINUE
      DO 20 I=1,N
        R(I)=(81.*PUAL/(8.*PIE*(RD(I)**4)))*Z(I)
        L(I)=(9.*RAL/(4.*PIE*RD(I)*RD(I)))*Z(I)
        C(I)=(3.*PIE*RD(I)**3/(2.*E(I)*H(I)))*Z(I)
   20 CONTINUE
      WRITE(2,82)(R(I),I=1,N)
      WRITE(2,82)(L(I),I=1,N)
      WRITE(2,82)(C(I),I=1,N)
      WRITE(2,82)(RD(I),I=1,N)
      WRITE(2,82)(Z(I),I=1,N)
      WRITE(2,82)(H(I),I=1,N)
      WRITE(2,82)(E(I),I=1,N)
      WRITE(2,82)R7,R10,PUAL,RAL
   82 FORMAT(4E15.7)
C     CALCULATE THE MATRIX A OF THE STATE EQUATION OF CVS MODEL
      N2=N*2
      DO 30 I=1,N2
      DO 30 J=1,N2
        A(I,J)=0.0
   30 CONTINUE
      A(1,1)=(-1.)*R(1)/L(1)
      A(1,2)=(-1.)/L(1)
      N1=N-1
      DO 40 I=1,N1
        NR=I+1
        I2=I*2
        I1=I2-1
        I3=I2+1
        A(I2,I1)=1./C(I)
        A(I2,I3)=-1./C(I)
        LI2=I2+1
        LI1=LI2-1
        LI3=LI2+1
        A(LI2,LI1)=1./L(NR)
        A(LI2,LI2)=-1.*R(NR)/L(NR)
        A(LI2,LI3)=-1./L(NR)
   40 CONTINUE
      A(6,11)=(-1.)/C(3)
      A(10,10)=A(10,11)/R8
      A(10,11)=0.0
      A(11,6)=A(11,10)
      A(11,10)=0.0
      A(14,13)=1./C(7)
      A(14,14)=(-1.)/(C(7)*R9)
      DO 51 I=1,N2
      WRITE(3,105)(A(I,J),J=1,N2)
   51 CONTINUE
  105  FORMAT(4E15.7)
      STOP
```

```
    END
$ENTRY
/*
//GO.FT01F001 DD *
4.,4.,4.,8.,16.,8.,8.
0.06,0.06,0.06,0.045,0.025,0.045,0.04
0.4,0.4,0.4,0.15,0.1,0.18,0.13
7.0,7.0,7.0,9.0,9.0,6.0,6.0
5355.6,3213.4
/*
//GO.FT02F001 DD DSN=YAN.A16.CPT,DISP=SHR
/*
//GO.FT03F001 DD DSN=YAN.A16.MTXA,DISP=SHR
/*

//YAN JOB
//STEP2 EXEC WATFIV,SIZE=256K
//SYSIN DD *
$JOB  WATFIV  EIGEN,NOEXT,NOWARN
//*******************************************************
//*                    MODULE NAME: EIGNMTXA
//*    THIS MODULE IS TO CALCULATE EIGENVALUES OF MATRIX A.
//*    USING A STANDARD SUBROUTINE.
//*******************************************************
      INTEGER N,IA,IJOB,IZ,IER
      REAL A(22,22),WK(22)
      COMPLEX W(22),Z(22,22)
      IA=22
      IZ=22
      N=22
      IJOB=0
      DO 30 I=1,N
       READ(2,10)(A(I,J),J=1,N)
10    FORMAT(4E15.7)
30    CONTINUE
      CALL EIGRF(A,N,IA,IJOB,W,Z,IZ,WK,IER)
      PRINT ,'IER=',IER
      DO 20 I=1,N
        PRINT ,W(I)
20    CONTINUE
      STOP
      END
$ENTRY
/*
//GO.FT02F001 DD DSN=YAN.A22.MTXA,DISP=SHR
/*

//YAN JOB
//STEP1 EXEC WATFIV,SIZE=256K
//SYSIN DD *
$JOB  WATFIV  STEN,NOEXT,NOWARN
//*************************************************************
//*                MODULE NAME: STENOSIS ANALYSIS
//*   THIS MODULE COMPUTE THE STENOSIS DROP AND FLOW ANALYSED
```

```
//*  RESULT: THREE INDEX NUMBERS.
//*  INPUT DATASET TYPE: STENOSIS DROP AND FLOW AND ITS DERIVATIVE
//*  OUTPUT DATASET TYPE: MEAN VALUE AND PEAK VALUE AND THREE INDEX
//*                       NUMBERS.
//*****************************************************************
      FUNCTION DMAX(N,X)
      DIMENSION X(101)
      DMAX=0.0
      DO 100 I=1,N
        IF (X(I).GT.DMAX) DMAX=X(I)
100 CONTINUE
      RETURN
      END
C
      FUNCTION DMEAN(N,X)
      DIMENSION X(101)
      DMEAN=0.0
      DO 100 I=1,N
        DMEAN=DMEAN+X(I)
100 CONTINUE
      DMEAN=DMEAN/N
      RETURN
      END
C
      DIMENSION DROP(101),FLOW(101),SUB(101),DFLOW(101)
      DIMENSION DM(10),DP(10),FM(10),FP(10),REP(10),REM(10)
      DIMENSION DFM(10),DFP(10)
      DIMENSION DIV(10),DIT(10),DII(10)
      INTEGER ZZ
      REAL PUAL,RAL,STENL,STENR,KV,KT,KI,PIE,AP,A0,A1,CV,CT,CI
      N=101
      PUAL=0.031
      RAL=1.05
C  FOR SEGMENT 9:
      STENL=1.0
      STENR=0.13
      PIE=3.141593
      SF=1.333E+5
      DO 111 ZZ=1,10
        READ(1,105)(DROP(I),I=1,N)
        READ(2,105)(FLOW(I),I=1,N)
        READ(3,105)(DFLOW(I),I=1,N)
105     FORMAT(4E15.7)
        DM(ZZ)=DMEAN(N,DROP)
        DP(ZZ)=DMAX(N,DROP)
        FM(ZZ)=DMEAN(N,FLOW)
        FP(ZZ)=DMAX(N,FLOW)
        DFM(ZZ)=DMEAN(N,DFLOW)
        DFP(ZZ)=DMAX(N,DFLOW)
        REP(ZZ)=2*RAL*FP(ZZ)/(PIE*STENR*PUAL)
        REM(ZZ)=2*RAL*FM(ZZ)/(PIE*STENR*PUAL)
        DO CASE ZZ
         CASE 1
C          0% STENOSIS
```

```
          KV=112.5
          KT=0.0
          KI=0.0
         CASE 2
C         10% STENOSIS
          KV=120.0
          KT=1.07
          KI=1.2
         CASE 3
C         20% STENOSIS
         KV=126.0
         KT=1.21
         KI=1.2
C
        CASE 4
C         30% STENOSIS
         KV=142.0
         KT=1.35
         KI=1.2
C
        CASE 5
C         40% STENOSIS
         KV=157.0
        KT=1.49
        KI=1.2
       CASE 6
C         50% STENOSIS
        KV=177.0
        KT=1.63
        KI=1.2
       CASE 7
C         60% STENOSIS
        KV=228.0
        KT=1.76
        KI=1.2
      CASE 8
C         70% STENOSIS
        KV=346.0
        KT=1.9
        KI=1.2
      CASE 9
C         80% STENOSIS
        KV=566.0
        KT=2.04
        KI=1.2
      CASE 10
C         90% STENOSIS
        KV=1456.0
        KT=2.18
        KI=1.2
      END CASE
C     ADJUST KV VALUES FOR DIFFERENT SEGMENT LIKE IN PEULER2
      KV=(0.18*KV/STENR)*STENL
      PRINT ,KV
C     INDEX NUMBER OF THE STENOSIS
```

```
      DIV(ZZ)=KV/REP(ZZ)
      DIT(ZZ)=0.5*KT*((1/(1-(ZZ-1)*.1))-1)**2
      DII(ZZ)=KI*STENL*DFP(ZZ)*PIE*(STENR**2)/(FP(ZZ)**2)
111   CONTINUE
      WRITE(4,82)(DIV(ZZ),DIT(ZZ),DII(ZZ),ZZ=1,10)
82    FORMAT(3E15.7)
      WRITE(4,81)(DM(ZZ),DP(ZZ),ZZ=1,10)
      WRITE(4,81)(FM(ZZ),FP(ZZ),ZZ=1,10)
      WRITE(4,81)(DFM(ZZ),DFP(ZZ),ZZ=1,10)
      WRITE(4,81)(REM(ZZ),REP(ZZ),ZZ=1,10)
81    FORMAT(2E15.7)
      STOP
      END
$ENTRY
/*
//GO.FT01F001 DD DSN=YAN.A7.STEDRP7,DISP=SHR
/*
//GO.FT02F001 DD DSN=YAN.A7.STEFLW7,DISP=SHR
/*
//GO.FT03F001 DD DSN=YAN.A7.DSTEFLW7,DISP=SHR
/*
//GO.FT04F001 DD DSN=YAN.A7.STENANA7,DISP=SHR
/*

//YAN JOB 'I=10,T=5','PIVA',MSGLEVEL=(1,1),CLASS=1
// EXEC WATFIV,SIZE=256K
//SYSIN DD *
$JOB  WATFIV   PIVA,NOEXT,NOWARN
//*************************************************************
//*                      MODULE NAME : PIVA
//*
//*    PURPOSE : TO CALCULATE THE MEAN VALUES OF IOP AND OCULAR
//*              VASCULAR VOLUME.
//*    INPUT DATASET TYPE : OBP
//*    OUTPUT DATASET TYPE : PIXVAX (Pim, Vam)
//*************************************************************
      FUNCTION CALCVAX(PAX)
C     THIS FUNCTION CALCULATES THE VALUE OF VAX BY SOLVING
C     THE RELATION ITERATIVELY
C     SET STARTING VALUES
      REAL A,B,C,D,F,G,CALCVAX,V1,V2,PAX
      COMMON A,B,C,F,G
      D = 4.
      CALCVAX = 1.0
      V1 = -(PAX - A * EXP(B * CALCVAX) + C) ** (-0.60) + G *
     CALOG(CALCVAX) + F
      IF (ABS(V1) .LT. 0.0001) GO TO 1
4     CALCVAX = CALCVAX + D
      V2 = -(PAX - A * EXP(B * CALCVAX) + C) ** (-0.60) + G *
     CALOG(CALCVAX) + F
      IF (ABS(V2) .LT. 0.0001) GO TO 1
      IF ((V2 * V1) .GT. 0) GO TO 3
      D = -D/2
5     V1 = V2
```

```
      GO TO 4
3     IF (ABS(V2) .LT. ABS(V1)) GO TO 5
      D = -D
      GO TO 5
1     RETURN
      END
C
      DIMENSION PAX(7,10)
      REAL PIX,VAX,A,B,C,F,G,KALPHA,ALPHA,PIO,VAO,E,SF
      INTEGER I,J,N,STEN
      COMMON A,B,C,F,G
C
C  READ TOTAL NUMBER OF ALL SEGMENTS IN THE DATASET
C
      READ ,N,PIO,VAO
      CALL GETPAX(N,PAX)
C  SET UP INITIAL VALUES
C
      KALPHA=0.805
      ALPHA=8./5.
      E=0.022
      SF=0.208
C
      A = (PIO+SF/E)*EXP((-1.)*E*VAO)
      B = E
      C = SF/E
      F = (PAX(1,1)-PIO)**(1.-ALPHA)-(1.-ALPHA)*KALPHA*ALOG(VAO)
      G = (1.-ALPHA)*KALPHA
C
      DO 1 I = 1,N
      WRITE(1,6)PIO,VAO
      DO 3 J=2,10
      VAX = CALCVAX(PAX(I,J))
      PIX = A * EXP(B * VAX) - C
      STEN = (J-1) * 10
      WRITE(1,6) PIX,VAX
3     CONTINUE
1     CONTINUE
6     FORMAT(2E15.7)
      STOP
      END
C
      FUNCTION MEAN(OBP)
      DIMENSION OBP(101)
      REAL TEMP,MEAN
      INTEGER I
      TEMP=0.
      DO 12 I=1,100
12      TEMP=TEMP+OBP(I)
      MEAN=TEMP/100.
      RETURN
      END
C
      SUBROUTINE GETPAX(N,PAX)
      DIMENSION PAX(7,10),OBP(101)
```

```
      INTEGER N
      REAL MAX,MIN,MEAN
      DO 18 I=1,N
      DO 17 J=1,10
      READ(2,19)(OBP(K),K=1,101)
 19   FORMAT(4E15.7)
      PAX(I,J)=MEAN(OBP)
 17   PAX(I,J)=PAX(I,J)*100.0
 18   CONTINUE
      RETURN
      END
$ENTRY
1,15.,32.37
/*
//GO.FT01F001 DD DSN=YAN.A16.PXVX,DISP=SHR
/*
//GO.FT02F001 DD DSN=YAN.A16.OBP6,DISP=SHR
/*

//YAN JOB 'I=80,T=3M','OBPIOPOP',MSGLEVEL=(1,1),CLASS=A
//STEP4 EXEC WATFIV,SIZE=256K
//SYSIN DD *
$JOB  WATFIV  DISPNEW,NOEXT,NOWARN
//*****************************************************************
//*                    MODULE NAME : OBPIOPOP (modified from [Jul84b])
//*    THIS MODULE COMPUTES IOP VARIATIONS, ABSOLUTE VALUES AND
//*    CORNEAL DISPLACEMENT (OPW). AS A FUNCTION OF CAROTID
//*    STENOSIS.
//*    INPUT DATASET TYPE: OBPS AS A FUNCTION OF STENOSIS FOR EACH
//*                              STENOSIS LOCATION (SEGMENTS 1-7).
//*
//*    OUTPUT DATASET TYPE: IOP VARIATIONS, IOP ABSOLUTE,AND  OPW.
//*****************************************************************
      FUNCTION DMIN(N,X)
C
C     SEARCH FOR THE MINIMUM IN A ONE-DIMENSIONAL ARRAY OF NUMBERS
C     N - DIMENSION OF THE ARRAY
C     X - THE ONE-DIMENSION ARRAY
C
      REAL X(101),DMIN
      DMIN=0.72E76
      DO 100 I=1,N
      IF (X(I).LT.DMIN) DMIN=X(I)
100   CONTINUE
      RETURN
      END
C
      FUNCTION MEAN(N,X)
      REAL X(101),MEAN
      N1=N-1
      SUM=0.0
      DO 1 I=1,N1
      SUM=SUM+X(I)
1     CONTINUE
```

```
      MEAN=SUM/FLOAT(N1)
      RETURN
      END
C
      DIMENSION PA(101),OP(101)
      DIMENSION OPDISP(101)
      INTEGER ZZ
      N=101
      M=5
      K=10
      T=1.0E-2
C
      NU=0.3
      H=15.0
      EF=15.0E4
      RSQ=(0.743E4)**2
C
C REPEAT LOOP FOR ALL 7 STENOSIS LOCATIONS
C
      DO 99 ZZ=7,7
C
      DO 3 J=1,K
C
C     READ PO,VAO FROM PIXVAX FILE.
C
      READ(11,27)PO,VAO
27    FORMAT(2E15.7)
C
C     READ OBP FUNCTION FOR STENOSIS ON SEGMENT ZZ
C
      READ(1,2)(PA(I),I=1,N)
2     FORMAT(4E15.7)
      L=(J-1)*10
C
C     SCALE INPUT DATA IN MMHG
C
      SF=1.0E2
      DO 1 I=1,N
1     PA(I)=PA(I)*SF
C
      CALL OBPIOP(OP,PA,PO,VAO)
      WRITE(10,2)(OP(I),I=1,N)
      DO 4 I=1,N
      OPDISP(I)=((1-NU)*RSQ*OP(I))/(4*H*EF)
4     CONTINUE
      OPMIN=DMIN(N,OP)
      DISPMIN=DMIN(N,OPDISP)
      DO 8 I=1,N
      OP(I)=OP(I)-OPMIN
      OPDISP(I)=OPDISP(I)-DISPMIN
8     CONTINUE
C
C
      WRITE(8,2)(OP(I),I=1,N)
```

```
      WRITE(9,2)(OPDISP(I),I=1,N)
6     FORMAT(4E13.5)
3     CONTINUE
99    CONTINUE
      STOP
      END
C-----------------------------------------------------------------
C     THIS SUBROUTINE IS TO CALCULATE OBP->IOP INTEGRAL.
C     P --- IOP RESULT.
C     PAL --- OBP INPUT.
C     PO  --- MEAN VALUE OF IOP.
C     VAO --- MEAN VALUE OF OCULAR BLOOD VOLUME.
C-----------------------------------------------------------------
      SUBROUTINE OBPIOP(P,PAL,PO,VAO)
      DIMENSION P(101),PAL(101)
      REAL KA,KT,PO,VAO,MEAN,PMEAN
      INTEGER A,I,J
      N=101
      A=8
      B=0.2
      E=0.022
      F=0.208
      VR=0.024
      KA=0.805
      STEP=0.1
      KT=(E*PO)+F
C     STARTING VALUE FOR INTEGRAL
      VA=VAO
      FPAO=(VA*KT)/(KA*(((-PO)**A)**B)+VA*KT)
C     COMPUTE INTEGRAL
      DO 1 I=1,N
      IS=IFIX(PAL(I)/STEP)
      IS1=IS-1
      SUMP=0
C     FINAL VALUE FOR INTEGRAL
      VA=VAO
      FPAL=(VA*KT)/(KA*((PAL(I)-PO)**A)**B+VA*KT)
C     COMPUTE INTERMEDIATE VALUES
      DO 2 J=1,IS1
      VA=VAO
      PA=J*STEP
      FPA=(VA*KT)/(KA*(((PA-PO)**A)**B)+VA*KT)
2     SUMP=SUMP+FPA
      P(I)=(STEP/2.0)*(FPAO+2.0*SUMP+FPAL)
1     CONTINUE
      PMEAN=MEAN(N,P)
      DO 90 I=1,N
      P(I)=P(I)-PMEAN+PO
90    CONTINUE
      RETURN
      END
$ENTRY
/*
//GO.FT01F001 DD DSN=YAN.A1.OBP6,DISP=SHR
/*
```

```
//GO.FT08F001 DD DSN=YAN.A1TRUE.IOPVAR6,DISP=SHR
/*
//GO.FT09F001 DD DSN=YAN.A1TRUE.OPW6,DISP=SHR
/*
//GO.FT10F001 DD DSN=YAN.A1TRUE.IOPABS6,DISP=SHR
/*
//GO.FT11F001 DD DSN=YAN.A1.PXVX6,DISP=SHR
/*

//YAN JOB 'I=50,T=40','SPECTM',MSGLEVEL=(1,1),CLASS=A
//STEP5 EXEC WATFIV,SIZE=256K
//SYSIN DD *
$JOB  WATFIV  SPECTM,NOEXT,NOWARN
//*****************************************************************
//*            MODULE NAME : SPECTM (modified from [Jul184b])
//*  THIS MODULE COMPUTES THE DFT SPECTRUM OF A SIGNAL.
//*    INPUT DATASET TYPE: WAVEFORM AS A FUNCITON OF STENOSIS LEVELS
//*    OUTPUT DATASET TYPE: MAGNITUDE AND PHASE DIFFERENCE SPECTRA.
//*****************************************************************
      SUBROUTINE DFT
C
C   PURPOSE
C     THE PROGRAM CAN BE USED TO EVALUATE THE DISCRETE FOURIER
C     TRANSFORM (DFT) OF AN N POINT SEQUENCE OF COMPLEX NUMBERS.
C     IT CAN ALSO EVALUATE THE INVERSE DFT.
C
C   METHOD
C     THE PROGRAM IS BASED ON THE DEFINITION OF THE DFT AND ITS
C     INVERSE.
C
C   USAGE
C     CALL DFT(N,NCHOCE,X1,X2)
C
C     N     - THE NUMBER OF GIVEN COMPLEX NUMBERS
C     NCHOCE - NCHOCE = -1 TO COMPUTE THE DFT, AND NCHOCE = 1
C           TO COMPUTE THE INVERSE DFT
C     X1    - THE NAME OF THE INPUT ARRAY WHICH HOLDS THE
C           SEQUENCE TO BE TRANSFORMED
C     X2    - THE NAME OF THE OUTPUT ARRAY WHICH HOLDS THE
C           SEQUENCE OF THE TRANSFORM
C
C   SUBROUTINES AND FUNCTION SUBPROGRAMS REQUIRED
C     NONE
C
C   REMARKS
C     DOUBLE PRECISION IS USED IN ALL THE COMPUTATIONS.
C     THE INPUT DATA ARE N, NCHOCE, AND X1. THE OUTPUT IS X2.
C
    SUBROUTINE DFT(N,NCHOCE,X1,X2)
    COMPLEX*16 X1(N),X2(N),W,CD,CDEXP
    W=(0.0,1.0)*6.2831853071796/DFLOAT(N)
    DO 2 K=1,N
    X2(K)=(0.0,0.0)
    DO 1 I=1,N
```

```
1     X2(K)=X2(K)+X1(I)*CDEXP(NCHOCE*W*(I-1)*(K-1))
      IF (NCHOCE.EQ.-1) X2(K)=X2(K)/DFLOAT(N)
2     CONTINUE
      RETURN
      END
C
      COMPLEX*16 X1(101),X2(101),XIN(101),XOUT(101,10)
      COMPLEX SINGLE
      DIMENSION R(101,10),JXY(2),XY(40,2),WK(101,2),VO(101),V1(101)
      DIMENSION WK1(40),WK2(40),SDFT(101,10)
      INTEGER ZZ
      REAL F1
      PIE=3.141593
      N=101

      N1=21
      N2=N-1
      K=10
C  REPEAT FOR EACH STENOSIS LOCATION (SEGMENTS 1-7)
      DO 99 ZZ=7,7
      DO 5 J=1,K
      READ(2,111)(R(I,J),I=1,N)
111   FORMAT(4E15.7)
      DO 2 I=1,N
2      X1(I)=CMPLX(R(I,J),0.E0)
      CALL DFT(N2,-1,X1,X2)
      DO 3 I=1,N1
      XOUT(I,J)=X2(I)
      SDFT(I,J)=CDABS(X2(I))
      SINGLE=X2(I)
      R(I,J)=ATAN2(AIMAG(SINGLE),REAL(SINGLE))
      R(I,J)=180.0*R(I,J)/PIE
3     CONTINUE
      WRITE(17,111)(SDFT(I,J),I=1,N1)
5     CONTINUE
      DO 6 J=2,K
      DO 7 I=1,N1
      R(I,J)=R(I,1)-R(I,J)
7     CONTINUE
      WRITE(1,111)(R(I,J),I=1,N1)
6     CONTINUE
99    CONTINUE
      STOP
      END
$ENTRY
/*
//GO.FT01F001 DD DSN=YAN.A1.OPW6.PHADIF,DISP=SHR
/*
//GO.FT02F001 DD DSN=YAN.A1.OPW6,DISP=SHR
/*
//GO.FT17F001 DD DSN=YAN.A1.OPW6.DFT,DISP=SHR
/*

//YAN JOB 'I=50,T=2','SPEDIF',MSGLEVEL=(1,1),CLASS=A
//STEP6 EXEC WATFIV,SIZE=256K
```

```
//SYSIN DD *
$JOB  WATFIV  SPEDIF,NOEXT,NOWARN
//*****************************************************************
//*          MODULE NAME : SPEDIF
//*   THIS MODULE IS TO CALCULATE DIF SPECTRUM.
//*   INPUT DATASET TYPE : DFT SPECTRUM.
//*   OUTPUT DATASET TYPE : DIF SPECTRUM.
//*****************************************************************
      SUBROUTINE DIF(SPE)
      REAL SPE(21),R(21)
      DO 10 I=2,21
        SPE(I-1)=(SPE(I)-SPE(I-1))/SPE(I-1)
10    CONTINUE
      DO 20 I=2,21
        SPE(I)=R(I)
20    CONTINUE
      SPE(1)=R(2)
      RETURN
      END
C
      DIMENSION R(21,10)
      INTEGER ZZ
      N=101
      N1=21
      N2=N-1
      K=10
C
      DO 99 ZZ=7,7
        READ(1,1)(R(I,1),I=1,N1)
        CALL DIF(R(1,1))
        DO 5 J=2,K
          READ(1,1)(R(I,J),I=1,N1)
1         FORMAT(4E15.7)
          CALL DIF(R(1,J))
          DO 10 II=1,N1
            R(II,J)=R(II,1)-R(II,J)
10        CONTINUE
          WRITE(2,1)(R(I,J),I=1,N1)
5     CONTINUE
99    CONTINUE
      STOP
      END
$ENTRY
/*
//GO.FT01F001 DD DSN=YAN.A1.OPW6.DFT,DISP=SHR
/*
//GO.FT02F001 DD DSN=YAN.A1.OPW6.DFTDIF,DISP=SHR
/*
```

(b) Plotting on MAC in MacrosoftBasic

```
''''''''''''''''''''''''''''''''''''''''''''''''''''''''''''''''''''''''''''''''''''''''''''''''''''''''''''''''''''''''''''''''''''''''''''''
''          MODULE : PLOT WAVEFORM
''    THIS MODULE IS TO PLOT ANY WAVEFORM OUTPUT
''    FORM THE MODELS.
''''''''''''''''''''''''''''''''''''''''''''''''''''''''''''''''''''''''''''''''''''''''''''''''''''''''''''''''''''''''''''''''''''''''''''''
REM ---- MAIN -PLOT WAVEFORM--
OPTION BASE 0
DIM OBP(100,9)
WIDE=426   '6 INCHES
HIGH=557   '8 INCHES
COORX=0
COORY=608  '8 INCHES   'THIS IS THE FRAME OF THE CHART.
DRTN=1!
N1=100:N2=9
FILENAME$=FILES$(1)      'LOADING THE DATA POINTS.
IF FILENAME$="" THEN END
OPEN FILENAME$ FOR INPUT AS #1
FOR I=0 TO N2
 FOR J=0 TO N1
   INPUT #1,OBP(J,I)
 NEXT J
NEXT I
CLOSE #1

REM ------SCALLING---
DIM YSET(1):DIM YSET1(1,9) 'YSET1 HOLDS THE MAX POINT OF THE TEN CURVES.
GOSUB MINMAX                'YSET(1) HOLDS THE MIN AND MAX VALUE OF THE DATA POINTS.
GRIDX=INT(DRTN/5*100+.5)/100
YSET(0)=INT(YSET(0))
GRIDY=INT((YSET(1)-YSET(0))/6)
YSET(1)=YSET(1)+GRIDY/5
X=YSET(0)+GRIDY*7-YSET(1)
XG=GRIDY/5
IF X<XG THEN YSET(1)=GRIDY*7+YSET(0)
GRDLEN=YSET(1)-YSET(0)

REM ----- GRAPH-----
 DIM XX(5):DIM YY(7):DIM PATTERN%(3)    'GRID LINE.
 WINDOW CLOSE 1
 WINDOW 3,"GRAPH",(0,0)-(460,700),3
 WINDOW OUTPUT 3
 CLS
 CALL SHOWPEN
 CALL PENMODE(9):CALL TEXTMODE(1):CALL PENSIZE(1,1)
 PICTURE ON
GRID:
 X1=COORX+45:X2=COORX+WIDE:XLEN=X2-X1
 Y1=COORY-20:Y2=COORY-HIGH:YLEN=Y1-Y2
  PATTERN%(0)=&HFF00:PATTERN%(1)=0
  PATTERN%(2)=&HFF00:PATTERN%(3)=0
```

```
 CALL PENPAT(VARPTR(PATTERN%(0)))
 FOR I=1 TO 4
  XX(I)=INT(X1+(I/5)*XLEN+.5)
  CALL MOVETO (XX(I),Y1):CALL LINETO (XX(I),Y2)
 NEXT I
 PATTERN%(0)=&H8888:PATTERN%(1)=&H8888
 PATTERN%(2)=&H8888:PATTERN%(3)=&H8888
 CALL PENPAT(VARPTR(PATTERN%(0)))
 FOR I=1 TO 6
  YY(I)=INT(Y1-(I*GRIDY/GRDLEN)*YLEN+.5)
  CALL MOVETO (X1,YY(I)):CALL LINETO (X2,YY(I))
 NEXT I
 CALL PENNORMAL
 CALL PENMODE(9):CALL TEXTMODE(1):CALL PENSIZE(1,1)
 XX(0)=INT(X1+.5):XX(5)=INT(X2+.5)    'Drawing the frame of the waveform
 LINE (XX(0),Y1)-(XX(0),Y2)
 LINE (XX(5),Y1)-(XX(5),Y2)
 YY(7)=Y2:YY(0)=Y1
 LINE (X1,Y1)-(X2,Y1)
 LINE (X1,Y2)-(X2,Y2)

LABEL:
 LIBRARY "TOOLLIB"
 FOR I=0 TO 5      'HORIZONTAL AXIS.
  A=Y1+15:AX=XX(I)-10:B=GRIDX*I
  CALL MOVETO(AX,A)
  'PRINT USING"#.#";B;
  LB$=LEFT$(STR$(B),3)
  DRAWTEXT LB$
 NEXT I
 FOR I=0 TO 6        'VERTICAL AXIS.
  A=X1-44:AY=YY(I):B=GRIDY*I+YSET(0)
  CALL MOVETO(A,AY)
  LB$=LEFT$(STR$(B),5)
  DRAWTEXT LB$
 NEXT I
 CALL MOVETO(A,Y2)
  IF X<XG THEN LB$=LEFT$(STR$(YSET(1)),3):DRAWTEXT LB$
  A=COORY+15:AX=INT((XX(3)-XX(2))/2+XX(2)-45.5)
 CALL TEXTFACE(1)
 CALL MOVETO(AX,A)
 DRAWTEXT "TIME [sec]"
 A=YY(6)+30:AX=X1-32:CALL MOVETO(AX,A)
 DRAWTEXT "OBP"
 A=A+15:AX=AX-20:CALL MOVETO(AX,A)
 DRAWTEXT "[mmHg]"
 CALL TEXTFACE(0)

REM --- PLOT ---
DIM LEGEND(1,9),SY$(9)      'FOR LEGEND
SY$(0)="0%":SY$(1)="10%":SY$(2)="20%":SY$(3)="30%":SY$(4)="40%"
SY$(5)="50%":SY$(6)="60%":SY$(7)="70%":SY$(8)="80%":SY$(9)="90%"
LEGEND(0,0)=XX(2)+12:LEGEND(1,0)=YY(7)+15
LEGEND(0,1)=LEGEND(0,0)+15:LEGEND(1,1)=LEGEND(1,0)+15
```

```
LEGEND(0,2)=LEGEND(0,0)+30:LEGEND(1,2)=LEGEND(1,0)+30
LEGEND(0,3)=LEGEND(0,0)+45:LEGEND(1,3)=LEGEND(1,0)+45
LEGEND(0,4)=LEGEND(0,0)+60:LEGEND(1,4)=LEGEND(1,0)+60
LEGEND(0,5)=LEGEND(0,0)+75:LEGEND(1,5)=LEGEND(1,0)+75
LEGEND(0,6)=LEGEND(0,0)+90:LEGEND(1,6)=LEGEND(1,0)+90
LEGEND(0,7)=LEGEND(0,0)+105:LEGEND(1,7)=LEGEND(1,0)+105
LEGEND(0,8)=LEGEND(0,0)+120:LEGEND(1,8)=LEGEND(1,0)+120
LEGEND(0,9)=LEGEND(0,0)+135:LEGEND(1,9)=LEGEND(1,0)+135
XMAX=GRIDX*5:YMAX=GRDLEN:FRSTX=X1
FOR I=0 TO N2      'PLOT LEGEND
   NYSET1=YSET1(0,I)
   NXTX=INT(X1+(DRTN/N1)*NYSET1/XMAX*XLEN+.5)
   NXTY=INT(Y1-(OBP(NYSET1,I)-YSET(0))/YMAX*YLEN+.5)
   CALL MOVETO(NXTX,NXTY)
   CALL LINETO(LEGEND(0,I),LEGEND(1,I))
   LX=LEGEND(0,I)+2:LY=LEGEND(1,I)
   CALL MOVETO(LX,LY)
   'PRINT SY$(I);
   DRAWTEXT SY$(I)
NEXT I
FOR I=0 TO N2       'PLOT THE WAVEFORM
 FRSTY=INT(Y1-(OBP(0,I)-YSET(0))/YMAX*YLEN+.5)
 CALL MOVETO(FRSTX,FRSTY)
 FOR J=1 TO N1
   NXTX=INT(X1+(DRTN/N1)*J/XMAX*XLEN+.5)
   NXTY=INT(Y1-(OBP(J,I)-YSET(0))/YMAX*YLEN+.5)
   CALL LINETO(NXTX,NXTY)
 NEXT J
NEXT I
PICTURE OFF
CLOSE #1
OPEN "CLIP:PICTURE" FOR OUTPUT AS#1
PRINT#1,PICTURE$
IMAGE$=PICTURE$
WINDOW CLOSE 3
WINDOW 4,"GRAPH",(0,0)-(608,722),3
CLS
PICTURE ON
PICTURE (76,38)-(550,720),IMAGE$
PICTURE OFF
IMAGE$=PICTURE$
WINDOW CLOSE 4
WINDOW 2,"GRAPH",(2,20)-(249,340),3
PICTURE (43,29)-(217,290),IMAGE$
123 : GOTO 123

MINMAX:
YSET(0)=10000:YSET(1)=-10000   'YSET(0)--MIN,YSET(1)--MAX
FOR I=0 TO N2
 YSET1(1,I)=-10000  'YSET1(1,I)--MAX, YSET1(0,I)--X-AXIS VALUE
 FOR J=0 TO N1
  IF OBP(J,I)>YSET(1) THEN YSET(1)=OBP(J,I)
  IF OBP(J,I)<YSET(0) THEN YSET(0)=OBP(J,I)
  IF OBP(J,I)>YSET1(1,I) THEN YSET1(1,I)=OBP(J,I):YSET1(0,I)=J
 NEXT J
```

```
NEXT I
RETURN

''''''''''''''''''''''''''''''''''''''''''''''''''''''''''''''''''''''''''''''''''''''''''''''''''''''''''''''''''''''''''''''''''''
''          MODULE : OBPIOP
''      THIS MODULE IS TO PLOT THE OBP-IOP RELATIONSHIP
''''''''''''''''''''''''''''''''''''''''''''''''''''''''''''''''''''''''''''''''''''''''''''''''''''''''''''''''''''''''''''''''''''
REM ----MAIN  OBPIOP10--
OPTION BASE 0
DIM OBP(100,9)
DIM IOP(100,9)
WIDE=426   ' 6 INCHES
HIGH=557   ' 8 INCHES
COORX=0
COORY=608  ' 8 INCHES    'THIS IS THE FRAME OF THE CHART.
DRTN=80!
N1=100:N2=9
FILENAME$=FILES$(1)       'LOADING THE OBP DATA POINTS.
IF FILENAME$="" THEN END
OPEN FILENAME$ FOR INPUT AS #1
FOR I=0 TO N2
 FOR J=0 TO N1
  INPUT #1,OBP(J,I)
  OBP(J,I)=OBP(J,I)*100
 NEXT J
NEXT I
CLOSE #1

FILENAME$=FILES$(1)       'LOADING THE IOP DATA POINTS
IF FILENAME$="" THEN END
OPEN FILENAME$ FOR INPUT AS #1
FOR I=0 TO N2
 FOR J=0 TO N1
  INPUT #1,IOP(J,I)
 NEXT J
NEXT I
CLOSE #1

REM ------SCALLING---
GOSUB PIXVAX  'FOR THE PIX VALUE ADJUSTMENT OF IOP.
DIM YSET(1):DIM YSET1(1,9) 'YSET1 HOLDS THE MAX POINT OF THE TEN CURVES.
GOSUB MINMAX                'YSET(1)  HOLDS THE MIN AND MAX VALUE INDEX  OF THE DATA POINTS.
GRIDX=INT(DRTN/5+.5)
YSET(0)=INT(YSET(0))
GRIDY=INT((YSET(1)-YSET(0))/6+.5)
YSET(1)=GRIDY*6+YSET(0)  'FOR TEMPARORY USE.
GRDLEN=YSET(1)-YSET(0)

REM ----- GRAPH-----
DIM XX(5):DIM YY(7):DIM PATTERN%(3)    'GRID LINE.
WINDOW CLOSE 1
WINDOW 3,"GRAPH",(0,0)-(460,700),3
WINDOW OUTPUT 3
CLS
```

```
 CALL SHOWPEN
 CALL PENMODE(9):CALL TEXTMODE(1):CALL PENSIZE(1,1)
 PICTURE ON
GRID:
 X1=COORX+45:X2=COORX+WIDE:XLEN=X2-X1
 Y1=COORY-20:Y2=COORY-HIGH:YLEN=Y1-Y2
  PATTERN%(0)=&HFF00:PATTERN%(1)=0
  PATTERN%(2)=&HFF00:PATTERN%(3)=0
  CALL PENPAT(VARPTR(PATTERN%(0)))
 FOR I=1 TO 4
   XX(I)=INT(X1+(I/5)*XLEN+.5)
    CALL MOVETO (XX(I),Y1):CALL LINETO (XX(I),Y2)
 NEXT I
  PATTERN%(0)=&H8888:PATTERN%(1)=&H8888
  PATTERN%(2)=&H8888:PATTERN%(3)=&H8888
  CALL PENPAT(VARPTR(PATTERN%(0)))
 FOR I=1 TO 6
   YY(I)=INT(Y1-(I*GRIDY/GRDLEN)*YLEN+.5)
    CALL MOVETO (X1,YY(I)):CALL LINETO (X2,YY(I))
 NEXT I
 CALL PENNORMAL
 CALL PENMODE(9):CALL TEXTMODE(1):CALL PENSIZE(1,1)
 XX(0)=INT(X1+.5):XX(5)=INT(X2+.5)     'Drawing the frame of the waveform
 LINE (XX(0),Y1)-(XX(0),Y2)
 LINE (XX(5),Y1)-(XX(5),Y2)
 YY(7)=Y2:YY(0)=Y1
 LINE (X1,Y1)-(X2,Y1)
 LINE (X1,Y2)-(X2,Y2)

LABEL:
 LIBRARY "TOOLLIB"
  FOR I=0 TO 5       'HORIZONTAL AXIS.
   A=Y1+15:AX=XX(I)-10:B=GRIDX*I
   CALL MOVETO(AX,A)
    LB$=LEFT$(STR$(B),3)
   DRAWTEXT LB$
  NEXT I
  FOR I=0 TO 6         'VERTICAL AXIS.
   A=X1-44:AY=YY(I):B=GRIDY*I+YSET(0)
   CALL MOVETO(A,AY)
   LB$=LEFT$(STR$(B),3)
   DRAWTEXT LB$
  NEXT I
  CALL MOVETO(A,Y2)
  A=COORY+15:AX=INT((XX(3)-XX(2))/2+XX(2)-45.5)
  CALL TEXTFACE(1)
  CALL MOVETO(AX,A)
  DRAWTEXT "OBP [mmHg]"
  A=YY(6)+30:AX=X1-32:CALL MOVETO(AX,A)
  DRAWTEXT "IOP"
  A=A+15:AX=AX-20:CALL MOVETO(AX,A)
  DRAWTEXT "[mmHg]"
  CALL TEXTFACE(0)
REM --- PLOT ---
```

```
 DIM LEGEND(1,9),SY$(9)      'FOR LEGEND
 SY$(0)="0%":SY$(1)="10%":SY$(2)="20%":SY$(3)="30%":SY$(4)="40%"
 SY$(5)="50%":SY$(6)="60%":SY$(7)="70%":SY$(8)="80%":SY$(9)="90%"
 LEGEND(0,0)=XX(2)+12:LEGEND(1,0)=YY(7)+15
 LEGEND(0,1)=LEGEND(0,0)+15:LEGEND(1,1)=LEGEND(1,0)+15
 LEGEND(0,2)=LEGEND(0,0)+30:LEGEND(1,2)=LEGEND(1,0)+30
 LEGEND(0,3)=LEGEND(0,0)+45:LEGEND(1,3)=LEGEND(1,0)+45
 LEGEND(0,4)=LEGEND(0,0)+60:LEGEND(1,4)=LEGEND(1,0)+60
 LEGEND(0,5)=LEGEND(0,0)+75:LEGEND(1,5)=LEGEND(1,0)+75
 LEGEND(0,6)=LEGEND(0,0)+90:LEGEND(1,6)=LEGEND(1,0)+90
 LEGEND(0,7)=LEGEND(0,0)+105:LEGEND(1,7)=LEGEND(1,0)+105
 LEGEND(0,8)=LEGEND(0,0)+120:LEGEND(1,8)=LEGEND(1,0)+120
 LEGEND(0,9)=LEGEND(0,0)+135:LEGEND(1,9)=LEGEND(1,0)+135
 XMAX=GRIDX*5:YMAX=GRDLEN:FRSTX=X1
 FOR I=0 TO N2       'PLOT LEGEND
    NYSET1=YSET1(0,I)
    NXTX=INT(X1+OBP(NYSET1,I)/XMAX*XLEN+.5)
    NXTY=INT(Y1-(IOP(NYSET1,I)-YSET(0))/YMAX*YLEN+.5)
    CALL MOVETO(NXTX,NXTY)
    CALL LINETO(LEGEND(0,I),LEGEND(1,I))
    NYSET1=YSET1(1,I)
    NXTX=INT(X1+OBP(NYSET1,I)/XMAX*XLEN+.5)
    NXTY=INT(Y1-(IOP(NYSET1,I)-YSET(0))/YMAX*YLEN+.5)
    CALL MOVETO(NXTX,NXTY)
    CALL LINETO(LEGEND(0,I),LEGEND(1,I))
    LX=LEGEND(0,I)+2:LY=LEGEND(1,I)
    CALL MOVETO(LX,LY)
    'PRINT SY$(I);
    DRAWTEXT SY$(I)
NEXT I
 FOR I=0 TO N2        'PLOT THE WAVEFORM
  FRSTX=INT(X1+(OBP(0,I))/XMAX*XLEN+.5)
  FRSTY=INT(Y1-(IOP(0,I)-YSET(0))/YMAX*YLEN+.5)
  CALL MOVETO(FRSTX,FRSTY)
  FOR J=1 TO N1
    NXTX=INT(X1+OBP(J,I)/XMAX*XLEN+.5)
    NXTY=INT(Y1-(IOP(J,I)-YSET(0))/YMAX*YLEN+.5)
    CALL LINETO(NXTX,NXTY)
  NEXT J
 NEXT I
PICTURE OFF
CLOSE #1
OPEN "CLIP:PICTURE" FOR OUTPUT AS#1
PRINT#1,PICTURE$
 IMAGE$=PICTURE$
 WINDOW CLOSE 3
 WINDOW 4,"GRAPH",(0,0)-(608,722),3
 CLS
 PICTURE ON
 PICTURE (76,38)-(550,720),IMAGE$
 PICTURE OFF
 IMAGE$=PICTURE$
 WINDOW CLOSE 4
 WINDOW 2,"GRAPH",(2,20)-(249,340),3
 PICTURE (43,29)-(217,290),IMAGE$
```

```
123 : GOTO 123

MINMAX:
 YSET(0)=IOP(0,0):YSET(1)=IOP(0,0)   'YSET(0)--MIN,YSET(1)--MAX
 FOR I=0 TO N2
  YSMAX=IOP(0,I)
  YSMIN=IOP(0,I)   'YSET1(1,I)--MIN INDEX, YSET1(0,I)--MAX INDEX.
  FOR J=0 TO N1
   IF IOP(J,I)>YSET(1) THEN YSET(1)=IOP(J,I)
   IF IOP(J,I)<YSET(0) THEN YSET(0)=IOP(J,I)
   IF IOP(J,I)>YSMAX THEN YSET1(0,I)=J:YSMAX=IOP(J,I)
   IF IOP(J,I)<YSMIN THEN YSET1(1,I)=J:YSMIN=IOP(J,I)
  NEXT J
 NEXT I
RETURN

PIXVAX: 'THIS USE THE A1.PIXVAX6 DATA.
 DIM PIX(9)
 PIX(0)=15
 PIX(1)=14.986
 PIX(2)=14.948
 PIX(3)=14.843
 PIX(4)=14.627
 PIX(5)=14.221
 PIX(6)=13.496
 PIX(7)=12.238
 PIX(8)=10.025
 PIX(9)=6.101
FOR I=0 TO N2
  IOPM=0!
  FOR J=1 TO N1
    IOPM=IOPM+IOP(J,I)
  NEXT J
  IOPM=IOPM/100!
  FOR J=0 TO N1
    IOP(J,I)=IOP(J,I)-IOPM+PIX(I)
  NEXT J
NEXT I
RETURN

''''''''''''''''''''''''''''''''''''''''''''''''''''''''''''''''''''''''''''''''''''''''''''''''''''''''''
''           MODULE: PLOT DIF
''    THIS MODULE IS TO PLOT THE DIF SPECTRAUM.
''''''''''''''''''''''''''''''''''''''''''''''''''''''''''''''''''''''''''''''''''''''''''''''''''''''''''''

REM ----MAIN dif--
OPTION BASE 0
DIM OBP(100,9)
DIM BUF(100,9)
WIDE=426   '6 INCHES
HIGH=557   '8 INCHES
COORX=0
COORY=608  '8 INCHES   'THIS IS THE FRAME OF THE CHART.
DRTN=20!
N1=20:N2=8
```

```
FILENAME$=FILES$(1)       'LOADING THE DATA POINTS.
IF FILENAME$="" THEN END
OPEN FILENAME$ FOR INPUT AS #1
FOR I=0 TO N2
 FOR J=0 TO N1
   INPUT #1,OBP(J,I)
 NEXT J
NEXT I
CLOSE #1
REM ------SCALLING---
DIM YSET(1):DIM YSET1(1,9) 'YSET1 HOLDS THE MAX POINT OF THE TEN CURVES.
GOSUB MINMAX                'YSET(1) HOLDS THE MIN AND MAX VALUE OF THE DATA POINTS.
GRIDX=INT(DRTN/5*100+.5)/100
'YSET(0)=INT(YSET(0)*10)/10   'This factor 10 is changable. This for MAGdDIF
'GRIDY=INT((YSET(1)-YSET(0))/6*10+.5)/10
YSET(0)=INT(YSET(0))                'This is for phadif.
GRIDY=INT((YSET(1)-YSET(0))/6+.5)
YSET(1)=YSET(1)+GRIDY/5
X=YSET(0)+GRIDY*7-YSET(1)
XG=GRIDY/5
IF X<XG THEN YSET(1)=GRIDY*7+YSET(0)
GRDLEN=YSET(1)-YSET(0)

REM ----- GRAPH-----
 DIM XX(5):DIM YY(7):DIM PATTERN%(3)    'GRID LINE.
 WINDOW CLOSE 1
 WINDOW 3,"GRAPH",(0,0)-(460,700),3
 WINDOW OUTPUT 3
 CLS
 CALL SHOWPEN
 CALL PENMODE(9):CALL TEXTMODE(1):CALL PENSIZE(1,1)
 PICTURE ON
GRID
 X1=COORX+45:X2=COORX+WIDE:XLEN=X2-X1
 Y1=COORY-20:Y2=COORY-HIGH:YLEN=Y1-Y2
 PATTERN%(0)=&HFF00:PATTERN%(1)=0
 PATTERN%(2)=&HFF00:PATTERN%(3)=0
 CALL PENPAT(VARPTR(PATTERN%(0)))
FOR I=1 TO 4
  XX(I)=INT(X1+(I/5)*XLEN+.5)
   CALL MOVETO (XX(I),Y1):CALL LINETO (XX(I),Y2)
NEXT I
 PATTERN%(0)=&H8888:PATTERN%(1)=&H8888
 PATTERN%(2)=&H8888:PATTERN%(3)=&H8888
 CALL PENPAT(VARPTR(PATTERN%(0)))
FOR I=1 TO 6
  YY(I)=INT(Y1-(I*GRIDY/GRDLEN)*YLEN+.5)
   CALL MOVETO (X1,YY(I)):CALL LINETO (X2,YY(I))
NEXT I
CALL PENNORMAL
CALL PENMODE(9):CALL TEXTMODE(1):CALL PENSIZE(1,1)
XX(0)=INT(X1+.5):XX(5)=INT(X2+.5)    'Drawing the frame of the waveform
LINE (XX(0),Y1)-(XX(0),Y2)
LINE (XX(5),Y1)-(XX(5),Y2)
YY(7)=Y2:YY(0)=Y1
```

```
 LINE (X1,Y1)-(X2,Y1)
 LINE (X1,Y2)-(X2,Y2)

LABEL:
 LIBRARY "TOOLLIB"
  FOR I=0 TO 5      'HORIZONTAL AXIS.
   A=Y1+15:AX=XX(I)-10:B=GRIDX*I
   CALL MOVETO(AX,A)
   LB$=LEFT$(STR$(B),4)
   DRAWTEXT LB$
  NEXT I
  FOR I=0 TO 6        'VERTICAL AXIS.
   A=X1-44:AY=YY(I)
'  B=INT((GRIDY*I+YSET(0))*10+.5)/10  'This factor 10 is changable.
   B=INT((GRIDY*I+YSET(0))+.5)  'This is for phadif.
   CALL MOVETO(A,AY)
    LB$=LEFT$(STR$(B),5)
   DRAWTEXT LB$
  NEXT I
  CALL MOVETO(A,Y2)
   IF X<XG THEN LB$=LEFT$(STR$(YSET(1)),5):DRAWTEXT LB$
   A=COORY+15:AX=INT((XX(3)-XX(2))/2+XX(2)-45.5)
  CALL TEXTFACE(1)
  CALL MOVETO(AX,A)
  DRAWTEXT "Frequency [Hz]"
  A=YY(6)+30:AX=X1-32:CALL MOVETO(AX,A)
  DRAWTEXT "Mag"
  A=A+15:AX=AX-20:CALL MOVETO(AX,A)
  CALL TEXTFACE(0)
REM --- PLOT ---
 adjx=5  'for letter position adjusting
 XMAX=GRIDX*5:YMAX=GRDLEN:FRSTX=X1-adjx
 ZERO=INT(Y1-(0!-YSET(0))/YMAX*YLEN+.5)
 LINE (X1,ZERO)-(X2,ZERO)
 CALL TEXTSIZE(9)
 FOR I=0 TO N2        'PLOT THE spectrum
  FRSTY=INT(Y1-(OBP(0,I)-YSET(0))/YMAX*YLEN+.5)-adjx
  CALL MOVETO(FRSTX,FRSTY)
  ISTEN=I+1:STEN$=LEFT$(STR$(ISTEN),2)
  DRAWTEXT STEN$
  FOR J=1 TO N1
    NXTX=INT(X1+(DRTN/N1)*J/XMAX*XLEN+.5)-adjx
    NXTY=INT(Y1-(OBP(J,I)-YSET(0))/YMAX*YLEN+.5)
    CALL MOVETO(NXTX,NXTY)
    DRAWTEXT STEN$
   NEXT J
 NEXT I
PICTURE OFF
CLOSE #1
OPEN "CLIP:PICTURE" FOR OUTPUT AS #1
PRINT #1,PICTURE$
 IMAGE$=PICTURE$
 WINDOW CLOSE 3
 WINDOW 4,"GRAPH",(0,0)-(608,722),3
```

```
CLS
PICTURE ON
PICTURE (76,38)-(550,720),IMAGE$
PICTURE OFF
IMAGE$=PICTURE$
WINDOW CLOSE 4
WINDOW 2,"GRAPH",(2,20)-(249,340),3
PICTURE (43,29)-(217,290),IMAGE$
123 : GOTO 123

MINMAX:
YSET(0)=10000:YSET(1)=-10000   'YSET(0)--MIN,YSET(1)--MAX
FOR I=0 TO N2
 YSET1(1,I)=-10000  'YSET1(1,I)--MAX, YSET1(0,I)--X-AXIS VALUE
 FOR J=0 TO N1
  IF OBP(J,I)>YSET(1) THEN YSET(1)=OBP(J,I)
  IF OBP(J,I)<YSET(0) THEN YSET(0)=OBP(J,I)
  IF OBP(J,I)>YSET1(1,I) THEN YSET1(1,I)=OBP(J,I):YSET1(0,I)=J
 NEXT J
NEXT I
RETURN
```